Interglacial climate variability during MIS 15 to Holocene: Insight from Coupled climate modelling

Dissertation zur Erlangung des Akademischen Grades eines Doktors der Naturwissenschaften

Dr. rer. nat

im Fachbereich 5 (Geowissenschaften)
der Universität Bremen

vorgelegt von

Rima Rachmayani

Bremen 2016

Versicherung an Eides Statt

gem. § 5 Abs. 5 der Promotionsordnung vom 15.07.2015

Ich, Rima Rachmayani, Duntzestr. 12, 28197 Bremen, 2276871
(Vorname, Name, Anschrift, ggf. Matr.-Nr.)

versichere an Eides Statt durch meine Unterschrift, dass ich die vorstehende Arbeit selbständig und ohne fremde Hilfe angefertigt und alle Stellen, die ich wörtlich dem Sinne nach aus Veröffentlichungen entnommen habe, als solche kenntlich gemacht habe, mich auch keiner anderen als der angegebenen Literatur oder sonstiger Hilfsmittel bedient habe, und die zu Prüfungszwecken beigelegte elektronische Version der Dissertation mit der abgegebenen gedruckten Version identisch ist.

Ich versichere an Eides Statt, dass ich die vorgenannten Angaben nach bestem Wissen und Gewissen gemacht habe und dass die Angaben der Wahrheit entsprechen und ich nichts verschwiegen habe.

Die Strafbarkeit einer falschen eidesstattlichen Versicherung ist mir bekannt, namentlich die Strafandrohung gemäß § 156 StGB bis zu drei Jahren Freiheitsstrafe oder Geldstrafe bei vorsätzlicher Begehung der Tat bzw. gemäß § 161 Abs. 1 StGB bis zu einem Jahr Freiheitsstrafe oder Geldstrafe bei fahrlässiger Begehung.

Bremen, 15-04-2016
Ort, Datum

Unterschrift

”Do you not see that Allah drives clouds? Then He brings them together, then He makes them into a mass, and you see the rain emerge from within it. And He sends down from the sky, mountains [of clouds] within which is hail, and He strikes with it whom He wills and averts it from whom He wills. The flash of its lightening almost takes away the eyesight.”

Q.S. An-Nur: 43

To my Husband Ayi and
my Daughter Khansa

Contents

Figures **10**

Tables **11**

Acknowledgements **12**

Abstract **13**

Zusammenfassung **15**

1 Introduction **17**

1.1 The effects of astronomical forcing and GHG on global surface climate during MIS 15, MIS 13, MIS 11, MIS 5, and MIS 1 17

1.2 Vegetation-precipitation feedback in Early-to-Mid- Holocene 19

1.3 Greenland Ice Sheet during MIS 5 and MIS 11 20

1.4 Research Objectives 21

1.5 Outline of the Thesis 22

1.6 Author contributions 23

2 Methodology **25**

2.1 Models 25

2.1.1 CCSM3-DGVM 25

2.1.2 GLIMMER ice-sheet model 26

3 Intra-interglacial climate variability: Model simulations of Marine Isotope Stages 1, 5, 11, 13, and 15 **27**

3.1 Abstract 27

3.2 Introduction 28

3.3 Experimental setup 30

3.3.1 Model description 30

3.3.2 Setup of experiments 30

3.3.3 Selection of interglacial time slices 31

3.3.4 Insolation anomalies 34

3.4 Results . . . 34
3.4.1 JJAS surface temperature anomalies . . . 34
3.4.2 DJF surface temperature anomalies . . . 36
3.4.3 JJAS precipitation anomalies . . . 38
3.4.4 Net Primary Production (NPP) anomalies . . . 41
3.4.5 Climatic effects of obliquity variations during MIS 11 and MIS 13 . 42
3.4.6 Evaluating the climatic effects of astronomical and GHG forcings through correlation maps . . . 45
3.5 Discussion . . . 50
3.6 Conclusions . . . 53
3.7 Acknowledgements . . . 54

4 North African vegetation-precipitation feedback in early and mid-Holocene climate simulations with CCSM3-DGVM 56
4.1 Abstract . . . 56
4.2 Introduction . . . 56
4.3 Experimental Design . . . 58
4.3.1 Model . . . 58
4.3.2 Setup of Experiments . . . 59
4.4 Results . . . 60
4.5 Discussion . . . 67
4.6 Conclusions . . . 73
4.7 Acknowledgement . . . 74

5 Sensitivity of the Greenland Ice Sheet to interglacial climate forcing: MIS 5 versus MIS 11 75
5.1 Abstract . . . 75
5.2 Introduction . . . 75
5.3 Experimental Setup . . . 77
5.3.1 Model . . . 77
5.3.2 Setup of Experiments . . . 78
5.4 Results . . . 79
5.5 Disscussion . . . 82
5.6 Conclusions . . . 86
5.7 Acknowledgments . . . 86

6 Summary and Outlook **87**
6.1 Summary of the results 87
6.2 Outlook 88

References **90**

Figures

3.1 Benthic δ^{18}O stack (Lisiecki and Raymo, 2005), climatic precession, obliquity, and insolation at July, 65° N (Berger, 1978) for the different interglacials. The points mark the time slices simulated in this study. 32

3.2 Insolation anomalies (relative to PI) for the time slices simulated in this study. Patterns of insolation anomaly are classified into Groups I, II, and III (see text). The calculation assumes a fixed present-day calendar with vernal equinox at 21 March. 35

3.3 Boreal summer surface temperature anomalies (relative to PI) for the different interglacial time slices. Classification into Groups I, II, and III (see text) is indicated. 37

3.4 As in Fig. 3.3, but for boreal winter. 39

3.5 As in Fig. 3.3, but for boreal summer precipitation. 40

3.6 As in Fig. 3.3, but for annual net primary production. 43

3.7 Differences in the seasonal and latitudinal distribution of insolation for (A) 416-394 ka, (B) 495-516 ka. 44

3.8 Differences in seasonal surface temperature (A)-(D) and boreal summer precipitation (E)-(F) for 416-394 ka (left) and 495-516 ka (right). 46

3.9 Linear correlation maps between surface temperature and GHG radiative forcing (A), obliquity (B), and climatic precession (C) as calculated from the entire set of experiments. Summer refers to JJAS, winter to DJF. Only significant values are shown according to a two-sided Student's t-test at 95% confidence level. 48

3.10 As in Fig. 3.9, but for precipitation. 49

4.1 Pre-industrial vegetation cover over North Africa simulated by CCSM3-DGVM. (A) Percentage coverage of tree PFTs, (B) same for grasses. 61

4.2 Change in total (i.e. all PFTs) percent vegetation cover for (A) the mid-Holocene (6 ka) and (B) the early Holocene (9 ka) experiment relative to pre-industrial (PI). 61

4.3 Changes of summer precipitation and near-surface winds for (A) the mid-Holocene and (B) the early Holocene experiment relative to PI in model simulations with dynamic vegetation. (C,D) Same as (A,B) but for fixed-vegetation simulations. (E,F) Differences between dynamic vegetation and fixed-vegetation experiments. Hatched areas in (E,F) display significant precipitation differences (95% confidence level) according to both a (non-parametric) Wilcoxon-Mann-Whitney test and a Student t-test. 63
4.4 As in Fig. 4.3, but for changes in summer surface temperature and 700 hPa winds. Hatched areas in (E,F) display significant temperature differences (95% confidence level) according to both a (non-parametric) Wilcoxon-Mann-Whitney test and a Student t-test. 64
4.5 As in Fig. 4.3, but for changes in summer moisture transport at 700 hPa. 66
4.6 Influence of vegetation initial conditions (9k North African vegetation cover versus bare soil) on pre-industrial and mid-Holocene North African climate simulations. Shown are differences in summer precipitation for (A) 0k9k-0k(OAV) and (B) 6k9k-6k(OAV). Hatched areas display significant precipitation differences (95% confidence level) according to both a (non-parametric) Wilcoxon-Mann-Whitney test and a Student t-test. The lower panel (C) shows the corresponding zonal averages over North Africa (20°W-30°E) along with standard errors. 68
4.7 Mean summer evapotranspiration versus precipitation over the region 10-25°N, 20°W-30°E in the 0k, 6k and 9k experiments with dynamic vegetation (OAV experiments; red) and with fixed vegetation (OAV_f experiments; blue). 72

5.1 Insolation anomalies (relative to PI) for the time slices 125 ka (A) and 410 ka (B). The calculation assumes a fixed present-day calendar with vernal equinox at 21 March. Benthic δ^{18}O stack (Lisiecki and Raymo, 2005), climatic precession, obliquity, July insolation at 65°N (Berger, 1978), and the integrated summer insolation with τ= 275 W/m^2 according to Huybers (2006) for the Holocene, MIS 5 and MIS 11 (C). The dots mark the time slices simulated in this study. 80
5.2 Results from the Glimmer MIS 5 and MIS 11 experiments: Timeseries of GrIS volume as equivalent sea-level height for (A) the 125 ka and (B) the 410 ka experiment (switching from modern to interglacial climate forcing at model year 50,000) using different tuning parameter settings (see Table 5.2). 82

5.3 Ablation rate anomalies (410 ka minus 125 ka experiment) at model year 500 after switching from modern to interglacial climate forcing for different tuning parameter settings (see Table 5.2). 83
5.4 Differences between 410 ka (MIS 11 experiment) and 125 ka (MIS 5 experiment) of climatic fields simulated by CCSM3: (A) boreal summer (JJA) surface temperature in and around Greenland, (B) annual snowfall, (C) AMOC (meridional overturning streamfunction in the Atlantic Ocean). 84

Tables

3.1 Atmospheric GHG concentrations used in the interglacial experiments. 33

3.2 Summer (JJAS) precipitation over North Africa (20° W-30° E and 10-25° N) and over India (70-100° E and 10-30° N) along with anomalies relative to PI. Absolute precipitation values are given with standard error (2σ) based on 100 simulation years of each experiment. 41

3.3 Simplified expressions for calculation of radiative forcing due to CO_2, CH_4, N_2O. C is CO_2 in ppmv, M is CH_4 in ppbv, N is N_2O in ppbv. The subscript 0 denotes the unperturbed GHG concentration of PI. 45

4.1 Summary of boundary conditions used in the experiments. Summer insolation refers to July, 21 at 20°N. 60

4.2 Mean summer (JJAS) precipitation over the region 10-25°N, 20°W-30°E in the various experiments. ΔP denotes anomalies relative to the corresponding 0k (PI) case. SE is the standard error. Precipitation values are normally distributed according to a Shapiro-Wilk normality test (95 % confidence level). 70

4.3 Changes of summer (JJAS) canopy evaporation, canopy transpiration and ground evaporation in the various early and mid-Holocene experiments over the region 10-25°N, 20°W-30°E. 71

4.4 Summer (JJAS) surface albedo values in the early and mid-Holocene experiments over the region 10-25°N, 20°W-30°E. 71

5.1 GHG concentrations used in the CCSM3 experiments. 79

5.2 Tuned parameter values used in the Glimmer ice-sheet experiments. The tuning parameters are *f* (enhancement flow factor), L_G (near-surface lapse rate), *G* (geothermal heat flux), α_s (PDD factor for snow), and α_i (PDD factor for ice). The experiment numbers (tuning parameter settings) are taken from Stone et al. (2010). For details the reader is referred to Stone et al. (2010). 81

Acknowledgements

Above all, I would like to thank Matthias Prange. He's not only introduced me to the fascinating world of past Interglacials climate change, but also took the risk giving a layperson like me the opportunity to work on this challenging and prevailing subject. Despite his numerous obligations, he always found time to provide important suggestions and helpful advice when problems arose. I must also thank my other supervisor Michael Schulz, for his enthusiasm and for ensuring continued progress and direction of the thesis. I am also grateful to both for allowing me to attend many International conferences and summer schools, which have been an invaluable experience. This thesis was funded by an INTERDYNAMIK project.

Thanks also to my thesis committee meeting, Ute Merkel and Torsten Beckert, who have provided helpful discussions and advice at our bi-annual meetings. Thank you to Andreas Manchske for answering many computing queries and solving any glitches that I have encountered on the way. Since I am also an external member of GLOMAR, I would like to thank to Dierk, Tina and Jutta for giving me valuable supports for family support and many courses that have been useful for my career. In addition, current members of Geosystem Modelling research group Amanda, Claudia, Leslie, Takasumi, Gerlinde, Benjamin, Jeroen, Andre, Kerstin, Andrea, Rike, Robin, Annagret, Kaveh, Alex, Sri, Diana, Ania, Irina, Charlotte, Huadong, Jürgen, Pepijn, Javier and former members Vidya, Nilima, Dian, Thejna, Xiao, Heather deserve special thanks for providing an agreeable working environment. Outside Bremen, I am also grateful to Dan J. Lunt and Emma J. Stone for their help during my research stay in University of Bristol on Greenland simulations. Within the COIN project, sincere thanks to Thomas Kleinen, Victor Brovkin, Pavel Tarasov for giving me a nice collaboration atmosphere and experiences.

The process of writing a thesis is a primarily time-consuming task. Therefore, further thanks go to all my Indonesian family "Keluarga Muslim Indonesia Bremen (KMIB)" especially Vidjaja family, Puti S. L. Kellermann, and Calon Doktor (CaTor) friends in Bremen for their lenience and neverending support during the last years. Last but no least, I am deeply indebted to my family, first and foremost my husband Ayi, my daughter Khansa, and my parents. Without their endless support, which not even halted during the hard times last years, this thesis could not have been completed. Thank you!

Abstract

Understanding the mechanisms and effects of natural long-term climate variability is essential for providing projections of possible climate change for the near future. This study examines the mechanisms of the climate variability over the time frame of the past 600 kyr using CCSM3-DGVM (Community Climate System Model version 3 with Dynamic Global Vegetation Model).

A set of 13 interglacial time slice experiments was carried out to study global climate variability between and within the Quaternary interglacials of Marine Isotope Stages (MISs) 1, 5, 11, 13, and 15. Here, this study focuses on the effect of different roles of obliquity, precession and greenhouse gases (GHG) forcing on global surface temperature and precipitation patterns. Local insolation anomalies induced by the astronomical forcing play a role in most regions of seasonal surface temperature anomalies. Climate feedbacks, however, may modify the surface temperature response in specific regions, most pronounced in the monsoon domains and the polar oceans. Especially in high latitudes and early Brunhes interglacials (MIS 13 and 15) when GHG concentrations were much lower than during the later interglacials, GHG forcing may also play an important role for seasonal temperature anomalies. During boreal summer, high-versus-low obliquity climates are generally characterized by strong warming over the Northern Hemisphere extratropics and slight cooling in the tropics. A moderate cooling over large portions of the Northern Hemisphere continents and a strong warming at high southern latitudes during winter is found. Additionally, a significant role of obliquity in forcing the West African monsoon is identified. In this case, other regional monsoon systems are less sensitive or not sensitive at all to obliquity variations during interglacials. Based on two specific time slices (394 and 615 ka), the model results suggest that the West African and Indian monsoon systems do not always vary in concert, challenging the concept of a global monsoon system at orbital timescales. Furthermore, GHG forcing is positively correlated with surface temperature over most regions of the globe in the annual mean and GHG radiative forcing exhibits no clear response in annual and seasonal precipitation during the interglacials except for the high latitudes in both hemispheres during annual, for southern high latitudes during summer, and for northern high latitudes during winter where the hydrologic cycle accelerates with higher GHG concentrations.

In order to disentangle the impact of dynamic vegetation on the early (9 ka) and mid-Holocene (6 ka) North African climate, experiments with the dynamic and fixed-vegetation

were carried out. In this study, the coupled model simulates enhanced summer rainfall and a northward migration of the West African monsoon trough along with an expansion of the vegetation cover for the early and middle Holocene compared to pre-industrial. With dynamic vegetation, the orbitally triggered summer precipitation anomaly is enhanced by approximately 20 % in the Sahara/Sahel region (10–25° N,20° W–30° E) in both the early and mid-Holocene experiments compared to their fixed-vegetation counterparts. The primary vegetation-rainfall feedback identified here operates through surface latent heat flux anomalies by canopy evaporation and transpiration and their effect on the mid-tropospheric African Easterly Jet, whereas the effects of vegetation changes on surface albedo and local water recycling play a negligible role.

Furthermore, this study constrains a three-dimensional thermomechanical-ice model Genie Land Ice Model with Multiple-Enabled Regions (GLIMMER) forced by CCSM3 climate model output for MIS 5 and MIS 11 time slices to simulate a sensitivity of Greenland ice sheet (GrIS). The GrIS is thought to have contributed substantially to high global sea levels during the interglacials of MIS 5 and MIS 11. Geological evidence suggests that the mass loss of the GrIS was similar or even greater during the interglacial of MIS 11 than MIS 5, despite a weaker insolation forcing. This study shows a stronger sensitivity of the GrIS to MIS 11 climate forcing than to MIS 5 forcing. The greater MIS 11 GrIS mass loss relative to MIS 5 is attributed to a larger heat transport towards high latitudes by a stronger Atlantic meridional ocean circulation in addition to a stronger GHG radiative forcing. The results, however, suggest a substantial modification of orbital insolation forcing by internal climate feedbacks, which add significant complexity to the traditional Milankovitch theory.

Zusammenfassung

Das Verständnis der Mechanismen und Auswirkungen von einer natürlichen langfristigen Klimaschwankung ist unerlässlich für die Bereitstellung von Projektionen möglicher Klimaänderungen für die nahe Zukunft. Diese Studie untersucht die Mechanismen der Klimavariabilität über den Zeitrahmen der vergangenen 600,000 Jahre durch die Verwendung von CCSM3-DGVM (Gemeinschaftsklima-System Modelversion 3 mit dem dynamischen globalen Vegetationsmodell).

Ein Satz von 13 interglazialen Scheibenexperimenten wurde durchgeführt, um globale Klimaschwankungen zwischen und innerhalb dem känozoischen Eiszeitalter der marinen Sauerstoff-Isotopenstufen 1, 5, 11, 13 , und 15 zu untersuchen. Hier, diese Studie konzentriert sich auf die verschiedenen Aspekte von Achsenneigung, Präzession und Antrieb durch Treibhausgas (THG) und deren Auswirkungen auf Oberflächentemperatur und Niederschlagsmuster. Lokale Sonneneinstrahlungs-Anomalien, induziert durch astronomische Kräfte, spielen in den meisten Regionen mit saisonalen Oberflächentemperaturanomalien eine Rolle. Jedoch können Klima-Feedbacks das Oberflächen-Temperaturverhalten in bestimmten Regionenändern. Am ausgeprägtesten zeigt sich dies in den Monsunregionen und den polaren Ozeanen. Vor allem in den hohen Breiten und frühen Brunhes-Interglazialen (MIS 13 und 15), als die Treibhausgaskonzentrationen viel niedriger als in den späteren Interglazialen waren, können die THG auch eine wichtige Rolle in Bezug auf die saisonalen Temperaturanomalien gespielt haben. Während des borealen Sommers, ist bei hoher im Gegensatz zu niedriger Achsenneigung, das Klima in der Regel durch eine starke Erwärmung in der nördlichen Hemisphäre und einer leichten Abkühlung in den Tropen gekennzeichnet. Während des borealen Winters hingegen findet eine moderate Abkühlung über grossen Teilen der nördlichen Hemisphäre statt und es wird eine starke Erwärmung der Kontinente in den hohen südlichen Breiten gefunden. Zusätzlich wird eine bedeutende Rolle der Achsenneigung im Antrieb des westafrikanischen Monsun identifiziert. In diesem Fall sind andere regionale Monsunsysteme weniger empfindlich oder ganz unempfindlich gegenüber den Achsenneigungsänderungen während der Interglaziale. Basierend auf zwei spezifische Zeitscheiben (394 und 615 ka) schlagen die Modellergebnisse vor, dass die westafrikanischen und indischen Monsun-Systeme nicht immer die gleichen Veränderungen aufweisen, sodass das Konzept eines globalen Monsunsystems auf einer orbitalen Zeitskala herausgefordert wird. Ausserdem können die Auswirkungen der THG im jährlichen Mittel über den meisten Regionen der Erde posi-

tiv mit der Oberflächentemperatur korreliert werden und die Strahlung aufgrund von THG zeigt keine klare Antwort in jährlichen und saisonalen Niederschlägen während der Interglaziale, mit Ausnahme der beiden hohen Breiten während des jahres. Dort zeigt sich für den Südsommer und für den im Nordwinter, dass sich der Wasserkreislauf mit höheren THG-Konzentrationen beschleunigt.

Um die Auswirkungen der dynamischen Vegetation auf das frühe (vor 9000 Jahren) und mittlere Holozäns (vor 6000 Jahren) auf das nordafrikanischen Klima zu entflechten, wurden Experimente durchgeführt, welche eine dynamische und eine unveränderliche Vegetation beinhalten. In dieser Studie simuliert das gekoppelte Modell erhöhte Sommerniederschläge und eine Wanderung des westafrikanischen Monsunstiefs in Richtung Norden, zusammen mit einer Ausbreitung der Vegetation im frühen und mittleren Holozän im Vergleich zur vorindustriellen Zeit. Mit der dynamischen Vegetation kann gezeigt werden, dass sich die orbital ausgelösten Sommerniederschlags-Anomalien in der Sahara/Sahel-Region (10–25° N, 20° W–30° E) um etwa 20% verstärken, sowohl im frühen als auch mittleren Holozän-Experimenten im Vergleich zur ihrem Pendant mit unveränderter Vegetation. Das primäre Vegetation-Niederschlags-Feedback, das hier identifiziert wurde, operiert über Oberflächen latente Wärmeflussanomalien, wie Verdunstung und Verdampfen über das Blätterdach und deren Wirkung auf den mittleren troposphären African Easterly Jet, während die Auswirkungen von Vegetationsveränderungen auf Bodenalbedo und das lokale Wasserrecycling kaum eine Rolle spielen.

Darüber hinaus, diese Studie beschränkt sich auf ein dreidimensionales thermomechanische Eis-Modell, das Genie Land Ice Modell mit multiplen aktivierten Regionen (GLIMMER), welches verursacht durch CCSM3 Klimamodelldaten für MIS 5- und MIS 11-Zeitscheiben, eine Empfindlichkeit für die Eisdecke Grönlands (GrIS) simuliert. Für das GrIS wird angenommen, dass es während der Warmzeiten von MIS 5 und MIS 11 erheblich zum hohen globalen Meeresspiegel beigetragen hat. Geologische Hinweise lassen darauf schliessen, dass während der Warmzeiten von MIS 5 und MIS der Masseverlust der GrIS ähnlich war oder während der Interglaziale von MIS 11 als MIS 5 noch weit höher war, trotz einer schwächeren Sonneneinstrahlung. Die Studie zeigt eine stärkere Empfindlichkeit der GrIS auf das MIS 11 Klima als auf das MIS 5 Klima. Der grössere GrIS Massenverlust von MIS 11 in Bezug auf MIS 5 wird auf einen grösseren Wärmetransport zu den hohen Breiten und eine stärkere atlantische meridionale Ozeanzirkulation zurückgeführt, zusätzlich zu einer stärkere THG Strahlung. Die Ergebnisse deuten jedoch darauf hin, dass eine wesentliche Änderung der orbitalen Sonneneinstrahlung durch interne Klima Feedbacks, der traditionellen Milankovitch-Theorie erheblich an Komplexität hinzufügen.

1 Introduction

The ability to predict future changes in global climate is essential for policymaking today and for human well-being in future. It is recognized in paleoclimate research that cyclic changes of global climate as a combined effect of the Earth's orbital configuration, greenhouse gasses (GHG) and internal feedback mechanisms (Prokopenko et al., 2010). This study investigates the combined effect during Marine Isotope Stages (MISs) 15, MIS 13, MIS 11, MIS 5, and current interglacial MIS 1 on global surface climate. Study of the current Holocene interglacial is therefore important for capturing the natural range of variability of interglacial climates in the sense that more or less similar orbital configurations with interglacials have repeatedly occurred in past. Early- and Mid- Holocene simulation focusing on the working mechanism of the vegetation-precipitation feedback by enabling dynamically vegetation in CCSM3 in particular area of North Africa is considered. Moreover, a higher than-present sea levels in the past interglacials is found when global mean temperature was warmer than the preindustrial (PI) (Dutton et al., 2015). This requires a contribution of mass loss from Greenland Ice Sheet (GrIS) as discussed in Reyes et al. (2014); Dutton et al. (2015) or more of the current polar ice-sheets (Dutton et al., 2015). Thus, understanding how GrIS lost mass during past warm periods of MIS 5 and MIS 11 can provide insights into their sensitivity to climate change.

1.1 The effects of astronomical forcing and GHG on global surface climate during MIS 15, MIS 13, MIS 11, MIS 5, and MIS 1

A cyclic growth and decay of continental ice sheets associated with global environmental changes is characteristic of the Quarternary period (e.g., Lisiecki and Raymo, 2005; Tzedakis et al., 2006; Jouzel et al., 2007; Lang and Wolff, 2011). While it is found that varying orbital insolation ultimately pace the transitions between glacial and interglacial stages (Hays et al., 1976), climate research is just beginning to understand the internal climate feedbacks that are required to shift the Earth system from one state to the other (e.g., van Nes et al., 2015). The astronomical forcing, with its characteristic periods of ca. 400 and 100 kyr (eccentricity), 41 kyr (obliquity), and ca. 21 kyr (precession) as in Berger (1978), also acts as an external driver for long-term climate change within the interglacials

(i.e. the long-term intra-interglacial climate variability) and likely contributes to interglacial diversity since the evolution of astronomical parameters differs between all Quaternary interglacial stages (cf. Tzedakis et al., 2009; Yin and Berger, 2015; Past Interglacials Working Group of PAGES, 2016).

For the interglacial of MIS 5 (Last Interglacial (LIG), MIS 5e; ca. 130-115 kyr ago), proxy data suggest a peak global mean temperature of about 1° C higher than during the pre-industrial period (e.g., Otto-Bliesner et al., 2013). The maximum global mean sea-level has been estimated to 6-9 m above the present-day level (Kopp et al., 2009; Dutton and Lambeck, 2012; Dutton et al., 2015). The interglacial of MIS 11 was unusually long, about 30,000 years (ca. 425-395 kyr ago). Global average temperatures of MIS 11 are highly uncertain, but a peak global mean temperature of up to 2° C relative to pre-industrial cannot be ruled out (Lang and Wolff, 2011; Dutton et al., 2015). Maximum global mean sea-level may have been 6-13 m higher than today (Raymo and Mitrovica, 2012; Dutton et al., 2015). Interglacials before MIS 11 (early Brunhes interglacials), like MIS 13 and 15, are generally characterized by lower global mean temperatures, larger continental ice-sheets, lower global sea level and lower atmospheric GHG concentrations relative to the more recent interglacials (e.g., Yin and Berger, 2010; Lang and Wolff, 2011; Dutton et al., 2015).

In this study, special focus on the sensitivity of the West African and Indian monsoon systems to obliquity and precession forcing on interglacials time scales is also carried out. In particular, the applicability of the global monsoon concept (Trenberth et al., 2000; Wang et al., 2014) is studied. West African monsoon rainfall turns out to be most sensitive to changes in summer insolation, whereas spring/early summer insolation is more important for monsoon rainfall over India as found by Braconnot et al. (2008). It has been argued that the reason is a resonant response of the Indian monsoon to the insolation forcing when maximum insolation anomalies occur near the summer solstice and a resonant response of the African monsoon – which has its rainfall maximum one month later in the annual cycle than the Indian monsoon – when the maximum insolation change is delayed after the summer solstice. The different responses to specific forcings and the sometimes out-of-phase behaviour of the African and Indian monsoon systems challenge the global monsoon concept – according to which all regional monsoon systems are part of one seasonally varying global-scale atmospheric overturning circulation in the tropics (Trenberth et al., 2000; Wang et al., 2014) – at astronomical timescales.

Furthermore, temperature and GHG co-evolve in climate system by affecting each other. An increase in GHG leads to a rise in atmospheric temperature, and, in turn, an

increase in temperature affects vegetation and upper ocean and thereby the carbon fluxes between the climate system components (Claussen, 2007). Hence, one has to understand temperature and atmospheric CO_2 fluctuations as feedback processes within the climate system (Claussen, 2007). Present-day concentrations of the atmospheric GHG carbon dioxide (CO_2), methane (CH_4) and nitrous oxide (N_2O) exceed the range of concentrations recorded in ice cores during the past 800 kyr (e.g. Schilt et al., 2010). Changes in atmospheric CO_2 concentration play an important role in glacial-interglacial cycles. Although the primary driver of glacial-interglacial cycles lies in the seasonal and latitudinal distribution of incoming solar energy driven by changes in the geometry of the Earth's orbit around the Sun (astronomical forcing), reconstructions and simulations together show that the full magnitude of glacial-interglacial temperature and ice volume changes cannot be explained without accounting for changes in atmospheric CO_2 content and the associated climate feedbacks (Masson-Delmotte et al., 2013).

1.2 Vegetation-precipitation feedback in Early-to-Mid-Holocene

Various positive feedbacks have been postulated to be crucial in shaping the early-to-mid Holocene North African humid period, involving vegetation and soil (e.g. Claussen et al., 1999; Levis et al., 2004a; Hales et al., 2006), sea-surface temperatures (e.g. Zhao et al., 2005; Zhao and Harrison, 2012), and surface-water coverage by lakes and wetlands (e.g. Krinner et al., 2012). The African Humid Period (AHP) was a dramatic climate change across North Africa from the hyperarid desert it is today to a nearly completely vegetated landscape during the early and middle Holocene as a direct result of African monsoonal climate responses to periodic variations in the Earth's orbital forcing (deMenocal and Tierney, 2012). Over time, the notion of a positive vegetation-precipitation feedback has received the greatest attention in the literature (e.g. Claussen, 2009). At present, North Africa is much drier than during the early and middle Holocene when a higher orbitally induced summer insolation triggered more humid and "greener" conditions in the Sahel and Saharan regions (e.g. Bartlein et al., 2011; Collins et al., 2013). It has been suggested (Otterman, 1974; Charney, 1975) that the effect of an expanded North African vegetation cover on surface albedo would be key in amplifying the early-to-mid Holocene West African monsoonal rainfall (e.g. Claussen and Gayler, 1997; Brovkin et al., 1998; Hales et al., 2006). A transition from the humid state to the arid state by a catastrophic bifurcation or "unstable collapse" (Liu et al., 2006, 2007) was suggested to have been abruptly terminating the AHP

around 5.5 ka (deMenocal et al., 2000). The abruptness of the North African climate transition (Lézine et al., 2011; Claussen et al., 2013; Francus et al., 2013) and the existence of a strong positive vegetation-precipitation feedback in North Africa (Levis et al., 2004a; Liu et al., 2006, 2007; Kröpelin et al., 2008; Notaro et al., 2008; Wang et al., 2008; Liu et al., 2010) will be investigated in this study to identify the strength of the vegetation-precipitation feedback in mid- to early Holocene simulations.

1.3 Greenland Ice Sheet during MIS 5 and MIS 11

Continental ice sheets are a major factor in the climate change debate, in particular due to their direct link to global sea level. The study of warm climates in the past may provide useful insight into the sensitivity of polar land ice to changing forcing. A growing body of evidence suggests particularly high global sea levels along with significant shrinking of the GrIS during the Quaternary interglacials of MIS 5 and MIS 11 (Dutton et al., 2015).

Summer temperature was up to 5° C in the Arctic region for last time at 125 ka higher than during PI (e.g., Montoya et al., 2000; Kaspar et al., 2005; Anderson et al., 2006; Otto-Bliesner et al., 2006; CAPE Last Interglacial Project Members, 2006; NEEM community members, 2013). As mentioned in section 1.1, compilations of relative sea level combined with modeling suggest a LIG peak global mean sea level of 6-9 m above present (Kopp et al., 2009; Dutton and Lambeck, 2012; Dutton et al., 2015). However, the contribution of GrIS melting to this sea level rise is highly uncertain, recent model results suggest a GrIS contribution between 1.4 and 4.3 m (Robinson et al., 2011; Born and Nisancioglu, 2012; Helsen et al., 2013; Masson-Delmotte et al., 2013; Stone et al., 2013; Quiquet et al., 2013), indicating that the size of the GrIS was still substantial during the LIG. It has been demonstrated, however, that the simulation of LIG GrIS mass loss is highly sensitive to poorly constrained model parameters (Stone et al., 2013). Interpretation of ice-core records during MIS 5 is controversial (Alley et al., 2010) and studies suggested different existed ice-area over Greenland at that time (Koerner, 1989; Koerner and Fischer, 2002; NorthGRIP, 2004; Otto-Bliesner et al., 2006; Willerslev et al., 2007; NEEM community members, 2013). Previous work investigated the sensitivity of ice-sheet evolution for the modern GrIS to five tuneable parameters which affect the ice-sheet dynamics and surface mass balance (Stone et al., 2010). Later on, it has been shown that these parameters strongly control the size of the modelled GrIS during the LIG (Stone et al., 2013).

Meanwhile, a warm interglacial during MIS 11 between 420-395 kyr ago (Milker et al., 2013; Dutton et al., 2015) is indicated by a higher sea surface temperatures (SST) at

about 1-2° C in North Atlantic compared to modern (McManus et al., 1999; Bauch et al., 2000; Helmke et al., 2003; Kandiano and Bauch, 2003; De Abreu et al., 2005; Kandiano et al., 2013). Some marine and continental records (Howard, 1997; Droxler et al., 2003) and geochronologic and geomorphic evidence (Raymo and Mitrovica, 2012) indicated that MIS 11 as unique interglacial includes the warmest interglacial of the past 500 kyr. As defned in section 1.1, the maximum global mean sea level (GMSL) at that time are estimated to be small at about 6-13 m higher than modern (Raymo and Mitrovica, 2012; Dutton et al., 2015), requiring a loss of most or all of the GrIS (Reyes et al., 2014). Taken together, mass loss of the GrIS was similar or even greater during the interglacial of MIS 11 than during the LIG. Since the changing seasonal insolation owing to varying astronomical parameters is thought to be a major forcing of polar ice-sheet evolution (Loutre et al., 2004; Huybers, 2006; van de Berg et al., 2011), the great GrIS mass loss during MIS 11 seems to be counterintuitive. Due to a low eccentricity of the Earth's orbit, climatic precession varied relatively little during MIS 11, and hence maximum boreal summer insolation was much smaller during the MIS 11 interglacial than during the LIG (Fig. 5.1, Chapter 5). By contrast, eccentricity was high during the LIG leading to high summer insolation values around 125 ka. Huybers (2006) pointed out that glaciers are sensitive to insolation integrated over the duration of the summer and introduced the concept of the integrated summer insolation as the dominant control on polar ice sheet evolution. Like maximum summer insolation, values for the integrated summer insolation were larger during the LIG than during MIS 11, and cannot explain a stronger GrIS melting during MIS 11 compared to MIS 5 (Fig. 5.1, Chapter 5).

And yet, simulating ice-coverage during MIS 11 is more challenging since the interpretation of the GrIS at this stage is highly unknown due to few reliable models and little proxy data exist in documenting the extent of the GrIS loss. Moreover, ice-loss estimation experiments over Greenland during MIS 11, such as at 410 ka have not been examined with ice-sheet modelling so far. In the present study, it shows the sensitivity to tuning parameters for the interglacial of MIS 11.

1.4 Research Objectives

The main objective of the thesis is to investigate the combined effect of Earth's orbital and GHG forcing together with the internal feedback mechanisms during the past warm interglacials of MIS 15, MIS 13, MIS 11, MIS 5, and MIS 1 on the climate. Since the dynamic vegetation is enabled in CCSM3, analysis of the vegetation-precipitation feedback in the

particular area of North Africa during Early- to Mid- Holocene is carried out. Sensitivity of GrIS to interglacial climate of MIS 5 and MIS 11 is also studied. To cover the main objective, the following research objectives are outlined:

- To investigate the effects of obliquity, precession and GHG on global surface climate during MIS 15, MIS 13, MIS 11, MIS 5, MIS 1 based on realistic orbital configurations and to test on the sensitivity of the West African and Indian monsoon systems to obliquity and precession forcing for astronomical timescales, in particular, the applicability of the global monsoon concept (Trenberth et al., 2000; Wang et al., 2014).

- To identify the sign, strength and working mechanism of the vegetation-precipitation feedback over North Africa in mid (6 ka) and early Holocene (9 ka) simulations by switching on and off interactive dynamic vegetation in this specific coupled model and to study the impact of vegetation initial conditions on mid-Holocene and modern (pre-industrial) climate-vegetation simulations and hence the existence of multiple equilibria in the North African climate-ecosystem.

- To analyze the sensitivity of GrIS mass loss to interglacial climate forcing of MIS 5 and 11, to address the conundrum as to why the GrIS mass loss may have been greater during MIS 11 than during MIS 5 despite a weaker insolation forcing and to investigate the impact of some poorly constrained parameters in large-scale ice-sheet modelling on the paleo-GrIS simulations.

1.5 Outline of the Thesis

The numerical model used for carrying out the experiments is described in Chapter 2. The results are presented in three manuscripts in Chapter 3, Chapter 4 and Chapter 5 respectively.

- Chapter 3 presents a different and complementary Coupled General Circulation Model (CGCM)-CCSM3 study which takes intra-interglacial climate variability into account by simulating two or more time slices for each interglacial stage of MIS 1, 5, 11, 13, and 15. Moreover, this study challenges the concept of a global monsoon system at astronomical timescales based on two specic time slices 394 and 615 ka.

- Chapter 4 analyses the impact of dynamic vegetation on the early and mid-Holocene North African climate by performing three sets of experiments with dynamic vegetation, fixed global PFT distribution, and without dynamic vegetation. Moreover, two additional simulations for PI and mid-Holocene were carried out to examine the role of DGVM initial conditions and the potential for bistable climate-vegetation states.

- Chapter 5 discusses potential mechanisms in the climate system that may have been responsible for the strong GrIS mass loss during MIS 11 compared to MIS 5. In addition, Glimmer experiments with different sets of parameters were performed to asses their sensitivity to the modelled GrIS during MIS 5 and MIS 11.

Chapter 6 includes the summary of the thesis and an outlook on modelling of earliear intergacials climates, sensitivity studies on uncertainties of the potential model-dependencies, and on modelling of interactively coupled CGCM-ice sheet transient experiments.

1.6 Author contributions

Chapter 3: Intra-interglacial climate variability: Model simulations of Marine Isotope Stages 1, 5, 11, 13, and 15.
R. Rachmayani, M. Prange, M. Schulz (published in Climate of the Past, doi:10.5194/cp-12-1-2016).
R. Rachmayani:

- performed all model experiments using CCSM3-DGVM.

- processed and analyzed model output.

- wrote the manuscript.

M. Prange: devised the project and improved the manuscript.

M. Schulz: devised the project and improved the manuscript.

Chapter 4: North African vegetation-precipitation feedback in early and mid-Holocene climate simulations with CCSM3-DGVM.

R. Rachmayani, M. Prange, M. Schulz (published in Climate of the Past, Special Issue: INTERDINAMIC (Integrated analysis of Interglacial climate dynamics), doi:10.5194/cp-11-175-2015)

R. Rachmayani:

- performed all model experiments using CCSM3-DGVM.
- processed and analyzed model output.
- wrote the manuscript.

M. Prange: implemented new parameterizations for canopy interception and soil evaporation into the land component of CLM, devised the project and improved the manuscript.

M. Schulz: improved the manuscript.

Chapter 5: Sensitivity of the Greenland Ice Sheet to interglacial climate forcing: MIS 5 versus MIS 11.

R. Rachmayani, M. Prange, D. J. Lunt, E. J. Stone, M. Schulz (Will be submitted for publication in Geophysical Research Letters).

R. Rachmayani:

- performed all model experiments using CCSM3-DGVM and Glimmer ice-sheet model.
- processed and analyzed model output.
- wrote the manuscript.

M. Prange: devised the project, improved the data analysis and the manuscript.

D. J. Lunt: improved the analysis of the ice-sheet model output.

E. J. Stone: selected optimal parameters based on different diagnostic skill scores which later used by author (R. Rachmayani) performed the senstivity experiments.

M. Schulz: improved the manuscript.

2 Methodology

2.1 Models

To study the response of climate under GHG and orbital forcings during the past interglacials, an approach of numerical modelling is applied. A General Circulation Models (GCMs) of Community Climate System Model version 3 with Dynamic Global Vegetation Model (CCSM3-DGVM) model is used. Moreover, the Glimmer (Genie Land Ice Model with Multiple-Enabled Regions) ice sheet model is utilized for the the ice-sheet modelling work simulated in this study. A brief description of models used in this study as follows:

2.1.1 CCSM3-DGVM

The NCARs (National Centre for Atmospheric Research) CCSM3 is a fully coupled GCM, composed of four separate components representing atmosphere, ocean, land and sea-ice connected by a flux coupler. The component models are CAM3 (Community Atmosphere Model version 3; (Collins et al., 2004, 2006a,b), POP (Parallel Ocean Program version 1.4.3; Smith and Gent (2002), CLM3 (Community Land surface Model version 3; Oleson et al. (2004) and CSIM5 (Community Sea Ice Model version 5; Briegleb et al. (2004). A low-resolution version is employed in all CCSM3 simulations in this study where the resolution of the atmospheric component is given by T31 (3.75° transform grid), with 26 layers in the vertical. The ocean has a nominal resolution of 3° (like the sea-ice component) with a vertical resolution of 25 levels.

The land model shares the same horizontal grid with the atmosphere and includes components for biogeophysics, biogeochemistry, the hydrological cycle as well as a DGVM as discussed in Sitch et al. (2003); Levis et al. (2004a); Bonan and Levis (2006). The DGVM predicts the distribution of 10 plant functional types (PFTs) which are differentiated by physiological, morphological, phenological, bioclimatic, and fire-response attributes (Levis et al., 2004a). In order to improve the simulation of land-surface hydrology and, hence, the vegetation cover, new parameterizations for canopy interception and soil evaporation were implemented into the land component (Oleson et al., 2008; Handiani et al., 2013; Rachmayani et al., 2015). PFT population densities are restored annually, while the land and atmosphere models are integrated with a 30 minutes time step.

2.1.2 GLIMMER ice-sheet model

Version 1.0.4 of Glimmer is used for consistency with previous work (e.g., Lunt et al., 2008, 2009). The core of the model is based on the ice-sheet model described by Payne (1999) and Rutt et al. (2009). The model includes a surface mass balance scheme, coupled ice flow, thermodynamics and ice thickness evolution and an isostatic readjustment component. The horizontal resolution of the model is 20 km with 11 vertical layers. Its design allows easy coupling to a wide variety of climate models. As such there are two main components to the model GLIDE and GLINT. GLIDE (General Land Ice Dynamic Elements) forms the core part of Glimmer, in which ice velocities, internal ice temperature distribution, isostatic readjustment and meltwater production are calculated. It takes boundary conditions from the climate which provides upper surface temperature and mass balance fields, from the isostasy model which provides the lower surface elevation, and finally a geothermal model which provides a geothermal heat flux through the lower surface of the ice. GLINT is an interface which allows any standard latitude longitude climate model to be coupled to GLIDE relatively easily. The surface mass balance is simulated using the positive degree day (PDD) approach described by Reeh (1991). The basis of the PDD method is the assumption that the melt that takes place at the surface of the ice sheet is proportional to the time-integrated temperature above the freezing point, known as the positive degree day. Two PDD factors are used, one each for snow and ice, to take account of the different albedos and densities of these materials. The use of PDD mass balance models is well-established in coupled atmosphere-ice sheet palaeoclimate modelling studies (DeConto and Pollard, 2003; Lunt et al., 2008, 2009)

Certain aspects concerning modelling the GrIS have not been included in the ice-sheet model simulations in this study. Firstly, the version of Glimmer used does not contain an ice-shelf component. The ice dynamics are represented with the widely used shallow-ice approximation (SIA) approach, which neglects longitudinal stresses in the ice sheet. This simplification is appropriate for ice masses that are thin compared with their horizontal extent.

Secondly, the process of calving is parameterised at the marine margin (no attempt at modelling the process of calving has been made). Thirdly, although basal sliding and basal hydrology are included as options in Glimmer they are simplistic in their attempt to model these components of the ice-sheet system (Rutt et al., 2009). Since modelling the GrIS in this thesis is centered around the criteria used in the BAMBER benchmark exercise basal sliding has not been included.

3 Intra-interglacial climate variability: Model simulations of Marine Isotope Stages 1, 5, 11, 13, and 15

R. Rachmayani, M. Prange, M. Schulz

3.1 Abstract

Using the Community Climate System Model version 3 (CCSM3) including a dynamic global vegetation model a set of 13 time slice experiments was carried out to study global climate variability between and within the Quaternary interglacials of Marine Isotope Stages (MISs) 1, 5, 11, 13, and 15. The selection of interglacial time slices was based on different aspects of inter- and intra-interglacial variability and associated astronomical forcing. The different effects of obliquity, precession and greenhouse gas (GHG) forcing on global surface temperature and precipitation fields are illuminated. In most regions seasonal surface temperature anomalies can largely be explained by local insolation anomalies induced by the astronomical forcing. Climate feedbacks, however, may modify the surface temperature response in specific regions, most pronounced in the monsoon domains and the polar oceans. GHG forcing may also play an important role for seasonal temperature anomalies, especially in high latitudes and early Brunhes interglacials (MIS 13 and 15) when GHG concentrations were much lower than during the later interglacials. High-versus-low obliquity climates are generally characterized by strong warming over the Northern Hemisphere extratropics and slight cooling in the tropics during boreal summer. During boreal winter, a moderate cooling over large portions of the Northern Hemisphere continents and a strong warming at high southern latitudes is found. Beside the well-known role of precession, a significant role of obliquity in forcing the West African monsoon is identified. Other regional monsoon systems are less sensitive or not sensitive at all to obliquity variations during interglacials. Moreover, based on two specific time slices (394 and 615 ka) it is explicitly shown that the West African and Indian monsoon systems do not always vary in concert, challenging the concept of a global monsoon sys-

tem at astronomical timescales. High obliquity can also explain relatively warm Northern Hemisphere high-latitude summer temperatures despite maximum precession around 495 ka (MIS 13). It is hypothesized that this obliquity-induced high-latitude warming may have prevented a glacial inception at that time.

3.2 Introduction

The Quaternary period is characterized by the cyclic growth and decay of continental ice sheets associated with global environmental changes (e.g., Lisiecki and Raymo, 2005; Tzedakis et al., 2006; Jouzel et al., 2007; Lang and Wolff, 2011). While it is commonly accepted that the transitions between glacial and interglacial stages are ultimately triggered by varying astronomical insolation forcing (Hays et al., 1976), climate research is just beginning to understand the internal climate feedbacks that are required to shift the Earth system from one state to the other (e.g., van Nes et al., 2015). The astronomical forcing, with its characteristic periods of ca. 400 and 100 kyr (eccentricity), 41 kyr (obliquity), and ca. 19 and 23 kyr (precession) as in Berger (1978), also acts as an external driver for long-term climate change within the interglacials (i.e. the long-term intra-interglacial climate variability) and likely contributes to interglacial diversity since the evolution of astronomical parameters differs between all Quaternary interglacial stages (cf. Tzedakis et al., 2009; Yin and Berger, 2015). Understanding both interglacial climate diversity and intra-interglacial variability helps to estimate the sensitivity of the Earth system to different forcings and to assess the rate and magnitude of current climate change relative to natural variability.

Numerous interglacial climate simulations have been performed in previous studies using Earth system models of intermediate complexity (e.g., Kubatzki et al., 2000; Crucifix and Loutre, 2002; Loutre and Berger, 2003; Yin and Berger, 2012, 2015). While the present and the last interglacial have also been extensively investigated with fully coupled atmosphere-ocean general circulation models (e.g., Braconnot et al., 2007; Lunt et al., 2013), earlier interglacial periods have received much less attention by climate modellers. Coupled general circulation model (CGCM) studies of earlier interglacial climates have recently been performed for Marine Isotope Stage (MIS) 11 (Milker et al., 2013; Kleinen et al., 2014) and MIS 13 (Muri et al., 2013). Using the CGCM CCSM3 (Community Climate System Model version 3), Herold et al. (2012) presented a set of interglacial climate simulations comprising the interglaciations of MIS 1, 5, 9, 11 and 19. Their study, however, focussed on peak interglacial forcing (i.e. Northern Hemisphere summer occurring at perihelion) and intercomparison of interglacials (i.e. interglacial diversity) only. In

particular, they found that, compared to the other interglacials, MIS 11 exhibits the closest resemblance to the present interglacial, especially during boreal summer.

Here, we present a different and complementary CGCM (CCSM3) study which takes intra-interglacial climate variability into account by simulating two or more time slices for each interglacial stage of MIS 1, 5, 11, 13, and 15. For the interglacial of MIS 5 (Last Interglacial, MIS 5e; ca. 130-115 kyr ago), proxy data suggest a peak global mean temperature of about 1° C higher than during the pre-industrial period (e.g., Otto-Bliesner et al., 2013; Dutton et al., 2015). The maximum global mean sea-level has been estimated to 6-9 m above the present-day level (Kopp et al., 2009; Dutton and Lambeck, 2012; Dutton et al., 2015). The interglacial of MIS 11 was unusually long, about 30,000 years (ca. 425-395 kyr ago). Global average temperatures of MIS 11 are highly uncertain, but a peak global mean temperature of up to 2° C relative to pre-industrial cannot be ruled out (Lang and Wolff, 2011; Dutton et al., 2015). Maximum global mean sea-level may have been 6-13 m higher than today (Raymo and Mitrovica, 2012; Dutton et al., 2015). Interglacials before MIS 11 (early Brunhes interglacials), like MIS 13 and 15, are generally characterized by lower global mean temperatures, larger continental ice-sheets, lower global sea level and lower atmospheric greenhouse gas (GHG) concentrations relative to the more recent interglacials (e.g., Yin and Berger, 2010; Lang and Wolff, 2011; Dutton et al., 2015).

The goal of this study is to disentangle the effects of obliquity, precession and GHG on global surface climate. Our selection of interglacial time slices takes into account different aspects of inter- and intra-interglacial variability and associated astronomical forcing. As such, our approach differs from and complements previous model studies that focussed on peak interglacial forcing and intercomparison of interglacials (Yin and Berger, 2012; Herold et al., 2012). The selection of the time slices is described in detail in Section 2.3.

In contrast to previously performed climate model experiments with idealized astronomical forcing, in which obliquity and precession have usually been set to extreme values (e.g., Tuenter et al., 2003; Mantsis et al., 2011, 2014; Erb et al., 2013; Bosmans et al., 2015), our analyzes are based on realistic astronomical configurations. We note that realistic and idealized forcing experiments are equally important and complementary. Idealized experiments provide important insight into the climate system's response to astronomical forcing. However, since this response may be non-linear, using extreme values of astronomical parameters in idealized experiments may hide important aspects of astronomical forcing. Obviously, realistically forced experiments have a stronger potential for model-data comparison.

Special focus is on the sensitivity of the West African and Indian monsoon systems to obliquity and precession forcing. In particular, the applicability of the global monsoon concept (Trenberth et al., 2000; Wang et al., 2014) will be tested for astronomical timescales.

3.3 Experimental setup

3.3.1 Model description

We use the fully coupled climate model CCSM3 with the atmosphere, ocean, sea-ice and land-surface components interactively connected by a flux coupler (Collins et al., 2006). We apply the low-resolution version of the model (Yeager et al., 2006) which enables us to simulate a large set of time slices. In this version, the resolution of the atmosphere is given by T31 spectral truncation (3.75° transform grid) with 26 layers, while the ocean model has a nominal horizontal resolution of 3° (as has the sea-ice component) with 25 levels in the vertical. The land model shares the same horizontal grid with the atmosphere and includes components for biogeophysics, biogeochemistry, the hydrological cycle as well as a Dynamic Global Vegetation Model (DGVM) based on the Lund-Potsdam-Jena (LPJ)-DGVM (Sitch et al., 2003; Levis et al., 2004a; Bonan and Levis, 2006). The DGVM predicts the distribution of 10 plant functional types (PFT) which are differentiated by physiological, morphological, phenological, bioclimatic, and fire-response attributes (Levis et al., 2004a). In order to improve the simulation of land-surface hydrology and hence the vegetation cover, new parameterizations for canopy interception and soil evaporation were implemented into the land component (Oleson et al., 2008; Handiani et al., 2013; Rachmayani et al., 2015). PFT population densities are restored annually, while the land and atmosphere models are integrated with a 30 minutes time step.

3.3.2 Setup of experiments

To serve as a reference climatic state, a standard pre-industrial (PI) control simulation was carried out following PMIP (Paleoclimate Modelling Intercomparison Project) guidelines with respect to the forcing (e.g., Braconnot et al., 2007). The PI boundary conditions include astronomical parameters of 1950 AD, atmospheric trace gas concentrations from the 18th century (Table 3.1) as well as pre-industrial distributions of atmospheric ozone, sulfate aerosols, and carbonaceous aerosols (Otto-Bliesner et al., 2006). The solar constant is set to 1365 W m^{-2}. The PI control run was integrated for 1000 years starting from modern initial conditions, except for the vegetation which starts from bare soil.

In total, 13 interglacial time slice experiments were carried out, all branching off from year 600 of the PI spin-up run and running for 400 years each. Note that the present study only focusses on the surface climate, for which this spin-up time should be sufficient, whereas the deep ocean usually needs more time to adjust to changes in forcing (Renssen et al., 2006b).

Boundary conditions for the selected time slices which are spanning the last 615 kyr comprise astronomical parameters (Berger, 1978) and GHG concentrations as given in Table 3.1, while other forcings (ice sheet configuration, ozone distribution, sulfate aerosols, carbonaceous aerosols, solar constant) were kept as in the PI control run. The mean of the last 100 simulation years of each experiment was used for analysis.

We note that a fixed calendar based on a 365-day year is used for all experiments (Joussaume and Braconnot, 1997; Chen et al., 2011). The greatest calender-biases are known to occur in boreal fall, whereas the effects in boreal summer and winter (the seasons discussed in the present study) are generally small (e.g., Timm et al., 2008).

3.3.3 Selection of interglacial time slices

For MIS 1, the mid-Holocene time slice of 6 ka using standard PMIP forcing (Braconnot et al., 2007) was complemented by an early-Holocene 9 ka simulation when Northern Hemisphere summer insolation was close to maximum (Fig. 3.1). Two time slices, 125 and 115 ka, were also chosen for the last interglacial (MIS 5e). Similar to 9 ka, the 125 ka time slice is also characterized by nearly peak interglacial forcing, although the MIS 5 insolation forcing is stronger due to a greater eccentricity of the Earth's orbit. Moreover, the global benthic δ^{18}O stack is at minimum around 125 ka (Lisiecki and Raymo, 2005). By contrast, boreal summer insolation is close to minimum at 115 ka, which marked the end of MIS 5e (Fig. 3.1). GHG concentrations for the MIS 5 time slices were taken as specified by PMIP-3 (Lunt et al., 2013).

For the unusually long interglacial of MIS 11 (e.g., Milker et al., 2013) three time slices were chosen, 394, 405, and 416 ka. The middle time slice (405 ka) coincides with the δ^{18}O minimum of MIS 11 (Lisiecki and Raymo, 2005; Milker et al., 2013). The time slices of 394 and 416 ka are characterized by almost identical precession and similar GHG concentrations (Table 3.1), but opposite extremes of obliquity (maximum at 416 ka, minimum at 394 ka; Fig. 3.1). This allows to study the quasi-isolated effect of obliquity forcing (Berger, 1978) during MIS 11 by directly comparing the results of these two time slices. As opposed to idealized simulations of obliquity forcing (e.g., Tuenter et al., 2003; Mantsis et al., 2011, 2014; Erb et al., 2013) our approach considers quasi-realistic climate states of the past using

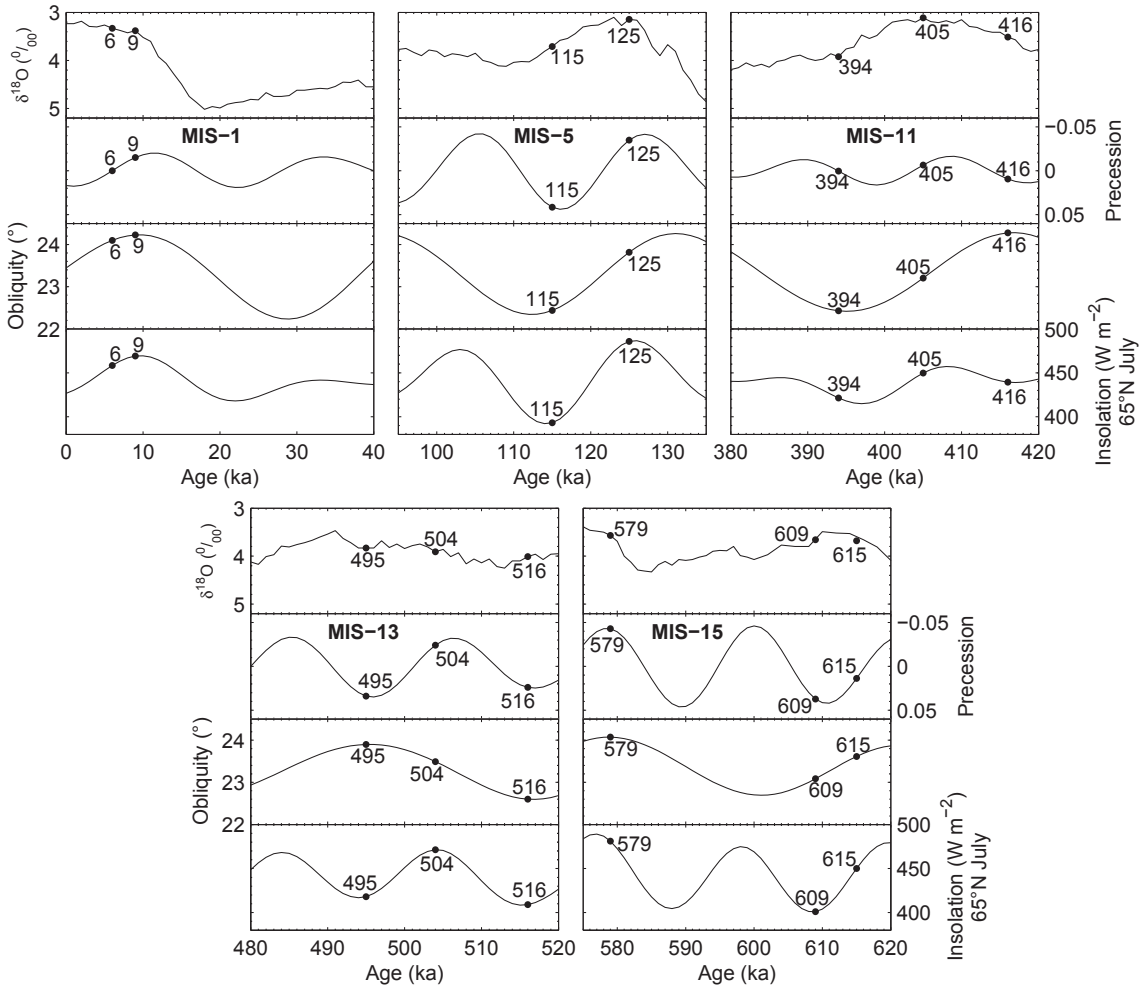

Figure 3.1 Benthic δ^{18}O stack (Lisiecki and Raymo, 2005), climatic precession, obliquity, and insolation at July, 65° N (Berger, 1978) for the different interglacials. The points mark the time slices simulated in this study.

Table 3.1 Atmospheric GHG concentrations used in the interglacial experiments.

Stage	Time slice (ka)	CO_2 (ppmv)	CH_4 (ppbv)	N_2O (ppbv)
MIS 1	0	280	760	270
	6	280	650	270
	9	265	680	260
MIS 5	115	273	472	251
	125	276	640	263
MIS 11	394	275	550	275
	405	280	660	285
	416	275	620	270
MIS 13	495	240	487	249
	504	240	525	278
	516	250	500	285
MIS 15	579	252	618	266
	609	259	583	274
	615	253	617	274

realistic forcings. In the same vein, time slices for MIS 13 have been chosen. Obliquity is at maximum at 495 ka and at minimum at 516 ka, while precession is almost identical. Unlike the 394 and 416 ka time slices of MIS 11 which are characterized by intermediate precession values, precession is at maximum at 495 and 516 ka, i.e. Northern Hemisphere summer occurs at aphelion causing weak insolation forcing (Yin et al., 2009). In addition, the 504 ka time slice was picked because of peak Northern Hemisphere summer insolation forcing, while obliquity has an intermediate value (Fig. 3.1).

Finally, two time slice experiments were performed for MIS 15 to assess the climatic response to minimum (579 ka) and maximum (609 ka) precession. Accordingly, Northern Hemisphere summer insolation is near maximum and minumum at 579 and 609 ka, respectively. In addition, a third MIS 15 experiment was carried out (615 ka) with insolation forcing in between the two others (Fig. 3.1). Moreover, the 615 ka time slice has a very special seasonal insolation pattern as we will see in the next section. All three MIS 15 time slices coincide with minimum $\delta^{18}O$ values (Lisiecki and Raymo, 2005).

Table 3.1 summarizes the GHG forcing of all experiments with values based on Lüthi et al. (2008), Loulergue et al. (2008), and Schilt et al. (2010) using the EPICA Dome C

timescale EDC3, except for the MIS 1 and MIS 5 experiments, where GHG values were chosen following the PMIP guidelines (see above). We note that due to the uneven distribution of methane sources and sinks over the latitudes, values of atmospheric CH_4 concentration derived from Antarctic ice cores present a lower estimate of global CH_4 concentration. We further note that some results from the MIS 1 (6 and 9 ka), MIS 5 (125 ka), and MIS 11 (394, 405, and 416 ka) experiments were previously published (Lunt et al., 2013; Milker et al., 2013; Kleinen et al., 2014; Rachmayani et al., 2015).

3.3.4 Insolation anomalies

Annual cycles of the latitudinal distribution of insolation at the top of the atmosphere (as anomalies relative to PI) are shown in Fig. 3.2 for each experiment. The insolation patterns can be divided into three groups which differ in their seasonal distribution of incoming energy. Group I is characterized by high Northern Hemisphere summer insolation as exhibited for the 6 and 9 ka (MIS 1), 125 ka (MIS 5), 405 and 416 ka (MIS 11), 504 ka (MIS 13), and 579 ka (MIS 15) time slices. In most (but not all, see below) cases this is due to an astronomical configuration with northern summer solstice at or close to perihelion. Group II comprises anomalies with low boreal summer insolation as shown for 115 ka (MIS 5), 495 and 516 ka (MIS 13), and 609 ka (MIS 15). In these cases, northern winter solstice is near perihelion. Group III is characterized by changes in the sign of the Northern Hemisphere insolation anomalies from spring to summer and consists of two dates (394 and 615 ka). At 394 (615 ka) the insolation anomaly spring-to-summer change is from positive (negative) to negative (positive). In these cases, spring equinox (394 ka) or fall equinox (615 ka) are close to perihelion.

3.4 Results

3.4.1 JJAS surface temperature anomalies

The response of boreal summer (June–July–August–September, JJAS) surface temperature to the combined effect of insolation and GHG in all individual climates (Fig. 3.3) shows warm conditions (relative to PI) over most parts of the continents in Group I (6, 9, 125, 405, 416, 504, and 579 ka) with the three warmest anomalies at 9, 125, and 579 ka. The warm surface conditions can largely be explained by the immediate effect of high summer insolation and a reduction of the Northern Hemisphere sea-ice area by about 15-20% (not shown) relative to PI. The large thermal capacity of the ocean explains a larger temperature response over land than over the ocean (Herold et al., 2012; Nikolova et al., 2013). Simulated

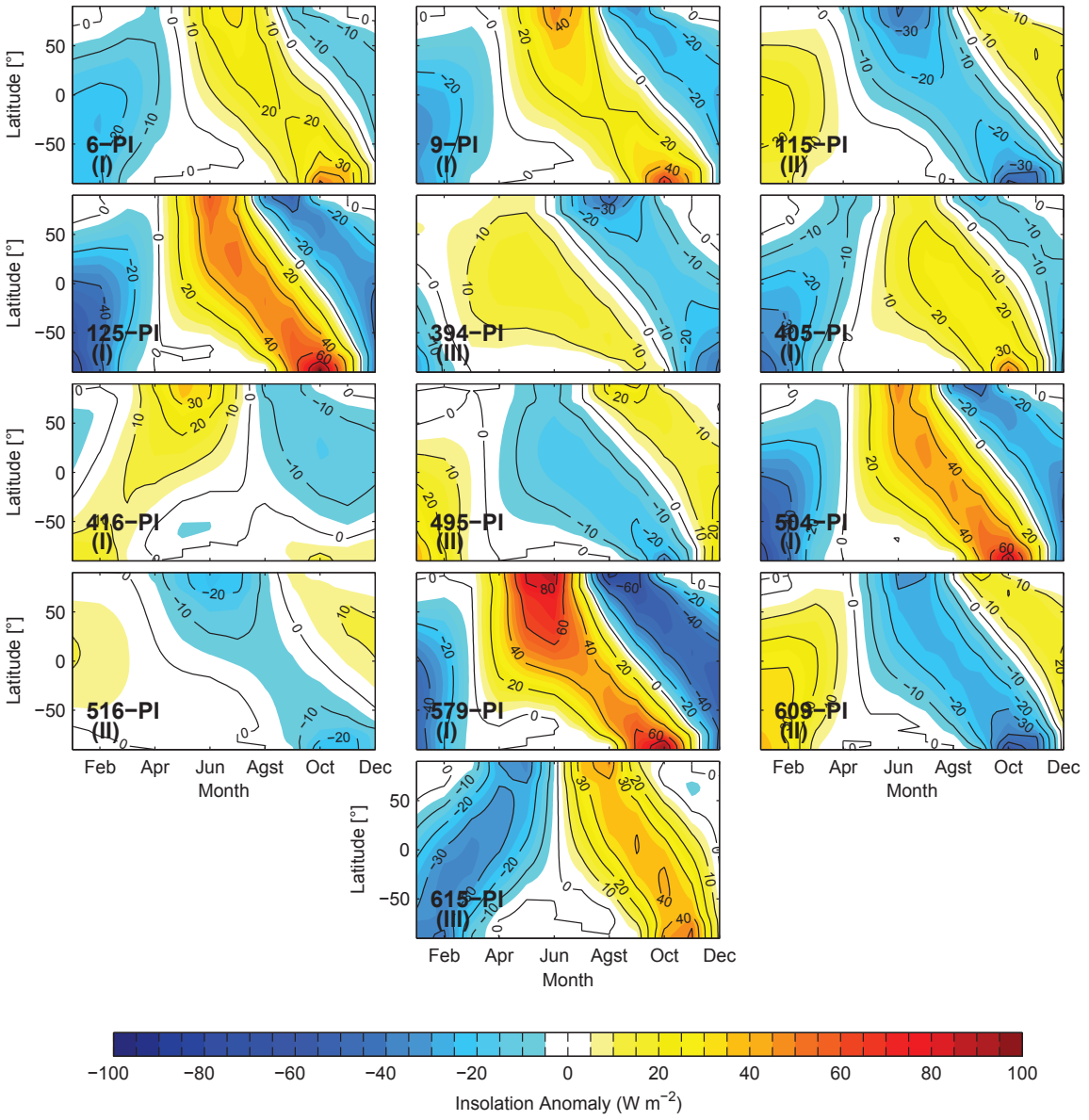

Figure 3.2 Insolation anomalies (relative to PI) for the time slices simulated in this study. Patterns of insolation anomaly are classified into Groups I, II, and III (see text). The calculation assumes a fixed present-day calendar with vernal equinox at 21 March.

cooling over North Africa (10-25° N) and India in the Group I experiments is caused by enhanced monsoonal rainfall in these regions, which is associated with increased cloud cover, i.e. reduced shortwave fluxes, and enhanced land surface evapotranspiration, i.e. greater latent cooling (e.g., Braconnot et al., 2002, 2004; Zheng and Braconnot, 2013). Cooling in some parts of the Southern Ocean in most Group I experiments is likely attributable to an austral summer remnant effect of local insolation (see below) as in Yin and Berger (2012). The 416 ka time slice, however, differs from the other Group I members by anomalously cold conditions over the Southern Hemisphere continents. Again, this behaviour can be explained by the immediate effect of the insolation, which shows negative anomalies in the Southern Hemisphere during the JJAS season (Fig. 3.2). As such, the 416 ka time slice must be considered a special case in Group I. While high Northern Hemisphere summer insolation is related to low precession in most Group I members, positive anomalies of Northern Hemisphere summer insolation at 416 ka are attributable to a maximum in obliquity (Fig. 3.1), yielding the Northern-versus-Southern Hemisphere insolation contrast.

In contrast to Group I, Group II climates exhibit anomalously cold JJAS surface temperatures globally with the three coldest anomalies at 115, 516, and 609 ka. Again, the temperature response can largely be explained by the direct response to insolation forcing, amplified in high latitudes by an increase of the sea-ice cover (about 5% in the Arctic compared to PI). Due to a particular combination of high precession and eccentricity with low obliquity the insolation forcing and surface temperature response is strongest for the 115 ka time slice. Group II warming in the North African and Indian monsoon regions is associated with increased aridity and reduced cloudiness.

Group III climates (394 and 615 ka) show rather complex temperature anomaly patterns, especially in the tropics. In the 394 ka time slice, however, northern continental regions show a distinct cooling, whereas continental regions exhibit an overall warming in the Southern Hemisphere (except for Antarctica). To a large extent, the 394 ka time slice shows a reversed JJAS temperature anomaly pattern compared to the 416 ka simulation over the continental regions, except for Antarctica.

3.4.2 DJF surface temperature anomalies

Boreal winter (December–January–February, DJF) surface temperature anomalies are presented in Fig. 3.4. Generally low DJF insolation in Group I time slices (Fig. 3.2) results in anomalously cold surface conditions over most of the globe, particularly strong in the 579 ka (MIS 15) time slice. However, anomalously warm conditions in the Arctic stand in contrast to the global DJF cooling at 6, 9, 125, 405, and 416 ka. The Arctic warming is

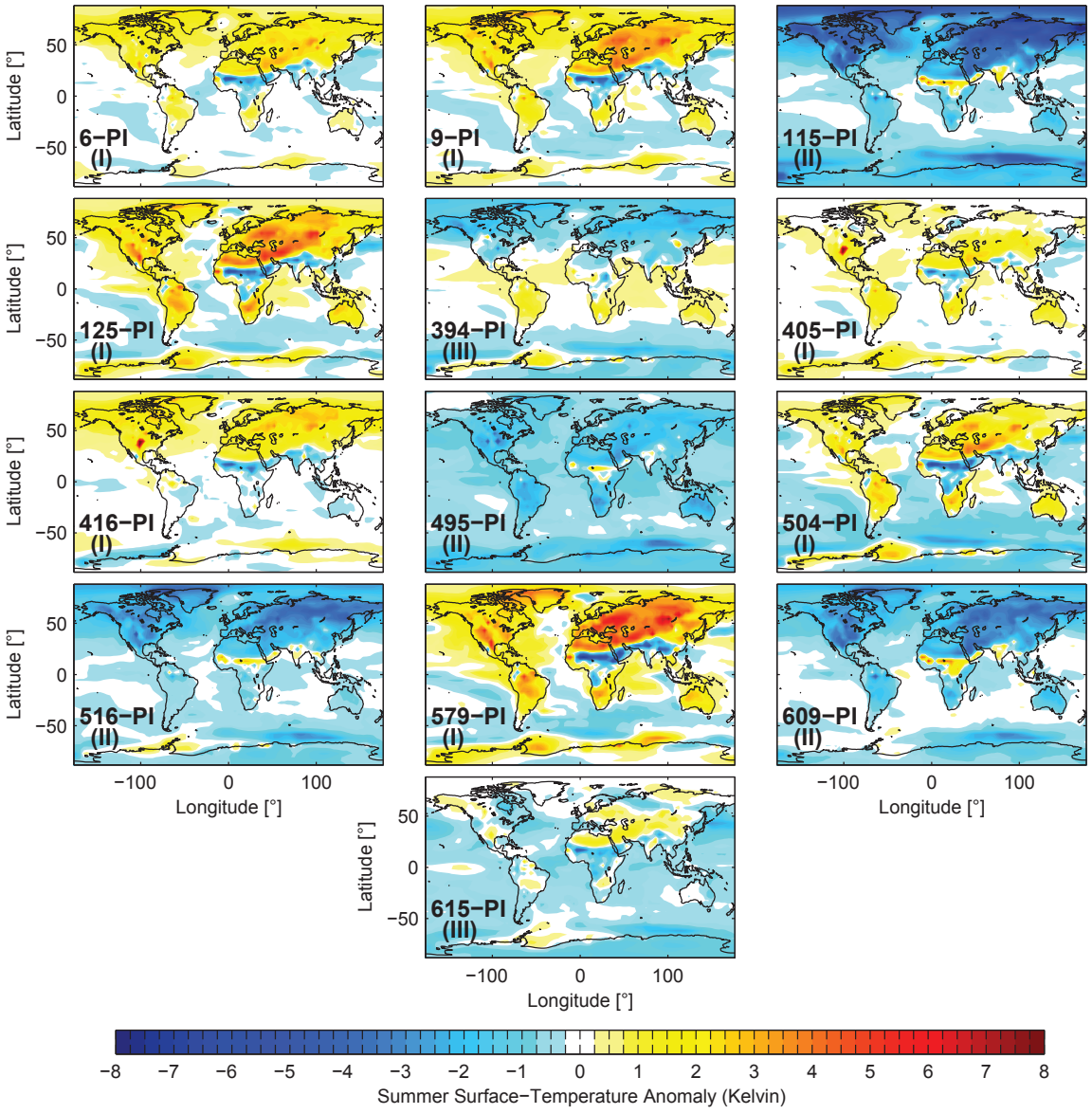

Figure 3.3 Boreal summer surface temperature anomalies (relative to PI) for the different interglacial time slices. Classification into Groups I, II, and III (see text) is indicated.

due to the remnant effect of the polar summer insolation through ocean–sea ice feedbacks (Fischer and Jungclaus, 2010; Herold et al., 2012; Yin and Berger, 2012; Kleinen et al., 2014). Anomalous shortwave radiation during the Arctic summer leads to enhanced melting of sea ice and warming of the upper polar ocean. The additional heat received by the upper ocean delays the formation of winter sea ice, reduces its thickness and finally leads to a warming of the winter surface atmospheric layer by enhanced ocean heat release (Yin and Berger, 2012). Arctic winter warming is not present in the 504 ka (MIS 13) and 579 ka (MIS 15) time slices in Group I, where the summer remnant effect in the Arctic is probably masked by a global cooling that is induced by low GHG concentrations typical for early Brunhes (MIS 13 and before) interglacials.

To a large extent, DJF surface temperature anomaly patterns are reversed in Group II with warming over most continental regions. Moreover, the summer remnant effect reverses to a substantial cooling in the Arctic region. Temperature anomaly patterns in Group III are, again, rather complex. Interestingly, most Northern Hemisphere continental regions remain relatively cold during boreal winter (as in summer) in the 394 ka simulation. Relatively low GHG concentrations, especially CH_4, contribute to the year-round extratropical cooling in this time slice.

3.4.3 JJAS precipitation anomalies

Boreal summer precipitation shown in Fig. 3.5 exhibits intensified rainfall in the monsoon belt from North Africa to India, via the Arabian Peninsula, in all Group I simulations in response to high summer insolation (Prell and Kutzbach, 1987; de Noblet et al., 1996; Tuenter et al., 2003; Braconnot et al., 2007). By contrast, the same monsoon regions experience anomalously dry conditions in the Group II (low boreal summer insolation) experiments. The most interesting results regarding the tropical rainfall response to astronomical forcing appear in Group III, where the monsoonal precipitation anomalies show opposite signs in North Africa (Sahel region) and India.

Table 3.2 summarizes the summer monsoonal rainfall amounts for the North African (20° W-30° E; 10-25° N) and Indian (70-100° E; 10-30° N) regions. Highest rainfall in the North African monsoon region occurs in the 9, 125, 504, and 579 ka time slice runs (all Group I) associated with low precession values (Fig. 3.1). Driest conditions occur at 115, 495, 516, and 609 ka (all Group II) associated with precession maxima (Fig. 3.1). As in North Africa, Group I (Group II) experiments exhibit anomalously wet (dry) monsoon conditions in India.

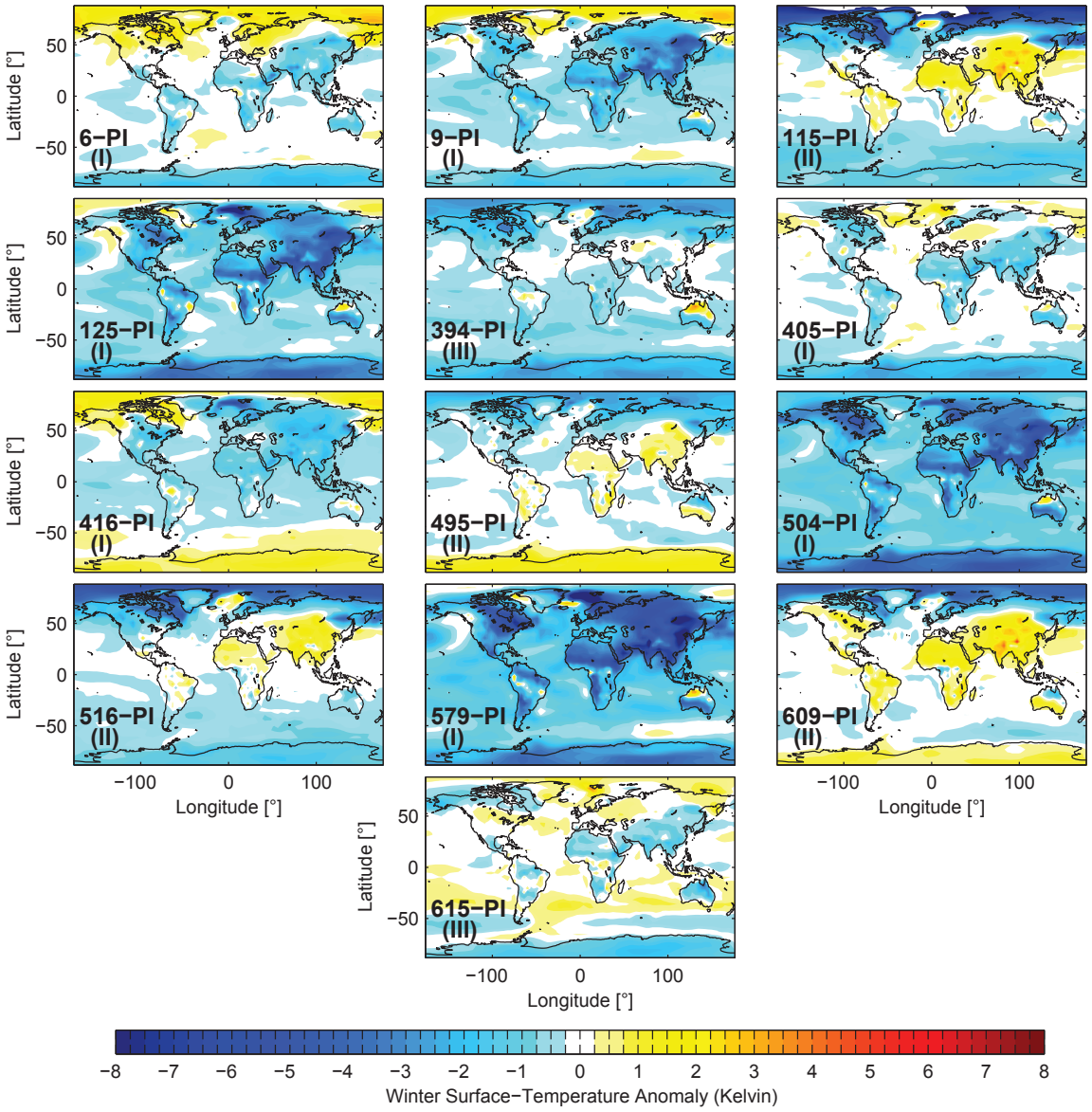

Figure 3.4 As in Fig. 3.3, but for boreal winter.

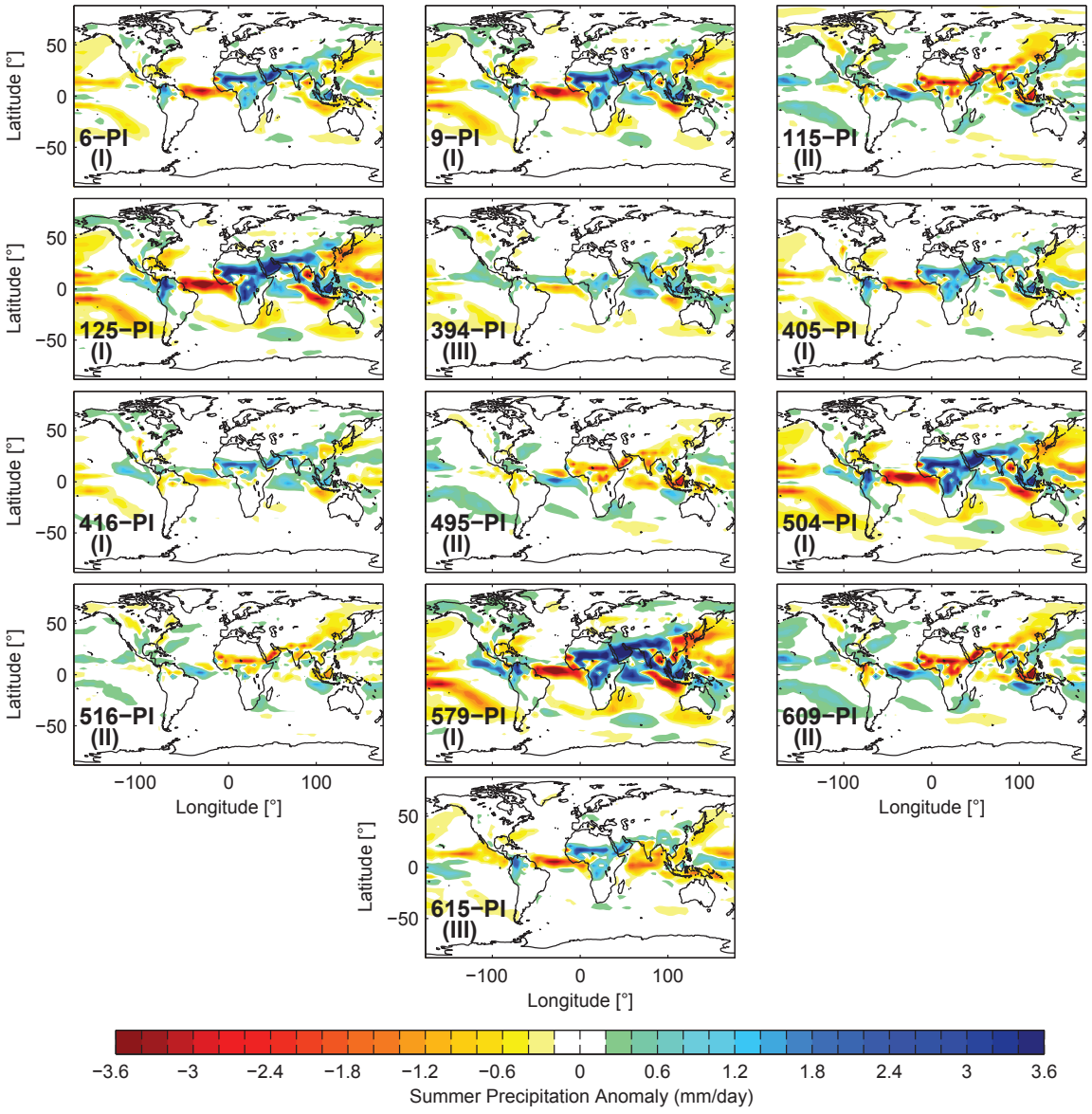

Figure 3.5 As in Fig. 3.3, but for boreal summer precipitation.

Table 3.2 Summer (JJAS) precipitation over North Africa (20° W-30° E and 10-25° N) and over India (70-100° E and 10-30° N) along with anomalies relative to PI. Absolute precipitation values are given with standard error (2σ) based on 100 simulation years of each experiment.

Stage	Time slice (ka)	North Africa (mm day $^{-1}$)	North Africa Anomaly (mm day $^{-1}$)	India (mm day $^{-1}$)	India Anomaly (mm day $^{-1}$)
MIS 1	0	2.44±0.04		6.59±0.12	
	6	3.41±0.04	0.97	6.91±0.10	0.32
	9	3.71±0.04	1.27	7.36±0.08	0.77
MIS 5	115	1.59±0.02	-0.85	5.90±0.15	-0.69
	125	3.79±0.04	1.35	7.26±0.07	0.67
MIS 11	394	2.37±0.04	-0.07	6.92±0.12	0.33
	405	3.20±0.04	0.76	6.95±0.11	0.36
	416	3.06±0.04	0.62	7.13±0.12	0.54
MIS 13	495	1.91±0.04	-0.53	6.11±0.13	-0.48
	504	3.72±0.04	1.28	7.11±0.08	0.52
	516	1.88±0.04	-0.56	6.22±0.13	-0.37
MIS 15	579	3.77±0.04	1.33	7.72±0.07	1.13
	609	1.49±0.02	-0.95	6.10±0.13	-0.49
	615	3.21±0.04	0.77	6.27±0.13	-0.32

3.4.4 Net Primary Production (NPP) anomalies

Vegetation responds to changes in surface temperature and precipitation and, in certain regions, may feedback to the climate (cf. Rachmayani et al., 2015). Figure 3.6 shows the simulated changes in NPP, reflecting increase/decrease and expansion/retreat of vegetation covers, relative to PI. In high Arctic latitudes, NPP increases in the Group I simulations, except for 405 ka where temperature changes are probably too small to substantially affect the vegetation. By contrast, Arctic NPP declines in the Group II experiments, albeit only in the easternmost part of Siberia in the 495 ka experiment. A substantial decline of Arctic NPP is also simulated for 394 ka (Group III). In the tropical regions, vegetation changes are mostly governed by precipitation. Consequently, enhanced rainfall results in increased NPP over North Africa, the Arabian Peninsula and India in all Group I experiments. In North Africa increased NPP is associated with a northward shift of the Sahel–Sahara boundary. The largest shifts are simulated for 125 and 579 ka in accordance with maximum North African rainfall anomalies. In these experiments, a complete greening of the Arabian Desert is simulated. Opposite NPP anomalies in the tropical monsoon regions are simulated in the Group

II experiments. In Group III, NPP increases result from anomalously high rainfall in North Africa (615 ka) or India (394 ka).

3.4.5 Climatic effects of obliquity variations during MIS 11 and MIS 13

The MIS 11 time slices 394 and 416 ka show opposite obliquity extremes (at similar precession), as do the MIS 13 time slices 495 and 516 ka (Fig. 3.1). Insolation differences between the high obliquity (416, 495 ka) and low obliquity (394, 516 ka) cases (i.e. 416 minus 394 and 495 minus 516 ka) are displayed in Fig. 3.7. The effect of high obliquity is to strengthen the seasonal insolation cycle. At low latitudes, the effect of obliquity on insolation is small.

For the maximum obliquity time slices (416 and 495 ka) relatively high boreal summer insolation directly translates into positive surface temperature anomalies over Northern Hemisphere continents, except for the low latitudes where reduced local insolation (especially in the MIS 13 case) and higher monsoon rainfall (especially in the MIS 11 case, see below) lead to surface cooling (Fig. 3.8a,b). By contrast, receiving anomalously low insolation during austral winter, Southern Hemisphere continents exhibit anomalously cold surface temperatures. For the 416–394 ka case, however, the Antarctic continent and the Southern Ocean show large-scale warming during the JJAS season, which can be attributed to a south polar summer remnant effect as the austral summer insolation anomaly is extremely high in this experiment (Fig. 3.7a). Higher GHG concentrations at 416 compared to 394 ka may add to this warming. Owing to a smaller south polar summer insolation anomaly (Fig. 3.7) the summer remnant effect is smaller in the 495–516 ka case and even surpassed by anomalously low GHG forcing in the 495 ka time slice, leading to negative austral winter temperature anomalies in the Southern Ocean and Antarctica (Fig. 3.7b).

During boreal winter, Northern Hemisphere continents show large-scale cooling in response to high obliquity (and hence relatively low insolation), except for the Arctic realm where the summer remnant effect results in substantial positive surface temperature anomalies (Fig. 3.8c and d). During the same season (DJF) anomalously high insolation causes surface warming in the Southern Hemisphere in response to high obliquity. As a general pattern in the annual mean, maximum-minus-minimum obliquity forcing causes anomalous surface warming at high latitudes and surface cooling at low latitudes caused by seasonal and annual insolation anomalies in combination with climate feedbacks like the polar summer remnant effect and monsoon rainfall.

Despite the weak insolation signal at low latitudes, substantial obliquity-induced changes in tropical precipitation are simulated (Fig. 3.8e and f). The strongest signal is

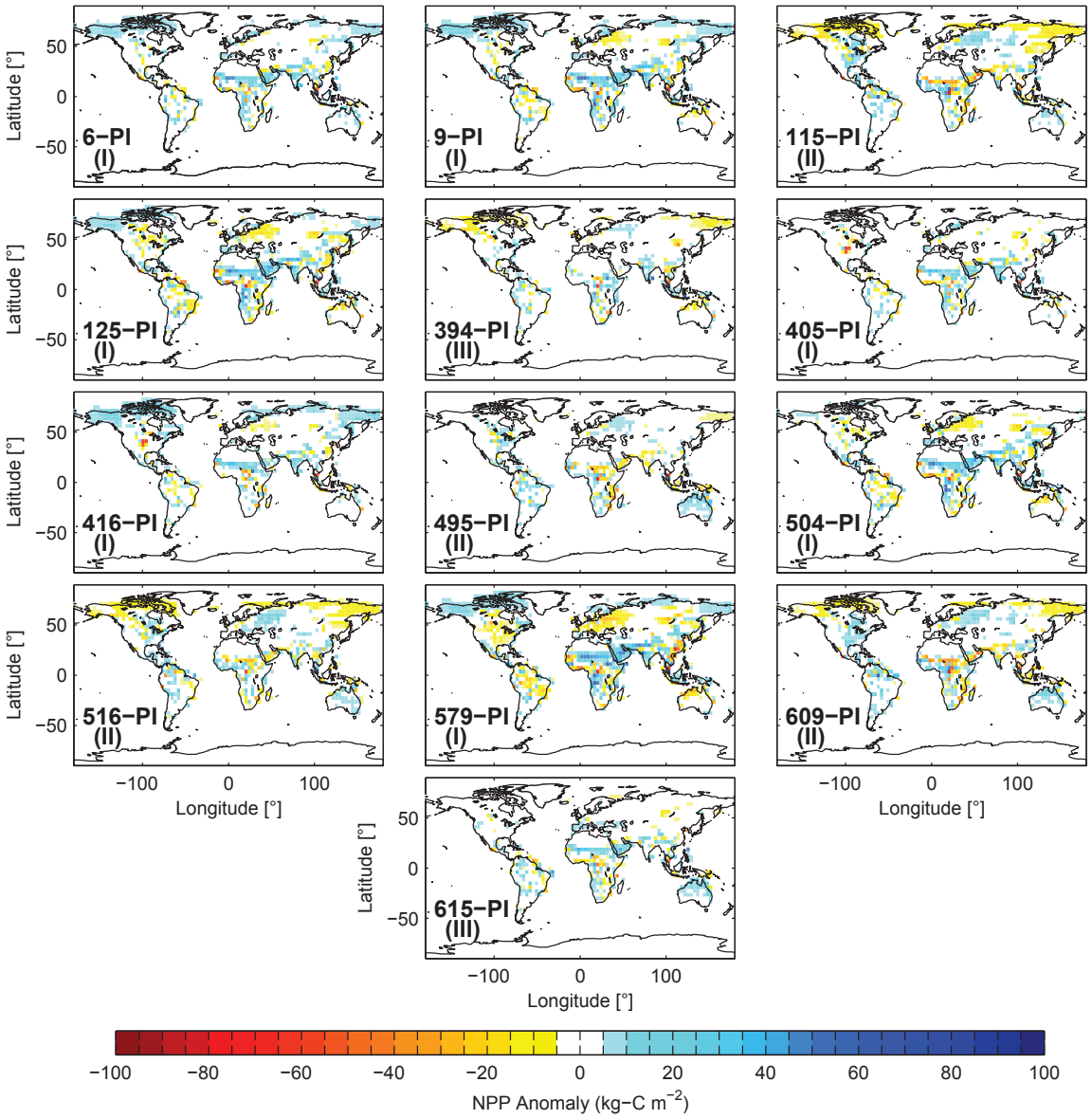

Figure 3.6 As in Fig. 3.3, but for annual net primary production.

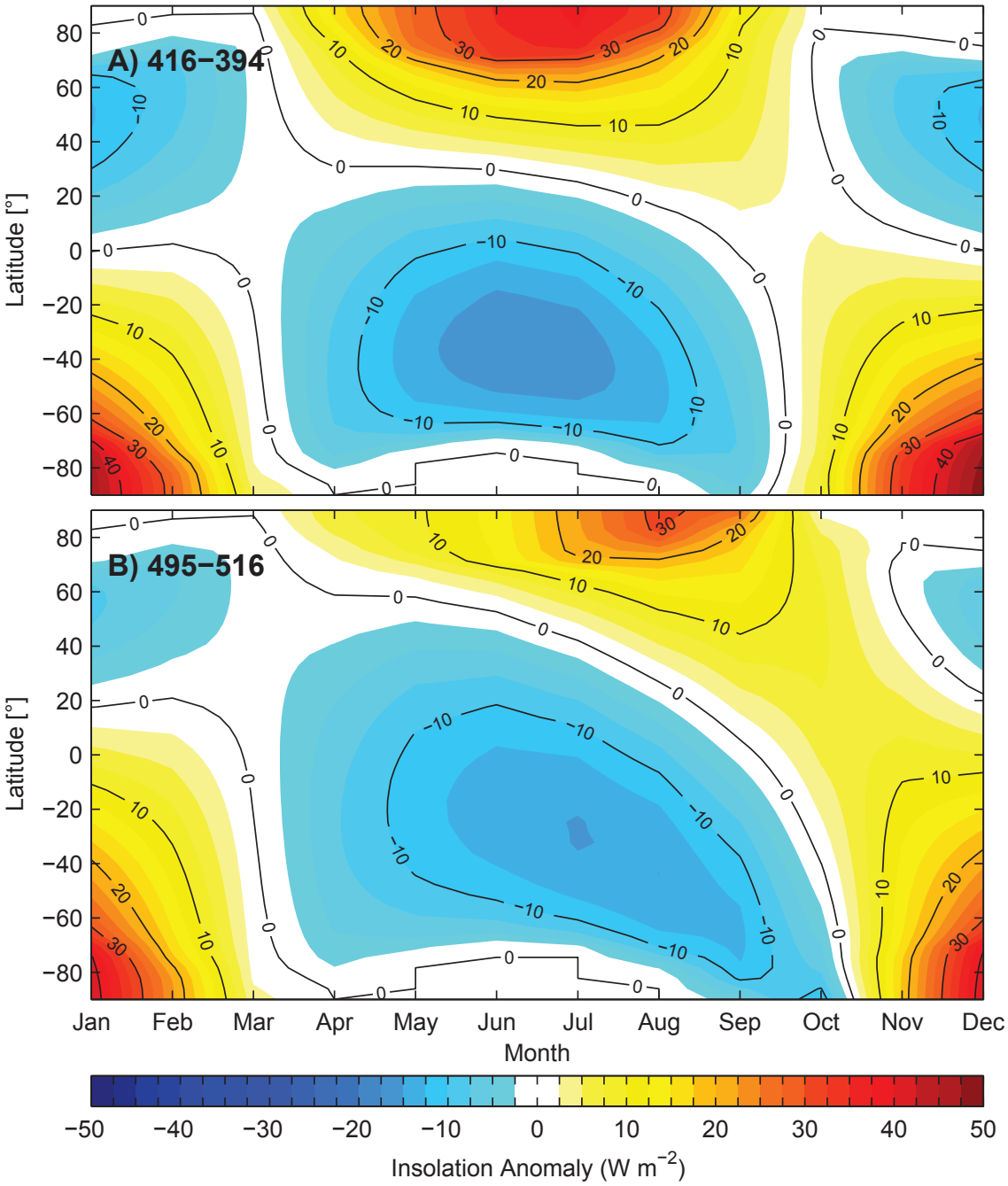

Figure 3.7 Differences in the seasonal and latitudinal distribution of insolation for (A) 416-394 ka, (B) 495-516 ka.

found in the North African monsoon region in the MIS 11 experiments, where greater JJAS precipitation occurs during maximum obliquity at 416 ka than during the obliquity minimum at 394 ka. A positive Sahel rainfall anomaly is also found in the MIS 13 experiments (495–516 ka), but much weaker than in the MIS 11 case (416–394 ka). We suppose that the obliquity-induced increase in North African monsoonal rainfall is counteracted by the high precession at 495 ka that tends to weaken the monsoon. Considering the spatiotemporal insolation patterns (Fig. 3.7) the Northern Hemisphere tropical summer insolation anomaly is less negative and the meridional summer insolation gradient anomalies are generally greater in the 416–394 ka case compared to the 495–516 ka case. Both features of the insolation anomaly favor a strong North African monsoon (see Discussion).

3.4.6 Evaluating the climatic effects of astronomical and GHG forcings through correlation maps

In order to evaluate the climatic effects of obliquity, precession and GHG concentrations, linear correlations between the individual forcing parameters and climatic fields (surface temperature, precipitation) were calculated from the 14 time slice experiments (13 interglacial time slices plus PI). To this end, each climate variable (temperature, precipitation) was averaged over the last 100 years of each experiment. Linear correlation coefficients between a climatological variable and a forcing parameter (obliquity, precession, GHG radiative forcing) were calculated at each grid point. Significance of correlations was tested by a two-sided Student's t test with 95% confidence level. Total radiative forcing from CO_2, CH_4, and N_2O in each experiment was calculated based on a simplified expression given in Table 3.3 (IPCC , 2001).

Table 3.3 Simplified expressions for calculation of radiative forcing due to CO_2, CH_4, N_2O. C is CO_2 in ppmv, M is CH_4 in ppbv, N is N_2O in ppbv. The subscript 0 denotes the unperturbed GHG concentration of PI.

Trace gas	Simplified expression Radiative forcing, ΔF (Wm^{-2})	Constants
CO_2	$\Delta F=\alpha(g(C)-g(C_0))$ where $g(C)= \ln(1+1.2C+0.005C^2 +1.4\times10^{-6}C^3)$	α=3.35
CH_4	$\Delta F=\alpha(\sqrt{M}-\sqrt{M_0})-(f(M,N_0)-f(M_0,N_0))$	α=0.036
N_2O	$\Delta F=\alpha(\sqrt{N}-\sqrt{N_0})-(f(M_0,N)-f(M_0,N_0))$ where $f(M,N)=0.47\ \ln[1+2.01\times10^{-5}(MN)^{0.75}+5.31\times10^{-15}M(MN)^{1.52}]$	α=0.12

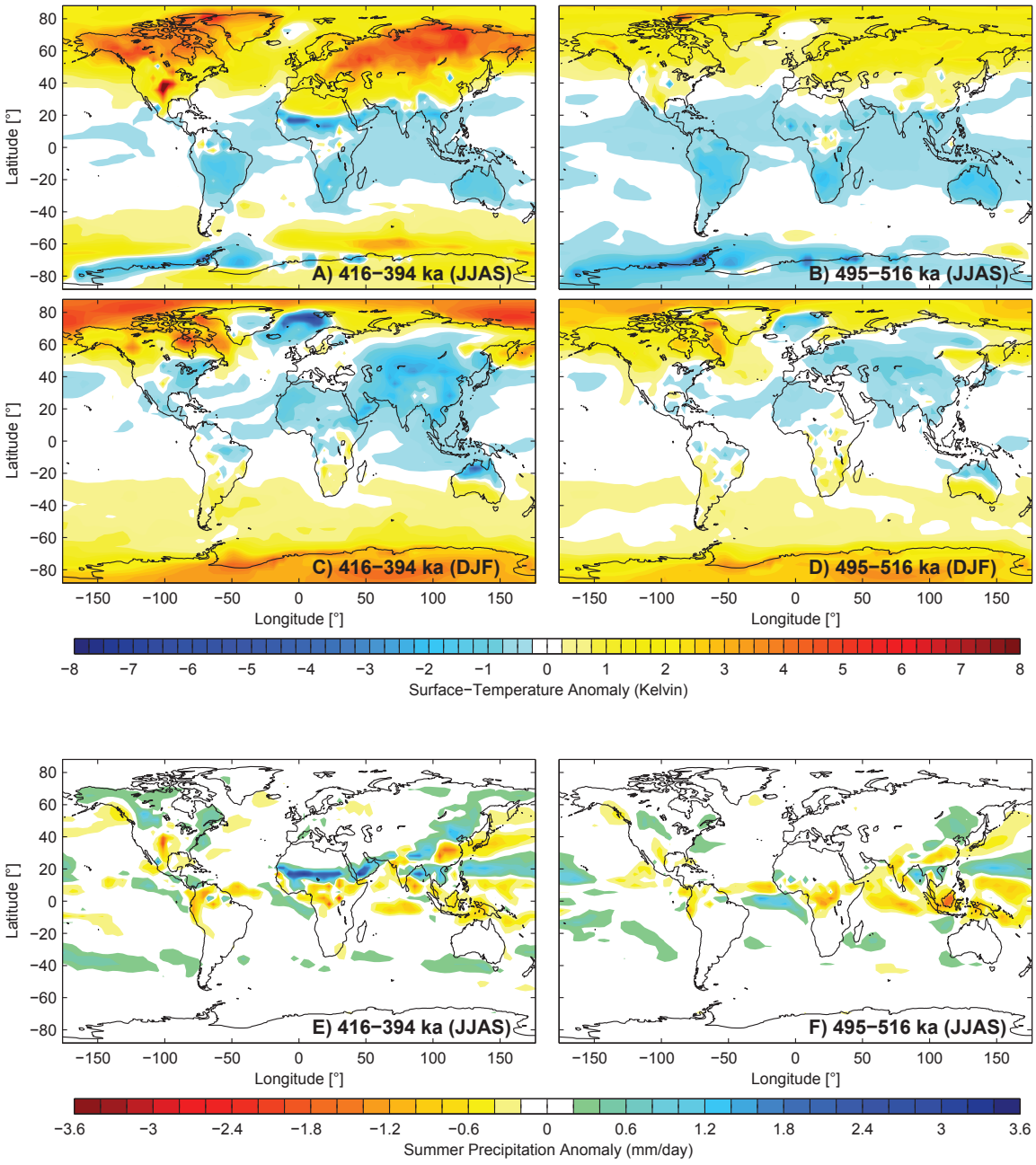

Figure 3.8 Differences in seasonal surface temperature (A)-(D) and boreal summer precipitation (E)-(F) for 416-394 ka (left) and 495-516 ka (right).

Figure 3.9 shows the corresponding correlation maps for annual mean, boreal summer, and boreal winter surface temperature. As expected, GHG forcing is positively correlated with surface temperature over most regions of the globe (Fig. 3.9a), which is particularly pronounced in the annual mean. For the seasonal correlation maps (boreal summer and winter) the correlation coefficients are smaller because of the dominant impact of obliquity and precession forcing.

As already described in the previous subsection, the general surface temperature pattern of high obliquity forcing is warming at high latitudes and cooling at low latitudes (Fig. 3.9b). High precession (northern solstice near aphelion) leads to boreal summer surface cooling over most extratropical regions (Fig. 3.9c). However, surface warming occurs in some tropical regions as a response to weaker monsoons. During boreal winter, anomalously high insolation causes anomalous surface warming except in the Arctic (due to the summer remnant effect) and northern Australia (due to a stronger regional monsoon).

Correlation maps for annual mean, boreal summer, and boreal winter precipitation are shown in Fig. 3.10. GHG radiative forcing exhibits no clear response in precipitation except for the high latitudes where the hydrologic cycle accelerates with higher GHG concentrations (Fig. 3.10a). Since the GHG variations are relatively small, the effects of astronomical forcing on the monsoons are way larger than the effects of GHG variations during the interglacials. Arctic precipitation is also amplified by high obliquity during summer (Fig. 3.10b). Obliquity also strengthens the monsoonal rainfall in North Africa (Sahel region), whereas no effect of obliquity can be detected for the Australian monsoon. The sensitivity of other monsoon systems to obliquity changes is also weak or even absent in our experiments. The most robust response of the hydrologic cycle is found for precession (Fig. 3.10c). In particular, high precession reduces summer rainfall in the monsoon belt from North Africa to India as well as in the Arctic realm. East Asian rainfall shows a somewhat heterogeneous pattern and is, in general, only weakly coupled with the Indian and African monsoons. This finding is consistent with a recent model intercomparison study by Dallmeyer et al. (2015). During boreal winter, the hydrologic cycle strengthens in the Arctic and Antarctic regions, while Southern Hemisphere monsoon systems amplify resulting in enhanced rainfall over South America, southern Africa, and northern Australia in response to high precession. We note that these monsoonal rainfall changes go along with distinct surface temperature signals in the annual mean (Fig. 3.9c).

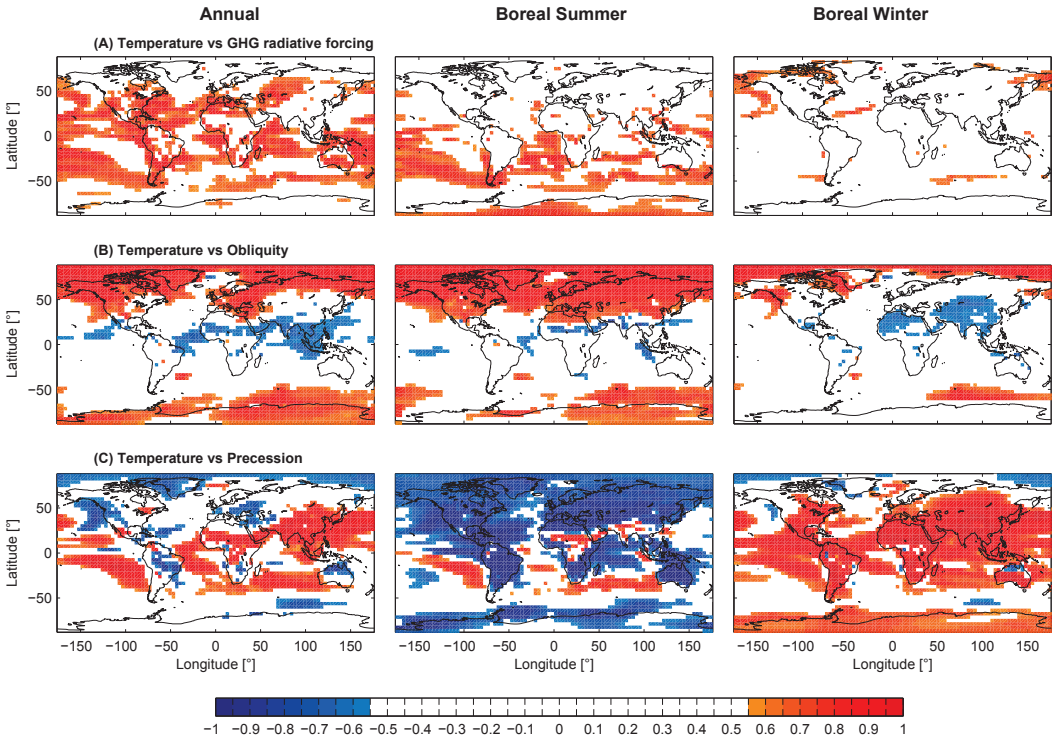

Figure 3.9 Linear correlation maps between surface temperature and GHG radiative forcing (A), obliquity (B), and climatic precession (C) as calculated from the entire set of experiments. Summer refers to JJAS, winter to DJF. Only significant values are shown according to a two-sided Student's t-test at 95% confidence level.

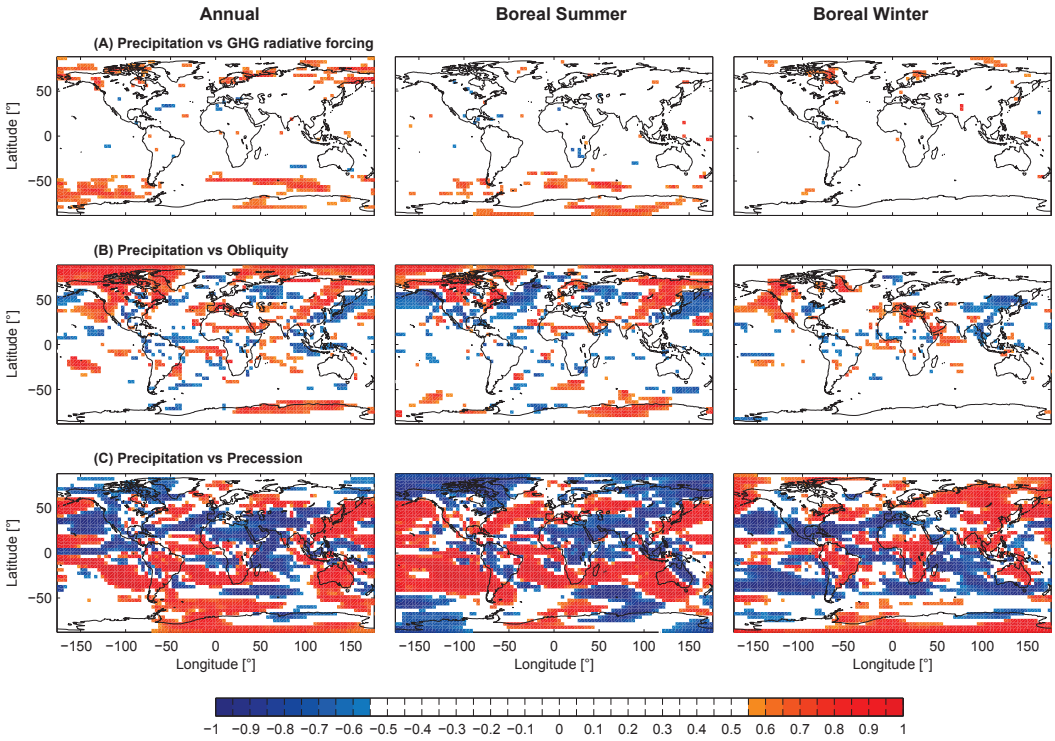

Figure 3.10 As in Fig. 3.9, but for precipitation.

3.5 Discussion

While most time slices presented in this study were simulated for the first time using a comprehensive CGCM, the 6, 115 and 125 ka time slices have been studied extensively in previous model studies. In general, the CCSM3 results are in line with these previous studies in terms of large-scale temperature and precipitation patterns. Warm boreal summer conditions (relative to PI) over most parts of the continents and the Arctic are a general feature in paleoclimatic simulations of the mid-Holocene (6 ka), while the North African and South Asian monsoon regions are anomalously cold due to enhanced rainfall (Braconnot et al., 2007). Though evidenced by proxy records (e.g., McClure, 1976; Hoelzmann et al., 1998; Fleitmann et al., 2003), several models fail to simulate wetter mid-Holocene conditions over the Arabian Peninsula (cf. `https://pmip3.lsce.ipsl.fr/database/maps/`), while CCSM3 simulates not only enhanced rainfall but also greening of the Arabian Desert. The 125 ka surface temperature pattern shows similar features than the 6 ka pattern, but much more pronounced due to the larger eccentricity and hence stronger precessional forcing. However, compared to other simulations of the last interglaciation, our CCSM3 simulation produces a relatively cold MIS 5e surface climate as shown by Lunt et al. (2013). At 115 ka, surface temperature anomalies show the opposite sign with dramatic cooling over the Arctic and the northern continental regions providing ideal conditions for glacial inception (e.g., Khodri et al., 2005; Kaspar and Cubasch , 2007; Jochum et al., 2012). A retreat of the vegetation at high northern latitudes tends to amplify the insolation-induced cooling (cf. Gallimore and Kutzbach, 1996; Meissner et al., 2003).

A recent simulation of the MIS 13 time slice at 506 ka using the CGCM HadCM3 (Muri et al., 2013) can be compared to our 504 ka time slice using CCSM3. Global patterns of surface temperature anomalies (relative to PI) are remarkably similar in the two different simulations with warm anomalies over all continents (except for the North African and South Asian monsoon regions) in boreal summer and worldwide cold anomalies during boreal winter. Moreover, both simulations show anomalously high boreal summer precipitation over northern South America, North and central Africa as well as the South Asian monsoon region.

Although our CCSM3 results show general agreement with other model studies, the validation of model results with data is usually not straightforward. The reader is referred to previous work where our CCSM3 simulation of 125 ka (Lunt et al., 2013) as well as the MIS 11 simulations have been extensively compared to proxy data (Milker et al., 2013; Kleinen et al., 2014). Taken together, these and other studies (e.g., Lohmann et al., 2013) indicate that CGCMs tend to produce generally smaller interglacial temperature anomalies

than suggested by the proxy records. So far, the reason for these discrepancies is unsolved (cf. Liu et al., 2014), but Hessler et al. (2014) pointed out that uncertainties associated with sea surface temperature reconstructions are generally larger than interglacial temperature anomalies. Thus, currently available surface temperature proxy data cannot serve as a target for benchmarking interglacial model simulations.

Two time slices of MIS 11 (394 vs. 416 ka) and two time slices of MIS 13 (495 vs. 516 ka) allow the investigation of (almost pure) obliquity effects on global climate, although the GHG and precession are not exactly the same between the time slices. As such, the results from these simulations can be compared to previously performed idealized model experiments in which obliquity has been changed from maximum to minimum values (Tuenter et al., 2003; Mantsis et al., 2011; Erb et al., 2013; Bosmans et al., 2015). The common results of those idealized and our experiments can be summarized as follows. High-versus-low obliquity climates are characterized by strong warming over the Northern Hemisphere extratropics and slight cooling in the tropics during boreal summer. During boreal winter, a moderate cooling over large portions of the Northern Hemisphere continents and a strong warming at high southern latitudes is found. The obliquity-induced Northern Hemisphere summer warming appears to be of particular interest for the MIS 13 climate evolution. At 495 ka, precession is at maximum, but the global benthic δ^{18}O stack by Lisiecki and Raymo (2005) does not show the expected increase towards heavier values which would indicate colder conditions and Northern Hemisphere cryosphere expansion (Fig. 3.1). In fact, despite high precession, the 495 ka simulation exhibits the warmest Northern Hemisphere summer temperatures from all Group II experiments (Fig. 3.3), which can be attributed to concomitant high obliquity. We therefore hypothesize that the Northern Hemisphere summer climate at 495 ka was not cold enough for ice sheets to grow and global ocean δ^{18}O to increase. We note, however, that the benthic δ^{18}O stack is subject to age model uncertainties of a few thousand years.

Moreover, our CCSM3 results as well as the studies by Tuenter et al. (2003) and Bosmans et al. (2015) suggest a significant effect of obliquity on West African monsoon rainfall despite the weak insolation signal at low latitudes. Bosmans et al. (2015) have shown that obliquity-induced changes in moisture transport towards North Africa result from changes in the meridional insolation gradient (Davis and Brewer, 2009). However, the impact of obliquity on the monsoon also depends on precession. In the 495–516 ka experiment the obliquity-effect on the West African monsoon is minor, as both time slices (495 and 516 ka) are characterized by precession maxima leading to extremely weak monsoonal circulation and rainfall in both cases. The existence of a 41 kyr cyclicity (in addition

to astronomical-related 100 and 19–23 kyr cycles) in reconstructions of North African aridity during the Quaternary has usually been attributed to obliquity-forced Northern Hemisphere cryosphere effects on the monsoon climate (e.g., Bloemendal and deMenocal, 1989; deMenocal et al., 1993; Tiedemann et al., 1994; deMenocal, 1995; Kroon et al., 1998). Our model results along with the studies by Tuenter et al. (2003) and Bosmans et al. (2015) complement this picture, showing that the direct insolation-gradient forcing associated with obliquity can contribute to West African monsoon changes without involving high-latitude remote climate forcing associated with Northern Hemisphere ice sheets.

According to the CCSM3 results, the Indian monsoon is less sensitive to direct obliquity (insolation gradient) forcing than the West African monsoon. This finding is consistent with proxy records from the Arabian Sea that show substantial 41 kyr (obliquity) periodicity only after the onset of Quaternary glacial cycles when waxing and waning of northern ice sheets could have worked as an agent for the transfer of obliquity forcing to the Indian monsoon region (Bloemendal and deMenocal, 1989). In general, it is found that the two monsoon systems do not always vary in concert. This is particularly evident in the Group III experiments (394 and 615 ka) where the precipitation anomalies over North Africa and India have opposite signs (Table 3.2). Considering the annual insolation maps of the 394 and 615 kyr experiments (Fig. 3.2), West African monsoon rainfall turns out to be most sensitive to changes in summer insolation, whereas spring/early summer insolation is more important for monsoon rainfall over India. Similar results have been found by Braconnot et al. (2008). It has been argued that the reason is a resonant response of the Indian monsoon to the insolation forcing when maximum insolation anomalies occur near the summer solstice and a resonant response of the African monsoon – which has its rainfall maximum one month later in the annual cycle than the Indian monsoon – when the maximum insolation change is delayed after the summer solstice. The different responses to specific forcings and the sometimes out-of-phase behaviour of the African and Indian monsoon systems challenge the global monsoon concept – according to which all regional monsoon systems are part of one seasonally varying global-scale atmospheric overturning circulation in the tropics (Trenberth et al., 2000; Wang et al., 2014) – at astronomical timescales.

Another important result of our study is associated with obliquity forcing of high-latitude precipitation anomalies. As obliquity increases, high latitudes become warmer and the gradient in solar heating between high and low latitudes decreases, while precipitation over high-latitude continental regions increases (Fig. 3.10b). This result clearly contradicts the "gradient hypothesis" by Raymo and Nisancioglu (2003) according to which low obliq-

uity would favour polar ice-sheet growth through enhanced delivery of moisture owing to an increased meridional solar heating gradient.

Since CO_2 and other GHG variations are relatively small during the interglacials, the effects of astronomical forcing on the monsoons are substantially larger. Hence, GHG forcing shows a clear response in precipitation only for the high latitudes where the hydrologic cycle accelerates with higher GHG concentrations. In the monsoon regions, interglacial rainfall variations are almost entirely controlled by astronomical forcing.

The use of a modern ice-sheet configuration for all interglacial time slice experiments, however, must be considered a limitation of the present study. Future studies should include the effects of changing ice sheets and associated meltwater fluxes in shaping interglacial climates. Large Northern Hemisphere ice sheets might have played an important role for regional and global climates especially during early Brunhes interglacials (MIS 13 and before) as suggested by, e.g., Yin et al. (2008) and Muri et al. (2013). But also during late Brunhes interglacial stages, like the Holocene, model studies suggest an influence of changing land ice on the interglacial climate evolution (Renssen et al., 2009; Marzin et al., 2013). The tremendous uncertainties regarding ice-sheet reconstructions beyond the present interglacial could be taken into account by performing sensitivity experiments.

3.6 Conclusions

Using CCSM3-DGVM, 13 interglacial time slice experiments were carried out to study global climate variability between and within Quaternary interglacials. The selection of interglacial time slices was based on different aspects of inter- and intra-interglacial variability and associated astronomical forcing. As such, our approach is complementary to both idealized astronomical forcing experiments (e.g., Tuenter et al., 2003; Mantsis et al., 2011, 2014; Erb et al., 2013; Bosmans et al., 2015) and climate simulations that focussed on peak interglacial forcing (Herold et al., 2012; Yin and Berger, 2012).

In this study, the different roles of obliquity, precession and GHG forcing on surface temperature and precipitation patterns have been disentangled. In most regions seasonal surface temperature anomalies could largely be explained by local insolation anomalies induced by the astronomical forcing. Climate feedbacks modify the surface temperature response in specific regions, particularly in the monsoon domains and the polar oceans. GHG forcing may also play a role for seasonal temperature anomalies, especially in high latitudes and the early Brunhes interglacials MIS 13 and 15 when GHG concentrations were much lower than during the later interglacials.

A significant role of obliquity in forcing the West African monsoon was found, whereas the Indian monsoon – as well as the other regional monsoon systems – appear to be less sensitive (or not sensitive at all) to obliquity changes during interglacials. Despite this important role of obliquity in West African monsoon variability, the response to precession is still stronger. Different responses to specific forcings and the obvious anti-phase behaviour of the African and Indian monsoon systems in the 394 and 615 ka experiments, where the North African rainfall anomaly has opposite sign compared to the Indian anomaly, clearly point to the fact that the two regional monsoon systems do not always vary in concert and challenge the global monsoon concept at the astronomical timescale.

As a general pattern in the annual mean, maximum-minus-minimum obliquity forcing causes anomalous surface warming at high latitudes and surface cooling at low latitudes caused by seasonal and annual insolation anomalies in combination with climate feedbacks like the polar summer remnant effect and monsoon rainfall. High obliquity may also explain relatively warm Northern Hemisphere high-latitude summer temperatures despite maximum precession around 495 ka (MIS 13). We hypothesize that this obliquity-induced high-latitude warming may have prevented a glacial inception at that time. Moreover, our results suggest high-latitude precipitation increase with increasing obliquity, contradicting the "gradient hypothesis" by (Raymo and Nisancioglu, 2003) according to which low obliquity would favour polar ice-sheet growth through enhanced delivery of moisture owing to an increased meridional solar heating gradient.

Future studies should include the effects of changing ice sheets and associated meltwater fluxes in shaping interglacial climates. With increasing computer power long-term transient simulations of interglacial climates will become more common. So far, transient CGCM simulations have been performed for the present (e.g., Lorenz and Lohmann , 2004; Varma et al., 2012; Liu et al., 2014) and the last interglacial (e.g., Bakker et al., 2013; Govin et al., 2014). More transient simulations of earlier interglacials, ideally with coupled interactive ice-sheet models, will help to develop a significantly deeper understanding of interglacial climate dynamics.

3.7 Acknowledgements

The study was funded by the Deutsche Forschungsgemeinschaft (DFG) through the Priority Programme INTERDYNAMIC. CCSM3 simulations were performed on the SGI Altix supercomputer of the Norddeutscher Verbund für Hoch- und Höchstleistungsrechnen (HLRN). The article processing charges for this open-access publication were covered by

the University of Bremen. We would like to thank the two anonymous reviewers for their constructive suggestions and helpful comments.

4 North African vegetation-precipitation feedback in early and mid-Holocene climate simulations with CCSM3-DGVM

R. Rachmayani, M. Prange, M. Schulz

4.1 Abstract

The present study analyses the sign, strength and working mechanism of the vegetation-precipitation feedback over North Africa in middle (6 ka) and early Holocene (9 ka) simulations using the comprehensive coupled climate-vegetation model CCSM3-DGVM. The coupled model simulates enhanced summer rainfall and a northward migration of the West African monsoon trough along with an expansion of the vegetation cover for the early and middle Holocene compared to pre-industrial. It is shown that dynamic vegetation enhances the orbitally triggered summer precipitation anomaly by approximately 20 % in the Sahara/Sahel region (10–25° N,20° W–30° E) in both the early and mid-Holocene experiments compared to their fixed-vegetation counterparts. The primary vegetation-rainfall feedback identified here operates through surface latent heat flux anomalies by canopy evaporation and transpiration and their effect on the mid-tropospheric African Easterly Jet, whereas the effects of vegetation changes on surface albedo and local water recycling play a negligible role. Even though CCSM3-DGVM simulates a positive vegetation-precipitation feedback in the North African region, this feedback is not strong enough to produce multiple equilibrium climate-ecosystem states on a regional scale.

4.2 Introduction

At present, North Africa is much drier than during the early and middle Holocene when a higher orbitally induced summer insolation triggered more humid and “greener” con-

ditions in the Sahel and Saharan regions (e.g. Kutzbach and Street-Perrot, 1985; Street-Perrott and Perrott, 1993; Jolly et al., 1998; Kohfeld and Harrison, 2000; Prentice et al., 2000; Bartlein et al., 2011; Collins et al., 2013). Following pioneering modelling work by Kutzbach (1981), numerous numerical climate model experiments have been conducted in order to examine climate sensitivity to Holocene orbital forcing in low latitudes, where insolation variations are strongly dominated by the precessional cycle. Even though these model studies have abundantly documented that an intensification and northward shift of the North African summer monsoon was induced by the enhanced seasonal insolation cycle during the early-to-mid Holocene, rainfall anomalies simulated by the models turned out to be significantly smaller than those reconstructed from lake level or pollen data (e.g. Jolly et al., 1998; Kohfeld and Harrison, 2000). Therefore, various positive feedbacks have been postulated to be crucial in shaping the early-to-mid Holocene North African humid period, involving vegetation and soil (e.g. Kutzbach et al., 1996; Claussen et al., 1999; Doherty et al., 2000; Levis et al., 2004a; Hales et al., 2006), sea-surface temperatures (e.g. Kutzbach and Liu, 1997; Zhao et al., 2005; Zhao and Harrison, 2012), and surface-water coverage by lakes and wetlands (e.g. Coe and Bonan, 1997; Krinner et al., 2012). Over time, the notion of a positive vegetation-precipitation feedback has received the greatest attention in the literature (see Claussen, 2009).

Based on early work by Otterman (1974) and Charney (1975), it has been suggested that the effect of an expanded North African vegetation cover on surface albedo would be key in amplifying the early-to-mid Holocene West African monsoonal rainfall (e.g. Claussen and Gayler, 1997; Brovkin et al., 1998; Hales et al., 2006). Provided that the positive vegetation-climate feedback is sufficiently strong to introduce non-linear dynamics into the climate-ecosystem, multiple equilibria of the atmosphere-vegetation state may exist (Claussen, 1994, 1997, 1998; Wang and Eltahir, 2000; Zheng and Neelin, 2000; Renssen et al., 2003; Patricola and Cook, 2008; Bathiany et al., 2012); a humid state with expanded vegetation cover and an arid state with expanded desert. In general circulation and conceptual model studies bi-stability was found only under late Holocene (i.e. after ~ 6 ka BP) orbital forcing, while only one stable state, the "green (West-) Sahara", was found for early-to-mid Holocene forcing (Claussen and Gayler, 1997; Brovkin et al., 1998; Claussen et al., 1998).

A transition from the humid state to the arid state by a catastrophic bifurcation or "unstable collapse" (Liu et al., 2006, 2007) was suggested to have been abruptly terminating the African humid period around 5.5 ka (deMenocal et al., 2000). Both the abruptness of the North African climate transition (Renssen et al., 2006a; Kröpelin et al., 2008; Lézine

et al., 2011; Claussen et al., 2013; Francus et al., 2013) as well as the existence of a strong positive vegetation-rainfall feedback in North Africa (Levis et al., 2004a; Liu et al., 2006, 2007; Kröpelin et al., 2008; Notaro et al., 2008; Wang et al., 2008; Liu et al., 2010) have later been challenged. In a model intercomparison study, two out of three coupled climate-vegetation models that participated in PMIP2 (Paleoclimate Modelling Intercomparison Project, Phase II) suggested a negative vegetation-precipitation feedback over North Africa in simulations of the middle Holocene, though no systematic feedback analysis has been performed (Braconnot et al., 2007). In particular, the Charney feedback operating via surface albedo changes has been called into question (Levis et al., 2004a; Notaro et al., 2008; Patricola and Cook, 2008; Wang et al., 2008; Liu et al., 2010).

In the current study, we investigate the sign, strength and working mechanism of the vegetation-precipitation feedback over North Africa in mid (6 ka) and early Holocene (9 ka) simulations with the comprehensive fully coupled climate-vegetation model CCSM3-DGVM. In contrast to statistical (lagged autocovariance) approaches (e.g. Notaro et al., 2008; Wang et al., 2008) to assess the existence and sign of the biogeophysical feedback, we apply a straightforward experimental design to assess the climate-vegetation feedback in North Africa by switching on and off interactive dynamic vegetation in this specific coupled model. Moreover, the impact of vegetation initial conditions on mid-Holocene and modern (pre-industrial) climate-vegetation simulations and hence the existence of multiple equilibria in the North African climate-ecosystem is studied systematically.

4.3 Experimental Design

4.3.1 Model

The National Center for Atmospheric Research (NCAR) Community Climate System Model version 3 (CCSM3) is composed of four components representing atmosphere, ocean, land (including the Dynamic Global Vegetation Model; DGVM) and sea ice connected by a flux coupler (Collins et al., 2006). Here we use the low-resolution version of the model, in which the resolution of the atmosphere and land components is given by T31 (3.75° transform grid), while the ocean has a nominal horizontal resolution of 3° (Yeager et al., 2006). The atmospheric and oceanic grids have 26 and 25 levels in the vertical, respectively. New parameterizations for canopy interception and soil evaporation have been implemented into the land component in order to improve the simulation of the land hydrology and vegetation cover (Oleson et al., 2008) as in Handiani et al. (2013). CCSM3's dynamic vegetation model DGVM is based on the Lund-Potsdam-Jena (LPJ) model (Sitch

et al., 2003; Levis et al., 2004b; Bonan and Levis, 2006) and simulates the tempo-spatial distribution of 10 plant functional types (PFTs; 7 tree PFTs and 3 grass PFTs) which are differentiated by physiological, morphological, phenological, bioclimatic, and fire-response attributes (Levis et al., 2004b). The land and atmosphere components are integrated with a 30 min time step, while vegetation structure and PFT population densities are updated annually (Levis et al., 2004b).

4.3.2 Setup of Experiments

In order to disentangle the impact of dynamic vegetation on the early and mid-Holocene North African climate three sets of experiments were carried out. The first set (OAV) uses the fully coupled CCSM3-DGVM inluding dynamic ocean (O), atmosphere (A), and vegetation (V) components as described above. A pre-industrial (PI) control run of CCSM3-DGVM was performed following the PMIP2 protocol with respect to the forcing (Braconnot et al., 2007). The PI simulation was integrated for 1000 years upon initialization with present-day hydrographic data and bare soil. Branched off from year 600 of the PI run, a middle (6 ka) and an early Holocene (9 ka) climate simulation was performed, each integrated for 400 years. Table 4.1 summarizes radiative forcings used in the set of model runs. Since variations in greenhouse gas concentrations over the three time slices are minor, the major forcing comes from variations in the Earth's orbital parameters. The orbitally induced summer insolation anomaly is larger at 9 ka than at 6 ka (Berger, 1978). The experiments with dynamic vegetation are referred to as 0k(OAV), 6k(OAV), and 9k(OAV), respectively. To examine the role of DGVM initial conditions and the potential for bistable climate-vegetation states, two additional 400-year long CCSM3-DGVM simulations for PI and the mid-Holocene were carried out, which were also initialized from year 600 of 0k(OAV) except for the vegetation cover (PFT distribution), which was taken from the final state of the 9k(OAV) experiment. These simulations are denoted by 0k9k(OAV) and 6k9k(OAV), respectively.

In the second set of experiments (OAV_f) the global PFT distribution is fixed. Three experiments with PI, 6 ka, and 9 ka boundary conditions (Table 4.1) were integrated for 400 years (again branched off from year 600 of 0k(OAV)) using the fixed vegetation cover taken from the final state of experiment 0k(OAV). These experiments are denoted by 0k(OAV_f), 6k(OAV_f), and 9k(OAV_f). The third set of experiments (OA) is identical to the OAV_f set of experiments, except that the observation-based modern vegetation cover from the standard CCSM3 setup without DGVM was prescribed. These runs are referred to as experiments 0k(OA), 6k(OA), and 9k(OA).

Table 4.1 Summary of boundary conditions used in the experiments. Summer insolation refers to July, 21 at 20°N.

Experiments	CO_2 (ppmv)	CH_4 (ppbv)	N_2O (ppbv)	Summer insolation (W m^{-2})
0k (PI)	280	760	270	453
6k (mid-Holocene)	280	650	270	477
9k (early Holocene)	265	680	260	486

In all simulations, ozone and aerosol distributions were kept at pre-industrial levels (Otto-Bliesner et al., 2006), and a fixed solar constant of 1365 W m^{-2} was applied. Moreover, all experiments were run with modern ice-sheet configuration and global sea level. For model output analyses, averages of the last 100 simulation years from each experiment were used and are presented here. Since this study focusses on the West African summer monsoon system, the analysis of climatologic quantities is limited to the months of June through September (JJAS). Note that a fixed calendar based on 365 days per year with vernal equinox fixed to March 21 (the Day/Month values refer to the present calendar) is used for all experiments (Joussaume and Braconnot, 1997; Chen et al., 2011). However, this does not affect the comparison of the different experiments for identical time slices.

4.4 Results

The North African vegetation cover from the 0k(OAV) control run is shown in Fig. 4.1, where the 10 PFTs simulated by the model are combined into two groups (trees and grasses). North of 18° N the model simulates desert with almost no vegetation. Between 12° N and 18° N, a semi-arid belt dominated by C_4 grass vegetation is simulated. To the south, the simulated vegetation cover mostly consists of trees in central and western tropical Africa. Similar to earlier dynamic vegetation modelling studies (Bonan et al., 2003; Sitch et al., 2003; Oleson et al., 2008), CCSM3-DGVM produces too much forest cover south of the Sahel compared to satellite observations (DeFries et al., 1999, 2000; Lawrence and Chase, 2007). Applying mid-Holocene boundary conditions in experiment 6k(OAV) results in a northward expansion of the North African vegetation cover (Fig. 4.2a), which is even more pronounced in experiment 9k(OAV) under early Holocene boundary conditions (Fig. 4.2b). The vegetation increase also captures the Arabian Peninsula and is mostly due to expansion of grasses.

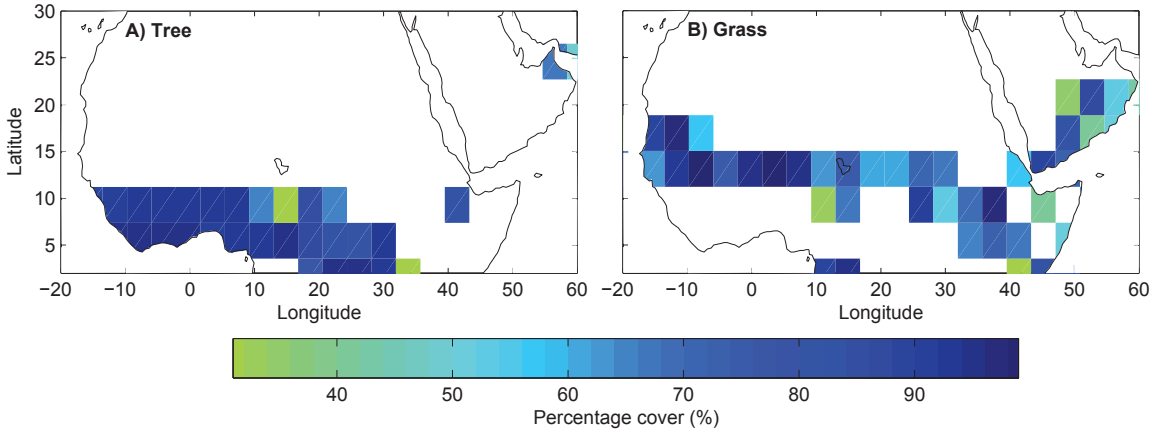

Figure 4.1 Pre-industrial vegetation cover over North Africa simulated by CCSM3-DGVM. (A) Percentage coverage of tree PFTs, (B) same for grasses.

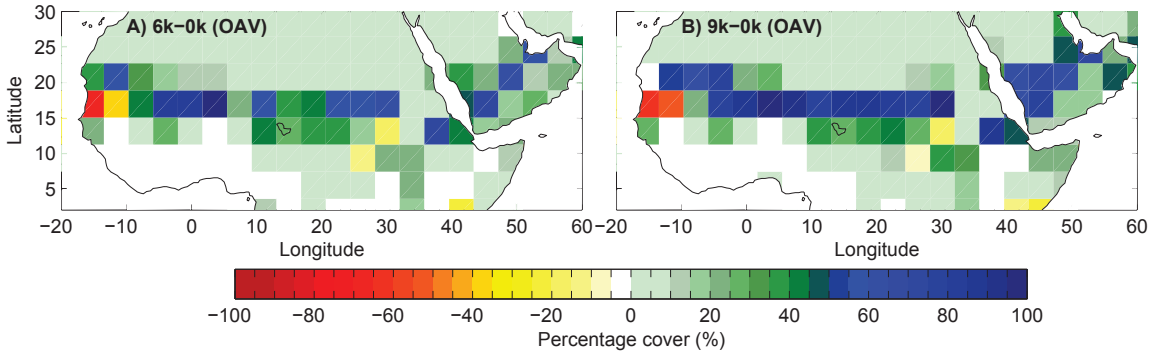

Figure 4.2 Change in total (i.e. all PFTs) percent vegetation cover for (A) the mid-Holocene (6 ka) and (B) the early Holocene (9 ka) experiment relative to pre-industrial (PI).

Figure 4.3a and b support that the greening of North Africa in the early-to-mid Holocene is associated with enhanced summer (JJAS) precipitation over this region, with largest rainfall anomalies between 10° N and 25° N. Averaged over this latitude range and between 20° W–30° E, the mid-Holocene summer rainfall anomaly amounts to 0.97 mm day^{-1} and lies well within the range of previously published 6 ka climate model simulations (Braconnot et al., 2007). For the 9k(OAV) simulation, the summer rainfall anomaly over this region is even larger (1.27 mm day^{-1}) due to stronger orbital forcing (Table 4.1). Southwesterly surface wind anomalies between 15° N and 25° N indicate that the enhanced precipitation is associated with a northward expansion of monsoon winds and a northward displacement of the monsoon trough (Fig. 4.3a and b).

In the simulations with fixed modern vegetation biogeography (OAV$_f$) the middle and early Holocene rainfall anomalies over North Africa are significantly smaller compared to their OAV counterparts (Fig. 4.3c–f). Averaged over the Sahara/Sahel region 10–25° N, 20° W–30° E the summer anomalies amount to only 0.80 and 1.04 mm day^{-1} for experiments 6k(OAV$_f$) and 9k(OAV$_f$), respectively, relative to PI. This result indicates a positive vegetation-precipitation feedback in North Africa. For both the 6 and 9 ka time slices, the implementation of the interactively coupled DGVM into the climate model enhances the orbitally triggered rainfall anomaly over the Sahara/Sahel region by approximately 20 %. Experiments without dynamic vegetation using the standard CCSM3 setup (OA) yield early and mid-Holocene rainfall anomalies over North Africa that are similar to the OAV$_f$ results (Table 4.2).

The wetter North African conditions in the early and mid-Holocene OAV experiments compared to their OAV$_f$ counterparts are not associated with a wholesale strengthening of the southwesterly monsoon flow that transports moist air from the equatorial Atlantic to the continent (Fig. 4.3e and f). However, spatially coherent anomalies in the wind system over North Africa can be found at mid-tropospheric levels related to changes in the African Easterly Jet (AEJ), which constitutes the equatorward portion of the Saharan High and dominates the sub-Saharan summer circulation over West Africa between 10° N and 20° N with maximum wind speeds between 700 hPa and 500 hPa. In all early and mid-Holocene simulations, a westerly wind anomaly develops at mid-levels south of $\approx$ 15° N, representing a weakening of the AEJ's southern flank relative to the modern situation, while the jet slightly intensifies at its northern flank (Fig. 4.4a–d), implying a northward shift of the jet. This behaviour is more pronounced in the OAV simulations than in their non-DGVM counterparts OAV$_f$ (Fig. 4.4e and f).

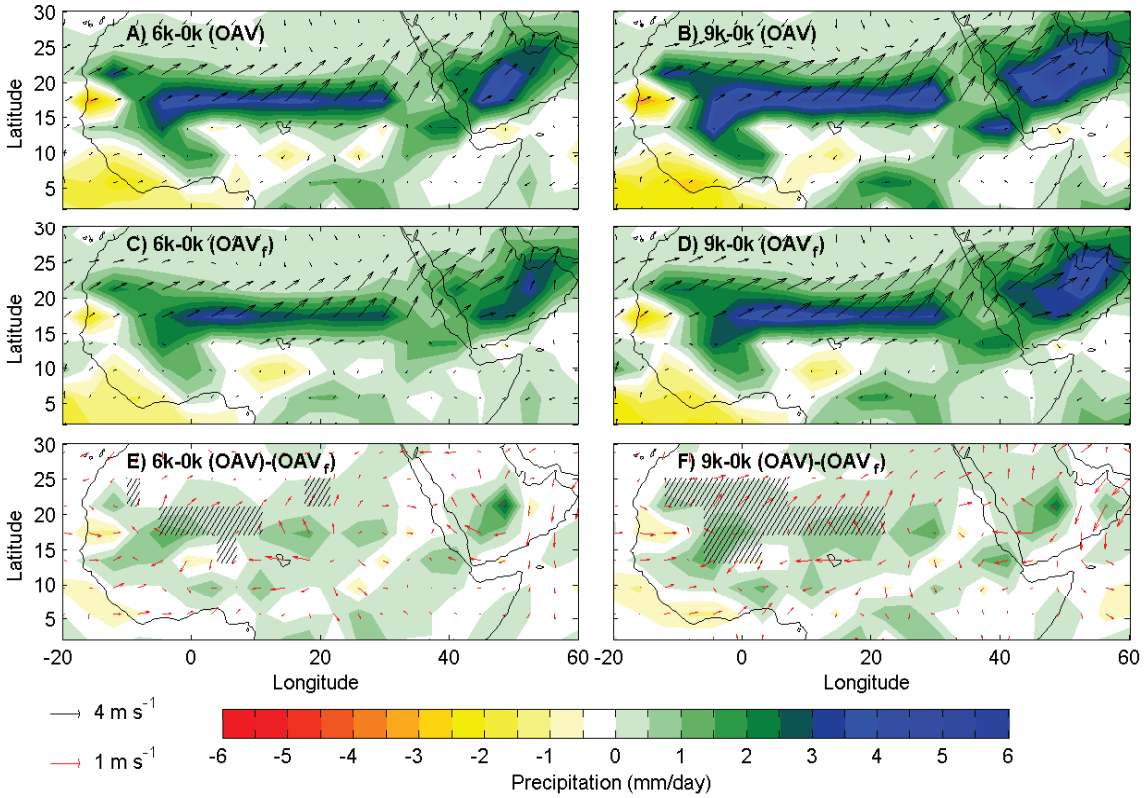

Figure 4.3 Changes of summer precipitation and near-surface winds for (A) the mid-Holocene and (B) the early Holocene experiment relative to PI in model simulations with dynamic vegetation. (C,D) Same as (A,B) but for fixed-vegetation simulations. (E,F) Differences between dynamic vegetation and fixed-vegetation experiments. Hatched areas in (E,F) display significant precipitation differences (95% confidence level) according to both a (non-parametric) Wilcoxon-Mann-Whitney test and a Student t-test.

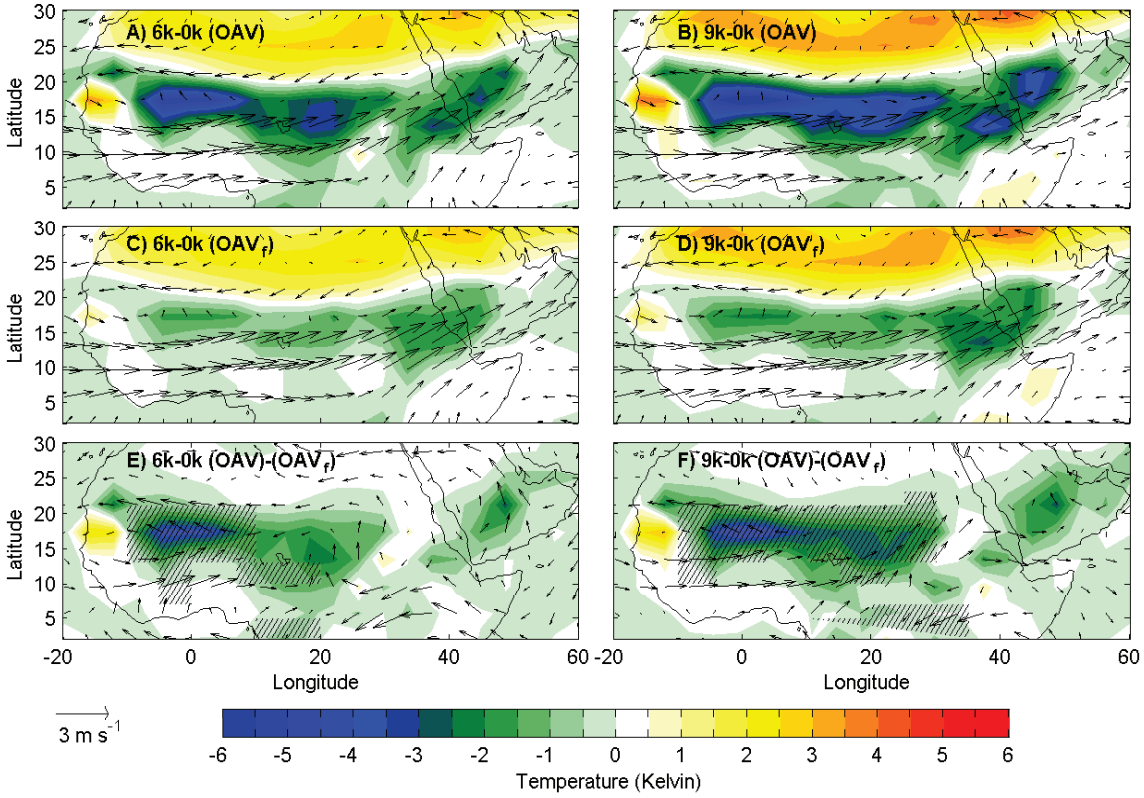

Figure 4.4 As in Fig. 4.3, but for changes in summer surface temperature and 700 hPa winds. Hatched areas in (E,F) display significant temperature differences (95% confidence level) according to both a (non-parametric) Wilcoxon-Mann-Whitney test and a Student t-test.

A close relationship exists between surface-temperature anomalies and mid-level wind anomalies over West Africa (Fig. 4.4). According to the thermal wind relation, anomalous horizontal temperature gradients induce vertical shear such that negative low-level temperature anomalies (communicated into the lower troposphere from the surface) are on the left of the anomalous mid-level wind vectors (cf. Cook, 1999). The negative surface temperature anomalies in the early and mid-Holocene experiments are substantial (more than 6K in the OAV experiments despite larger incoming shortwave radiation at the top of the atmosphere), in line with temperature reconstructions from groundwater samples (Beyerle et al., 2003), and associated with increased cloudiness due to enhanced convection, reflecting solar radiation back to space (cf. Braconnot et al., 2007; Patricola and Cook, 2007; Bosmans et al., 2012). Even more relevant in the context of vegetation-rainfall feedbacks is enhanced latent surface cooling by larger evapotranspiration in the wetter regions. Table 4.3 summarizes the changes in the different components of surface evapotranspiration over the Sahara/Sahel region for the set of experiments. With enhanced rainfall in the early and mid-Holocene experiments, evapotranspiration increases. This increase is much stronger when dynamic vegetation is enabled (OAV) due to enhanced canopy evaporation and transpiration in the "greener" regions. In the early and mid-Holocene experiments with fixed vegetation (OAV_f and OA) changes in canopy evaporation and transpiration are negligible, whereas ground evaporation substantially increases. This increase in ground evaporation, however, is smaller than the rise in total evapotranspiration in the OAV experiments. As a result, latent surface cooling and hence changes in the AEJ are much more pronounced in the early and mid-Holocene experiments with dynamic vegetation (Fig. 4.4e and f).

Previous work has shown that the AEJ plays a key role in controlling sub-Saharan precipitation by transporting moisture off the continent below the level of condensation, thus increasing moisture divergence over West Africa (e.g. Cook, 1999; Rowell, 2003). Figure 4.5 displays moisture transport anomalies at the AEJ level for the early and mid-Holocene experiments. In all experiments, eastward moisture flux anomalies appear at the southern flank of the AEJ south of 15° N, effectively reducing the westward moisture export from the North African region to the Atlantic. Owing to a stronger mid-level circulation change, the moisture export across the West African coastline is more strongly reduced in the early and mid-Holocene experiments with interactive dynamic vegetation compared to their fixed-vegetation counterparts (Fig. 4.5e and f), thus keeping more moisture available to feed the rain in the West African monsoon region.

Initializing the 0k and 6k simulations of CCSM3-DGVM with the expanded North African vegetation cover from experiment 9k(OAV) (cf. Fig. 4.2b) rather than with bare soil

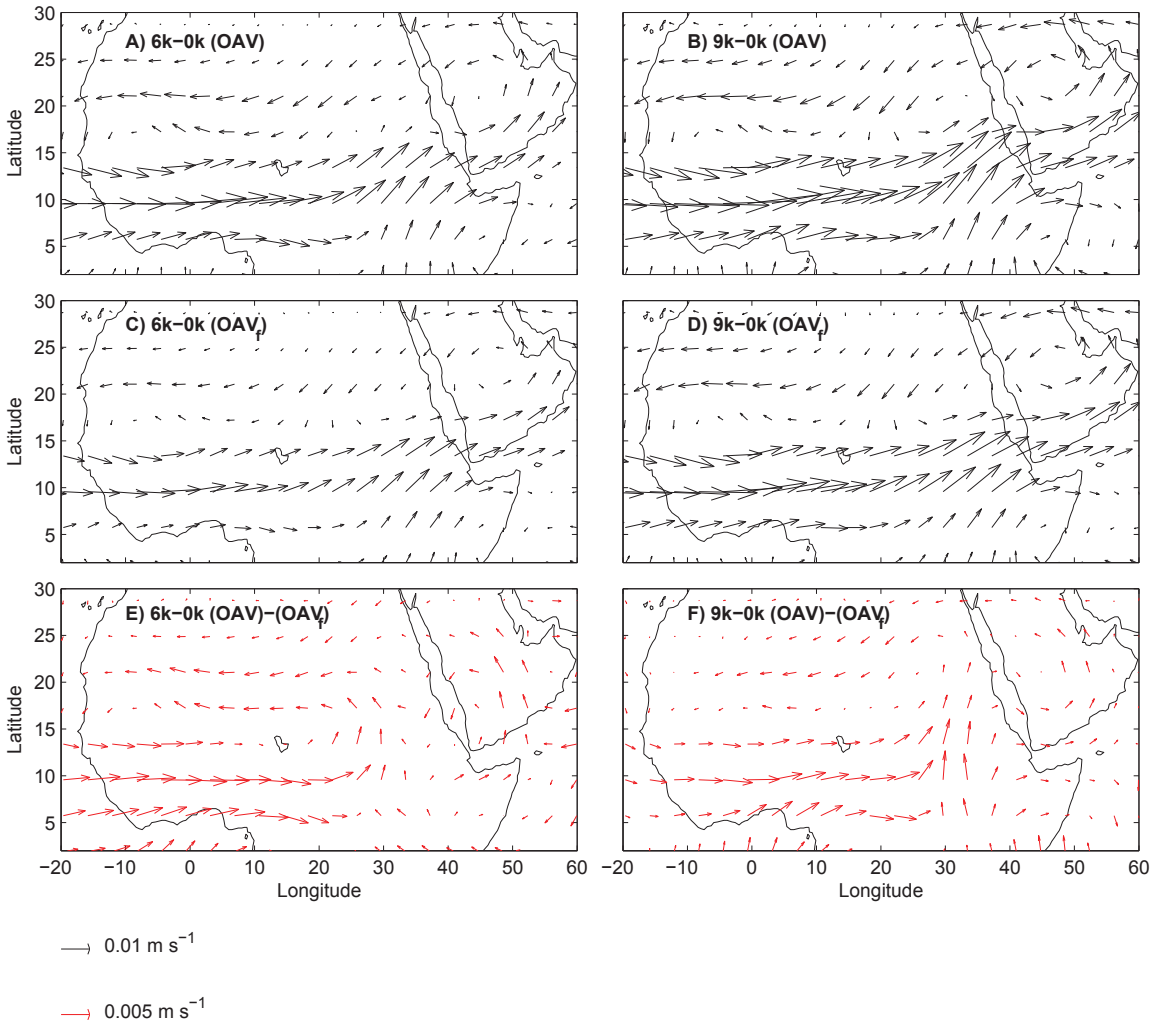

Figure 4.5 As in Fig. 4.3, but for changes in summer moisture transport at 700 hPa.

has a negligible effect on the region-averaged (10–25° N, 20° W–30° E) precipitation and evapotranspiration (see experiments 0k9k(OAV) and 6k9k(OAV) in Tables 4.2 and 4.3). A closer inspection of the North African precipitation fields, however, reveals small but statistically significant differences between the experiments 0k9k(OAV) and 0k(OAV) in a region between 10° N and 15° N (Fig. 4.6a and c). No such coherent pattern is found for the precipitation difference between experiments 6k9k(OAV) and 6k(OAV), suggesting that there is no significant influence of the initial vegetation cover on CCSM3-DGVM's simulation of mid-Holocene climate in North Africa (Fig. 4.6b and c).

4.5 Discussion

In response to enhanced summer insolation CCSM3-DGVM simulates increased rainfall over North Africa along with a northward shift of the monsoon trough during the early and middle Holocene. In the model experiments, higher rainfall is simulated at 9 ka than at 6 ka due to stronger insolation forcing. This result should be taken with care, however, since other forcings than orbital and greenhouse gases were not taken into account. In particular, remnants of the Laurentide ice sheet and enhanced meltwater flux into the adjacent ocean might have affected North African rainfall during the early Holocene (Niedermeyer et al., 2009; Lézine et al., 2011; Marzin et al., 2013). Early-to-mid Holocene wet conditions are also simulated for southern Arabia in accordance with geological evidence (e.g. McClure, 1976; Hoelzmann et al., 1998; Fleitmann et al., 2003).

The early and mid-Holocene North African precipitation increase goes along with a northward expansion of the vegetation cover. Substantial greening is also simulated over the Arabian Peninsula in line with vegetation reconstructions (e.g. Hoelzmann et al., 1998). Our sensitivity experiments reveal that the expansion of vegetation acts as a positive feedback on the rainfall increase in both North Africa and the Arabian Peninsula. In the Sahara/Sahel region (10–25° N,20° W–30° E) the dynamic vegetation enhances the orbitally triggered rainfall anomaly by approximately 20 % in both the early and mid-Holocene experiments. Despite the enhanced anomalous rainfall when dynamic vegetation is enabled, CCSM3-DGVM still underestimates early-to-mid Holocene monsoonal rainfall in the Saharan region by roughly a factor of two when compared to mid-Holocene reconstructions (Bartlein et al., 2011). Likewise, the northward expansion of savanna-type vegetation in North Africa also seems to be undersimulated (e.g. Hoelzmann et al., 1998; Jolly et al., 1998; Prentice et al., 2000). Underestimation of the northward extent and intensity of precipitation (and vegetation) changes is a common problem in coupled climate model simu-

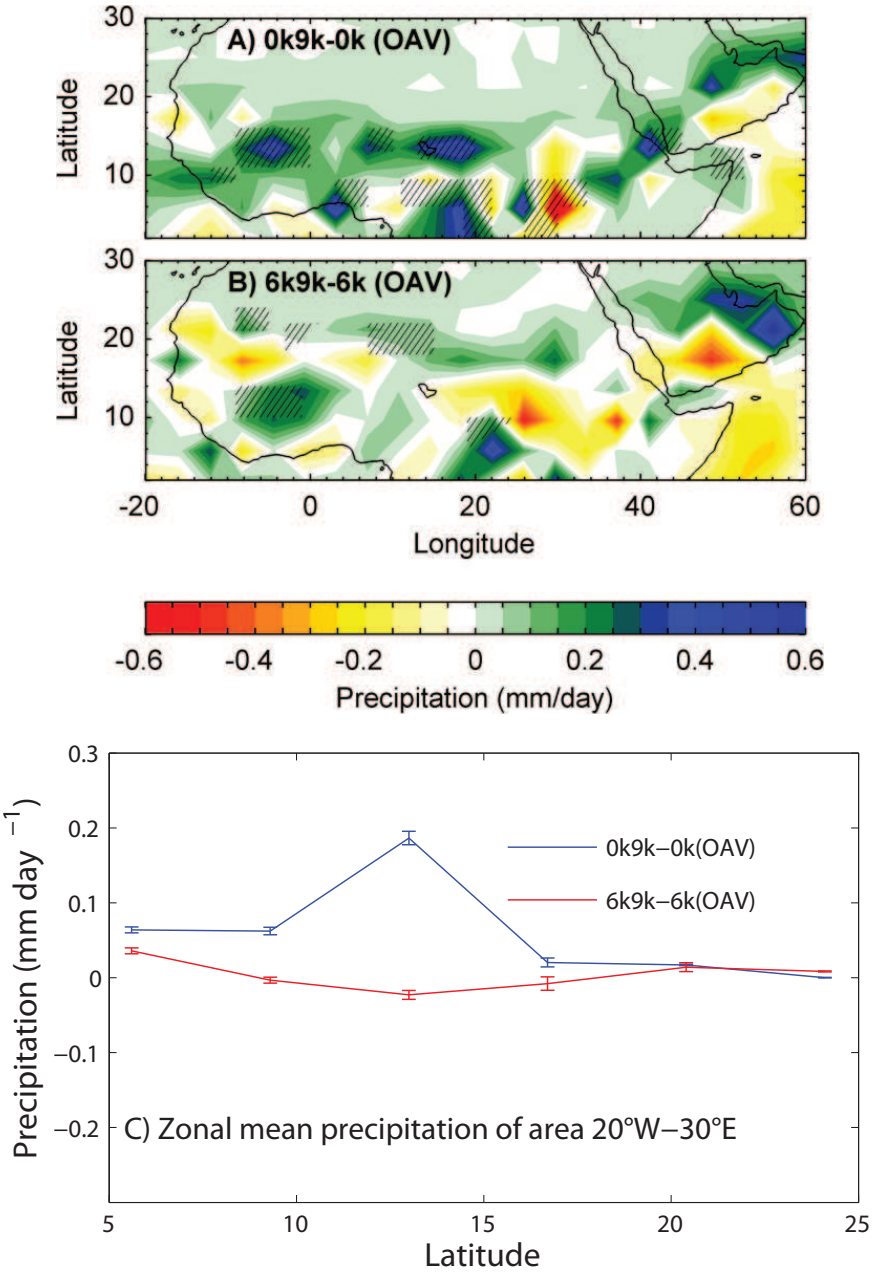

Figure 4.6 Influence of vegetation initial conditions (9k North African vegetation cover versus bare soil) on pre-industrial and mid-Holocene North African climate simulations. Shown are differences in summer precipitation for (A) 0k9k-0k(OAV) and (B) 6k9k-6k(OAV). Hatched areas display significant precipitation differences (95% confidence level) according to both a (non-parametric) Wilcoxon-Mann-Whitney test and a Student t-test. The lower panel (C) shows the corresponding zonal averages over North Africa (20°W-30°E) along with standard errors.

lations of the mid-Holocene (e.g. Zheng and Braconnot, 2013), which might reflect shortcomings in physical model parameterizations and/or missing land surface feedbacks (soil, lakes) or could be related to coarse model resolution (Bosmans et al., 2012).

A closer inspection of the mid-tropospheric wind field has identified changes in the AEJ as a key component of the positive vegetation-precipitation feedback mechanism in CCSM3-DGVM. More vegetation north of 15° N facilitates enhanced latent surface cooling through canopy evaporation and transpiration which, according to the thermal wind balance, results in a substantial deceleration of the jet's southern flank associated with a northward AEJ shift. Previous work has shown that a slowdown and/or northward shift of the AEJ is associated with positive Sahelian rainfall anomalies (e.g. Rowell et al., 1992; Xue and Shukla, 1993, 1996; Cook, 1999; Nicholson and Grist, 2001; Rowell, 2003; Cook and Vizy, 2006; Patricola and Cook, 2007; Nicholson, 2008; Bouimetarhan et al., 2012). A latitudinal displacement of the AEJ may affect Sahel rainfall through changes in horizontal and vertical wind shear and associated dynamic instabilities (Grist and Nicholson, 2001; Nicholson and Grist, 2001), a mechanism poorly resolved in coarse-resolution global climate models. Another way to connect changes in the AEJ with rainfall anomalies is through the large-scale column moisture budget (Cook, 1999; Rowell, 2003; Patricola and Cook, 2007; Mulitza et al., 2008). The mid-level jet plays a major role in the North African moisture budget by exporting large amounts of water vapor from the continent to the Atlantic Ocean below the level of condensation. Calculation of horizontal vapour transports in our experiments has revealed a reduction of this moisture export out of the North African realm in the early and middle Holocene. This reduction is amplified by stronger surface cooling in the OAV experiments with dynamic vegetation (Fig. 4.4e and f), such that more moisture is available to feed the rain in the monsoonal region, providing for a positive vegetation-precipitation feedback.

A positive feedback between the AEJ and sub-Saharan rainfall has been suggested in previous studies (Rowell et al., 1992; Cook, 1999; Rowell, 2003). Our experiments suggest that this feedback is boosted by a dynamic vegetation cover through modification of surface latent heat fluxes and low-level temperature gradients. As such, our results are largely consistent with the regional atmosphere model simulations by Patricola and Cook (2008) who found a close link between Saharan/Sahelian vegetation, North African rainfall, and moisture transports by the AEJ, whereas changes in vegetation have almost no effect on the southerly surface winds from the Gulf of Guinea and the associated near surface moisture import to the West African monsoon system. However, contrary to Patricola and Cook (2008) who found increasing low-level moist static energy and hence increasing convective

Table 4.2 Mean summer (JJAS) precipitation over the region 10-25°N, 20°W-30°E in the various experiments. ΔP denotes anomalies relative to the corresponding 0k (PI) case. SE is the standard error. Precipitation values are normally distributed according to a Shapiro-Wilk normality test (95 % confidence level).

Experiments	Precipitation (P)±2SE (mm day $^{-1}$)	ΔP (mm day $^{-1}$)
0k(OAV)	2.44±0.04	
6k(OAV)	3.41±0.04	0.97
9k(OAV)	3.71±0.04	1.27
0k(OAV$_f$)	2.47±0.04	
6k(OAV$_f$)	3.27±0.06	0.80
9k(OAV$_f$)	3.51±0.06	1.04
0k(OA)	2.48±0.04	
6k(OA)	3.29±0.04	0.81
9k(OA)	3.47±0.06	0.99
0k9k(OAV)	2.47±0.06	$<2SE$
6k9k(OAV)	3.42±0.04	0.98

instability where vegetation expands, changing vegetation has no effect on low-level moist static energy in our CCSM3-DGVM simulations (not shown).

The positive vegetation-precipitation feedback via mid-tropospheric atmosphere dynamics (AEJ) identified in our model experiments is induced by changes in surface latent heat fluxes. Water vapor, and hence latent heat, is introduced into the atmosphere via plant transpiration and the evaporation of water from the soil and free water on the vegetation canopy (the summed rate is called evapotranspiration). An expanded vegetation cover in North Africa during the early-to-mid Holocene favours evapotranspiration (cf. Ripley, 1976). Evapotranspiration increases with precipitation, but the slope is steeper when dynamic vegetation is enabled (Fig. 4.7). Whether the additional moisture introduced into the atmosphere from the expanded vegetation canopy contributes to enhanced rainfall through local water recycling has been assessed by calculating the Budyko recycling coefficient (representing the ratio of total precipitation to advected precipitation over a specified area) as defined by Brubaker et al. (1993) for the Sahara/Sahel region (10–25° N,20° W–30° E). We found that enhanced water recycling plays no role in the model's positive vegetation-rainfall feedback. For instance, the regional recycling coefficient surprisingly decreases from 1.98 in the pre-industrial control run 0k(OAV) to 1.59 in the early Holocene experiment 9k(OAV) when dynamic vegetation is enabled, whereas it increases from 1.66

Table 4.3 Changes of summer (JJAS) canopy evaporation, canopy transpiration and ground evaporation in the various early and mid-Holocene experiments over the region 10-25°N, 20°W-30°E.

Experiments	Canopy Evaporation (mm day $^{-1}$)	Canopy Transpiration (mm day $^{-1}$)	Ground Evaporation (mm day $^{-1}$)
6k-0k(OAV)	0.18	0.23	0.06
9k-0k(OAV)	0.23	0.29	0.11
6k-0k(OAV$_f$)	0.00	-0.03	0.34
9k-0k(OAV$_f$)	0.00	-0.03	0.45
6k-0k(OA)	0.00	-0.01	0.29
9k-0k(OA)	0.07	0.04	0.23
0k9k-0k(OAV)	0.03	0.04	-0.04
6k9k-0k(OAV)	0.18	0.22	0.07

Table 4.4 Summer (JJAS) surface albedo values in the early and mid-Holocene experiments over the region 10-25°N, 20°W-30°E.

Experiments	Surface Albedo
0k(OAV)	0.218
6k(OAV)	0.209
9k(OAV)	0.204
0k(OAV$_f$)	0.217
6k(OAV$_f$)	0.208
9k(OAV$_f$)	0.206

(pre-industrial) to 2.03 (early Holocene) in the fixed-vegetation experiments 0k(OAV$_f$) and 9k(OAV$_f$), respectively.

A closer inspection of the changes in evapotranspiration reveals enhanced evaporative surface cooling due to canopy evaporation and transpiration during the early-to-mid Holocene. Model studies who have shown a negative vegetation-precipitation feedback in North Africa (Liu et al., 2007, 2010) did not include a canopy evaporation term in the formulation of surface hydrology. However, including canopy evaporation in our simulations is crucial for obtaining enough evaporative surface cooling to trigger the positive vegetation-precipitation feedback via mid-tropospheric atmosphere dynamics. In fact, if canopy evaporation was neglected in our simulations (and would not have been compensated by enhanced transpiration or ground evaporation), the feedback would disappear or even become negative (cf. Table 4.3).

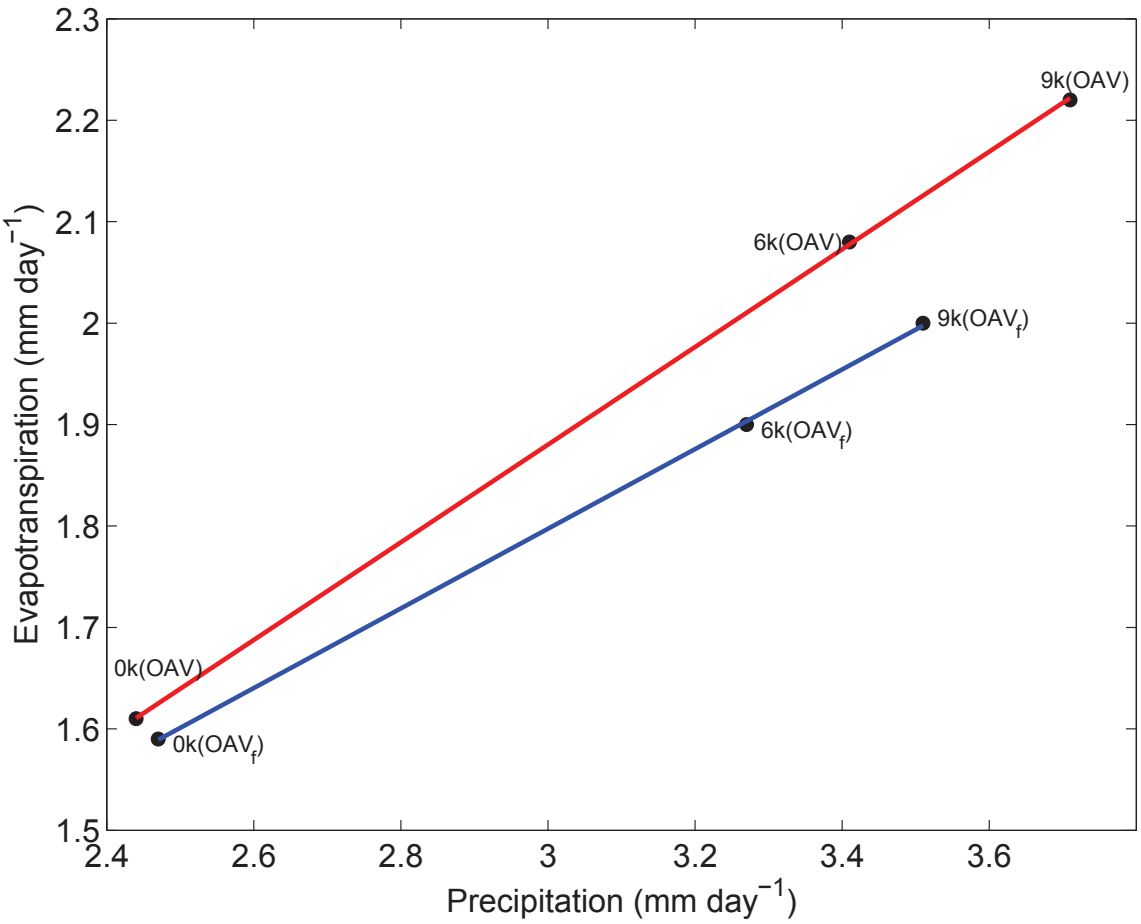

Figure 4.7 Mean summer evapotranspiration versus precipitation over the region 10-25°N, 20°W-30°E in the 0k, 6k and 9k experiments with dynamic vegetation (OAV experiments; red) and with fixed vegetation (OAV$_f$ experiments; blue).

Vegetation-induced changes in surface albedo (Charney feedback), which would increase low-level moist static energy (resulting in atmospheric destabilization) through enhanced surface warming – or more precisely, less pronounced surface cooling (Charney et al., 1976) – play no substantial role for creating a positive vegetation-rainfall feedback in our model study, unlike in earlier studies (e.g. Kutzbach et al., 1996; Claussen and Gayler, 1997; Hales et al., 2006). By contrast, the positive feedback through AEJ dynamics as found in our study relies on North African surface cooling rather than enhanced surface warming by decreasing surface albedo, consistent with the regional model study by Patricola and Cook (2008). It is important to note that soil albedo values in CCSM3-DGVM depend on the volumetric water content of the first soil layer and can locally be as small as 0.09 for saturated soils in the visible range (Oleson et al., 2004). This strongly diminishes the effect of vegetation on North African surface albedo (Levis et al., 2004a; Notaro et al., 2008) as seen in Table 4.4.

The results from experiments 0k9k(OAV) and 6k9k(OAV) suggest that the simulation of modern and mid-Holocene regional climate in North Africa does not depend on the initial vegetation cover as also shown by Renssen et al. (2006b). Despite the existence of a positive vegetation-rainfall feedback multiple equilibrium states were not found on the regional scale, which would rule out the potential for abrupt climate-vegetation transitions in the Holocene due to a catastrophic bifurcation or "unstable collapse" (Liu et al., 2006, 2007). However, statistical significance tests did not rule out the possibility of multiple states at the local scale between 10°N and 15°N under modern boundary conditions. This implies that, locally, unstable collapses could occur such that late Holocene proxy records from specific sites may show abrupt transitions while records from other sites do not (cf. Bathiany et al., 2012). Similar ideas were put forward by Brovkin and Claussen (2008); Williams et al. (2011) and Claussen et al. (2013). For the middle Holocene, the climate-ecosystem turned out to be mono-stable in CCSM3-DGVM even at the local scale, which is consistent with earlier findings by Brovkin et al. (1998) who suggested that the system is prone to bi-stability only in the late Holocene, whereas the early-to-mid Holocene was mono-stable.

4.6 Conclusions

Model experiments with CCSM3-DGVM support the findings of increased summer rainfall and expansion of vegetation in the early-to-mid Holocene over North Africa as in previous coupled general circulation model studies. By enabling interactive dynamic vegetation

(OAV experiments), rainfall intensification is much more pronounced in this model. In the Sahara/Sahel region, the dynamic vegetation enhances the orbitally triggered summer rainfall anomaly by approximately 20 % in both the early (9 ka) and mid-Holocene (6 ka) experiments.

The primary vegetation-atmosphere feedback identified here operates through surface latent heat flux anomalies by canopy evapotranspiration and their effect on the AEJ. As such, the vegetation feedback relies on enhanced surface (evaporational) cooling as opposed to the Charney feedback which operates through atmospheric instability by decreased surface albedo. Neglecting canopy evaporation, as in some previous model studies, could substantially affect the simulation of evaporative cooling such that the positive vegetation-atmosphere feedback might disappear. This type of climate-vegetation feedback over North Africa does not apply to other monsoon regions, since the feedback mechanism is closely linked to the characteristics of the regional atmospheric circulation (e.g. the presence of the AEJ). However, the North African climate-vegetation feedback should work also in other epochs than the Holocene. Even though CCSM3-DGVM simulates a positive vegetation-precipitation feedback over North Africa, this feedback is not strong enough to produce multiple equilibrium climate-ecosystem states on a regional scale.

In order to cope with the uncertainties regarding the potential model-dependencies, further sensitivity studies are needed to assess the the robustness of our results. Besides model resolution and PFT characteristics in the vegetation model, sensitivity studies should particularly address the effects of different parameterizations for land surface evaporation, transpiration and albedo.

4.7 Acknowledgement

This study has been supported by the Deutsche Forschungsgemeinschaft (DFG) through the Priority Programme INTERDYNAMIC. The CCSM3-DGVM model simulations have been carried out on the HLRN-II (SGI Altix) supercomputer.

5 Sensitivity of the Greenland Ice Sheet to interglacial climate forcing: MIS 5 versus MIS 11

R. Rachmayani, M. Prange, D. J. Lunt, E. J. Stone, M. Schulz

5.1 Abstract

The Greenland Ice Sheet (GrIS) is thought to have contributed substantially to high global sea levels during the interglacials of Marine Isotope Stage (MIS) 5 and 11. Geological evidence suggests that the mass loss of the GrIS was similar or even greater during the interglacial of MIS 11 than MIS 5, despite a weaker insolation forcing. In the present study, this conundrum is addressed by using the three-dimensional thermomechanical ice-sheet model Glimmer forced by CCSM3 climate model output for MIS 5 and MIS 11 time slices. Our results suggest a stronger sensitivity of the GrIS to MIS 11 climate forcing than to MIS 5 forcing. The greater MIS 11 GrIS mass loss relative to MIS 5 is attributed to a larger heat transport towards high latitudes by a stronger Atlantic meridional ocean circulation in addition to a stronger greenhouse gas radiative forcing. The results suggest a substantial modification of orbital insolation forcing by internal climate feedbacks, which add significant complexity to the traditional Milankovitch theory.

5.2 Introduction

Continental ice sheets are a major factor in the climate change debate, in particular due to their direct link to global sea level. The study of warm climates in the past may provide useful insight into the sensitivity of polar land ice to changing forcing. A growing body of evidence suggests particularly high global sea levels along with significant shrinking of the Greenland Ice Sheet (GrIS) during the Quaternary interglacials of Marine Isotope Stage (MIS) 5 and MIS 11 (Dutton et al., 2015).

For the interglacial of MIS 5, the Last Interglacial (LIG; ca. 130-115 kyr ago), global mean annual temperature was estimated to have been 1° C warmer than during the pre-industrial (Otto-Bliesner et al., 2013; Dutton et al., 2015), while summer temperature

anomalies might have been up to 5° C above present in the Arctic region reflecting substantial polar amplification (e.g., Otto-Bliesner et al., 2006; CAPE Last Interglacial Project Members, 2006; NEEM community members, 2013). Compilations of relative sea level combined with modeling suggest a LIG peak global mean sea level of 6-9 m above present (Kopp et al., 2009; Dutton and Lambeck, 2012; Masson-Delmotte et al., 2013; Kopp et al., 2013; O'Leary et al., 2013; Dutton et al., 2015). The contribution of GrIS melting to this sea level rise is highly uncertain, but recent model results suggest a GrIS contribution between 1.4 and 4.3 m (Robinson et al., 2011; Born and Nisancioglu, 2012; Helsen et al., 2013; Masson-Delmotte et al., 2013; Stone et al., 2013; Quiquet et al., 2013), indicating that the size of the GrIS was still substantial during the LIG. It has been demonstrated, however, that the simulation of LIG GrIS mass loss is highly sensitive to poorly constrained model parameters (Stone et al., 2013).

Meanwhile, a warm interglacial during MIS 11 ca. 420-395 kyr ago (Milker et al., 2013; Dutton et al., 2015) has been suggested as the best analogue for present and future climate (Loutre and Berger, 2000, 2003; Droxler et al., 2003; Alley et al., 2010; Bowen, 2010) when orbital geometry was similar to the configuration during the present interglacial (Berger and Loutre, 1991). Global average temperatures of MIS 11 are highly uncertain, but a peak global mean temperature anomaly of up to 2° C relative to pre-industrial cannot be ruled out (Masson-Delmotte et al., 2010; Lang and Wolff, 2011; Dutton et al., 2015). Evidence from marine sediment cores points to sea surface temperatures (SST) in the North Atlantic 1-2° higher than today (McManus et al., 1999; Bauch et al., 2000; Helmke et al., 2003; Kandiano and Bauch, 2003; De Abreu et al., 2005). Maximum global mean sea level during the MIS 11 interglacial likely was 6-13 m higher than today (Muhs et al., 2012; Roberts et al., 2012; Raymo and Mitrovica, 2012; Chen et al., 2014; Dutton et al., 2015), requiring a loss of most or all of the GrIS (Reyes et al., 2014).

Taken together, mass loss of the GrIS was similar or even greater during the interglacial of MIS 11 than during the LIG. Since the changing seasonal insolation owing to varying astronomical parameters is thought to be a major forcing of polar ice-sheet evolution (e.g., Loutre et al., 2004; Huybers, 2006; van de Berg et al., 2011), the great GrIS mass loss during MIS 11 seems to be counterintuitive. Due to a low eccentricity of the Earth's orbit, climatic precession varied relatively little during MIS 11, and hence maximum boreal summer insolation was much smaller during the MIS 11 interglacial than during the LIG (Fig. 5.1). By contrast, eccentricity was high during the LIG leading to high summer insolation values around 125 ka. Huybers (2006) pointed out that glaciers are sensitive to insolation integrated over the duration of the summer and introduced the concept of the

integrated summer insolation as the dominant control on polar ice-sheet evolution. Like maximum summer insolation, values for the integrated summer insolation were larger during the LIG than during MIS 11, and cannot explain a stronger GrIS melting during MIS 11 compared to MIS 5 (Fig. 5.1).

The goal of the present study is twofold. Using the three-dimensional thermomechanical ice-sheet model Glimmer (Genie land ice model with multiply-enabled regions) the sensitivity of GrIS mass loss to interglacial climate forcing of MIS 5 and 11 is studied. Climate forcing comes from MIS 5 and MIS 11 simulations with the Community Climate System Model version 3 (CCSM3). We will address the conundrum as to why the GrIS mass loss may have been greater during MIS 11 than during MIS 5 despite a weaker insolation forcing. In addition, we will study the impact of some poorly constrained parameters in large-scale ice-sheet modelling on the paleo-GrIS simulations. Previous work investigated the sensitivity of ice-sheet evolution for the modern GrIS to five tuneable parameters which affect the ice-sheet dynamics and surface mass balance (Stone et al., 2010). Later on, it has been shown that these parameters strongly control the size of the modelled GrIS during the LIG (Stone et al., 2013). In the present study, we will show the sensitivity to tuning parameters for the interglacial of MIS 11.

5.3 Experimental Setup

5.3.1 Model

CCSM3 Global Climate Model

The coupled general circulation model (CGCM) CCSM3 is composed of four components representing atmosphere, ocean, sea ice and land surface (Collins et al., 2006a). We used the low-resolution (T31) version of the model (Yeager et al., 2006). In this version, the horizontal resolution of the atmosphere and land components is 3.75° with 26 layers in the atmosphere, while the nominal resolution of the ocean/sea-ice grid is 3° .The ocean grid consists of 25 levels in the vertical. In this study, the dynamic global vegetation model (DGVM) is included along with some improvements of land hydrology parameterizations (Oleson et al., 2008) as in previous studies (e.g., Handiani et al., 2013; Rachmayani et al., 2015, 2016).

Glimmer Ice-sheet Model

To simulate the GrIS response to interglacial climate forcing provided by CCSM3, we use the three-dimensional thermomechanical ice-sheet model Glimmer version 1.0.4 (Payne,

1999; Rutt et al., 2009). The horizontal resolution of the model is 20 km with 11 vertical layers. Ice dynamics are represented by the widely used shallow-ice approximation. The model is formulated on a Cartesian grid and takes the surface mass balance and near-surface air temperature as input at each time-step. Here, the ice-dynamics time-step is one year. The surface mass balance is simulated using the positive degree day (PDD) approach described in Reeh (1991); DeConto and Pollard (2003); Lunt et al. (2008, 2009). The PDD method is based on the assumption that the surface ice melt is proportional to the time-integrated temperature above freezing point which provides for the energy available for melting. Here, two PDD factors are used, one each for snow and ice, to take account of the different albedos and densities (Stone et al., 2013). Glimmer further assumes an elastic isostatic response of the lithosphere to changes in ice mass. The forcing data from the low-resolution CCSM3 climate model are transformed onto the ice-model grid using bilinear interpolation. In the case of surface air temperature, a vertical lapse-rate correction is applied. The use of a lapse-rate correction in transforming the CCSM3 climate to the Glimmer grid represents the local aspect of the ice-elevation feedback. Further details on the ice-sheet model and its offline coupling to the atmosphere can be found in Lunt et al. (2008) and Stone et al. (2010, 2013).

5.3.2 Setup of Experiments

Climate forcing for the ice-sheet model is provided by two CCSM3 interglacial time-slice experiments, one with 125 ka boundary conditions (MIS 5) and the other with 410 ka boundary conditions (MIS 11). These boundary conditions include astronomical parameters (Berger, 1978) and atmospheric greenhouse gas (GHG) concentrations as given in Table 5.1, while other forcings (ice-sheet configuration, ozone distribution, sulfate aerosols, carbonaceous aerosols, solar constant) were kept as in the modern (pre-industrial, PI) control run. Both interglacial time-slice simulations were branched off from year 600 of the PI spin-up run and integrated for 400 years each, which was sufficient for the surface climate to equilibrate. For details on the CCSM3 PI and interglacial time-slice experiments the reader is referred to Lunt et al. (2013); Kleinen et al. (2014); Rachmayani et al. (2016). Monthly means of precipitation and near-surface air temperature from the last 100 years of each experiment were taken to force the Glimmer ice-sheet model.

The ice-sheet model was spun up for 50,000 years using climatological ERA-40 datasets (Hanna et al., 2005; ECMWF, 2006; Hanna et al., 2008) and the Greenland bedrock topography of Bamber et al. (2001). Subsequently, the forcing was switched to interglacial climate of the 125 ka and 410 ka time-slices, respectively, using simulated precipitation

Table 5.1 GHG concentrations used in the CCSM3 experiments.

Experiments	CO_2 (ppmv)	CH_4 (ppbv)	N_2O (ppbv)
0 ka (PI)	280	760	270
125 ka (MIS 5)	276	640	263
410 ka (MIS 11)	284	710	282

and temperature anomalies (relative to the control run) superimposed onto the ERA-40 climatology (Stone et al., 2010, 2013).

The goal of our model experiments is not to simulate a realistic evolution of the GrIS during the interglacials of MIS 5 and MIS 11, as this would require a transient climate forcing as well as feedbacks from the ice sheet to the climate model components. Instead, our goal is to identify potential mechanisms in the climate system that may have been responsible for the strong GrIS mass loss during MIS 11 compared to the LIG. Since we consider the 125 ka and 410 ka time slices representative of the LIG and the peak interglacial of MIS 11 in terms of insolation (Fig. 5.1) and GHG (Table 5.1) forcing, we deem our time-slice approach appropriate for this purpose. The approach is also appropriate to assess the sensitivity of the modelled GrIS to tunable parameters. To this end, we have performed all Glimmer experiments six times with different sets of parameters as shown in Table 5.2. These parameter sets have been identified by Stone et al. (2010) as optimal for the simulation of the modern GrIS based on different diagnostic skill scores.

5.4 Results

A rapid decline of the GrIS volume takes place within a few thousand years after switching the climate forcing from modern to either 125 ka (Fig. 5.2a) or 410 ka (Fig. 5.2b). For both time slices it is evident that the simulated size of the GrIS strongly depends on the set of tuning parameters used. For both interglacials, experiment 67 reveals the highest sensitivity to the 125 ka and 410 ka forcings such that the GrIS almost disappears in less than 5000 years. Experiment 67 is characterized by the largest lapse rate L_G (Table 5.2), which probably leads to an overestimation of the positive ice-elevation feedback. However, independent of the tuning parameter set used, the GrIS mass loss is always greater in the MIS 11 experiments compared to the MIS 5 experiments. Surface ablation is the dominant factor for the greater MIS 11 ice loss. Fig. 5.3 shows higher ablation rates in the MIS 11 experiments compared to the LIG, especially in northern, northeastern and western Greenland, indepen-

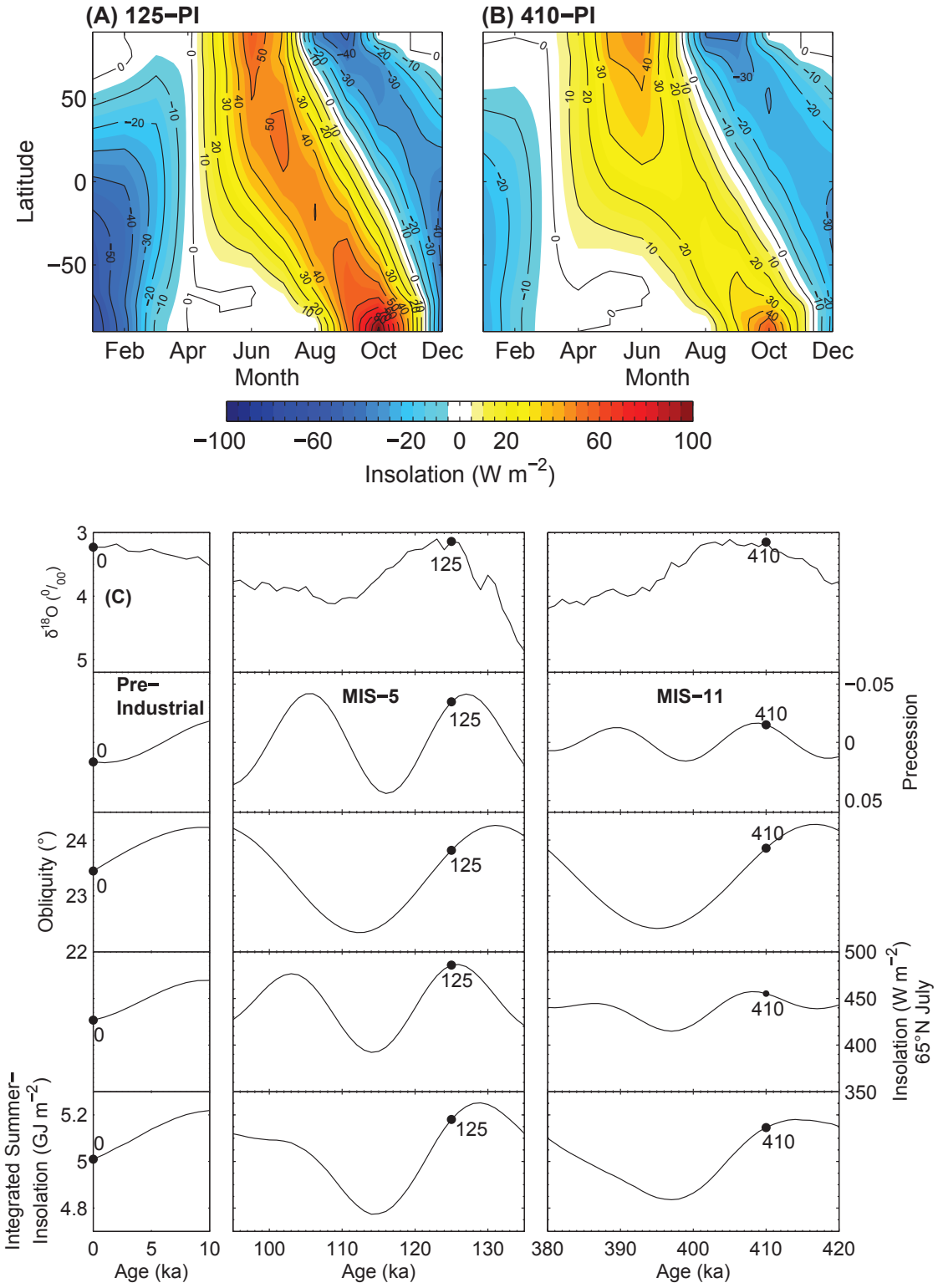

Figure 5.1 Insolation anomalies (relative to PI) for the time slices 125 ka (A) and 410 ka (B). The calculation assumes a fixed present-day calendar with vernal equinox at 21 March. Benthic δ^{18}O stack (Lisiecki and Raymo, 2005), climatic precession, obliquity, July insolation at 65°N (Berger, 1978), and the integrated summer insolation with τ= 275 W/m^2 according to Huybers (2006) for the Holocene, MIS 5 and MIS 11 (C). The dots mark the time slices simulated in this study.

Table 5.2 Tuned parameter values used in the Glimmer ice-sheet experiments. The tuning parameters are *f* (enhancement flow factor), L_G (near-surface lapse rate), *G* (geothermal heat flux), α_s (PDD factor for snow), and α_i (PDD factor for ice). The experiment numbers (tuning parameter settings) are taken from Stone et al. (2010). For details the reader is referred to Stone et al. (2010).

Experiment No.	f	L_G (°C km^{-1})	G (mW m^{-2})	α_s (mm d^{-1} °C^{-1})	α_i (mm d^{-1} °C^{-1})
10	4.5838	-4.2047	-52.630	3.7243	19.878
233	4.8585	-4.0754	-46.667	4.2425	16.344
99	1.2838	-4.5334	-41.758	4.7844	18.710
165	3.1036	-4.2456	-47.709	4.5763	19.455
67	2.6165	-8.1157	-53.421	3.9951	13.502
240	2.5551	-6.0820	-59.070	3.6258	10.221

dent of the tuning parameter settings. Given the weaker insolation forcing during MIS 11 compared to the LIG (Fig. 5.1), the generally higher ablation rates seem counterintuitive.

Fig. 5.4 shows the difference between the climate forcings of MIS 11 (410 ka) and MIS 5 (125 ka) as provided by CCSM3. Higher MIS 11 summer (June-July-August, JJA) air temperatures all over Greenland compared to the LIG provide for the energy required for the enhanced surface melting (Fig. 5.4a), while the annual deposition of snow due to precipitation is greater in MIS 11 than in MIS 5 over most parts of Greenland except for the southernmost and southwestern portion (Fig. 5.4b). Therefore, enhanced snowfall tends to counteract the larger MIS 11 GrIS mass loss associated with surface ablation over large regions. Higher GHG concentrations (Table 5.1) contribute to the anomalously warm conditions in Greenland during MIS 11 (cf. Yin and Berger (2015)). However, a closer inspection of the summer surface temperature anomaly pattern reveals a maximum in the North Atlantic and Nordic Seas pointing to changes in the large-scale ocean circulation (Fig. 5.4a). A comparison of the ocean circulations between the different experiments shows that the Atlantic Meridional Overturning Circulation (AMOC) is about 1.7 Sv (1 Sv = 10^6 m^3/s) stronger in the MIS 11 time slice compared to the LIG experiment (Fig. 5.4c), thus transporting more heat (ca. 8-15% increase depending on latitude) from the tropical North Atlantic to subpolar regions, where air-sea heat exchange takes place with impact on the climate over Greenland. Compared to the modern control run, the AMOC at 125 ka is even 2.2 Sv weaker.

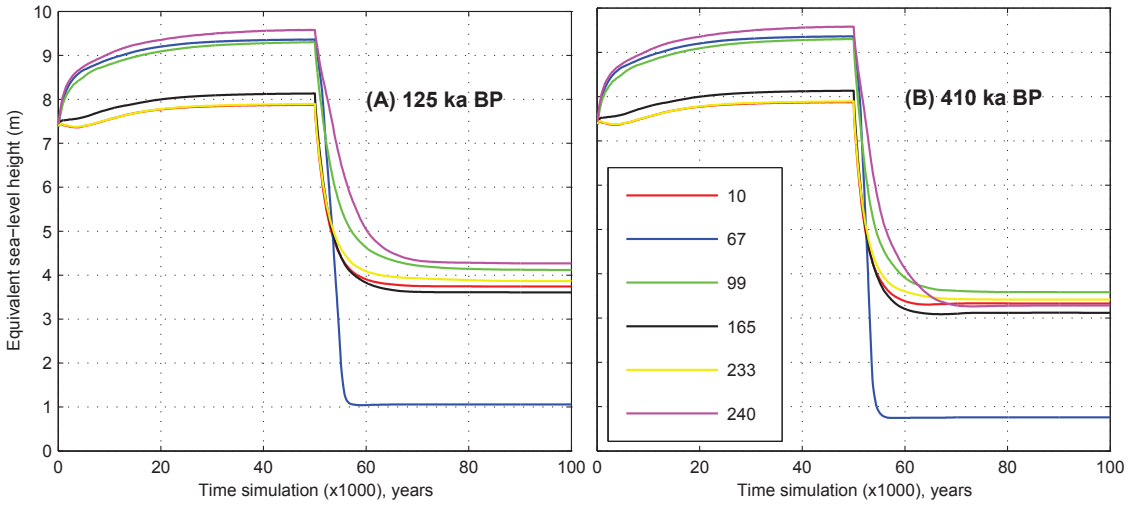

Figure 5.2 Results from the Glimmer MIS 5 and MIS 11 experiments: Timeseries of GrIS volume as equivalent sea-level height for (A) the 125 ka and (B) the 410 ka experiment (switching from modern to interglacial climate forcing at model year 50,000) using different tuning parameter settings (see Table 5.2).

5.5 Disscussion

Equal or even greater GrIS mass loss during the interglacial of MIS 11 compared to the LIG is difficult to explain with pure insolation forcing. In harmony with geological evidence our model experiments suggest stronger GrIS melt during the interglacial of MIS 11 than during the LIG. The northern and western regions of Greenland show the strongest sensitivities to MIS 11 interglacial climate forcing. The stronger MIS 11 ice loss relative to MIS 5 is attributable to larger GHG radiative forcing (cf. Yin and Berger (2015)) and a stronger AMOC transporting more heat towards the North Atlantic and Nordic Seas. Analyzing the reason for the MIS 11 amplification of the AMOC would require additional specific ocean model experiments, which is beyond the scope of the present study. Through changes in surface albedo, a smaller Arctic sea-ice area during the MIS 11 interglacial (not shown) may act as a positive feedback to the anomalous warming in high latitudes. Hence, our model results suggest that internal climate feedbacks may strongly modify the orbital insolation forcing, adding significant complexity to the traditional Milankovitch theory.

Warm Greenland summer conditions during the LIG in response to high insolation have been simulated by numerous climate models (e.g., Montoya et al., 2000; Kaspar et al., 2005; Otto-Bliesner et al., 2006; Lunt et al., 2013; Stone et al., 2013). Unfortunately, only few model studies exist regarding the climate of MIS 11. Simulations with the Earth system model of intermediate complexity LOVECLIM show colder Greenland summer temper-

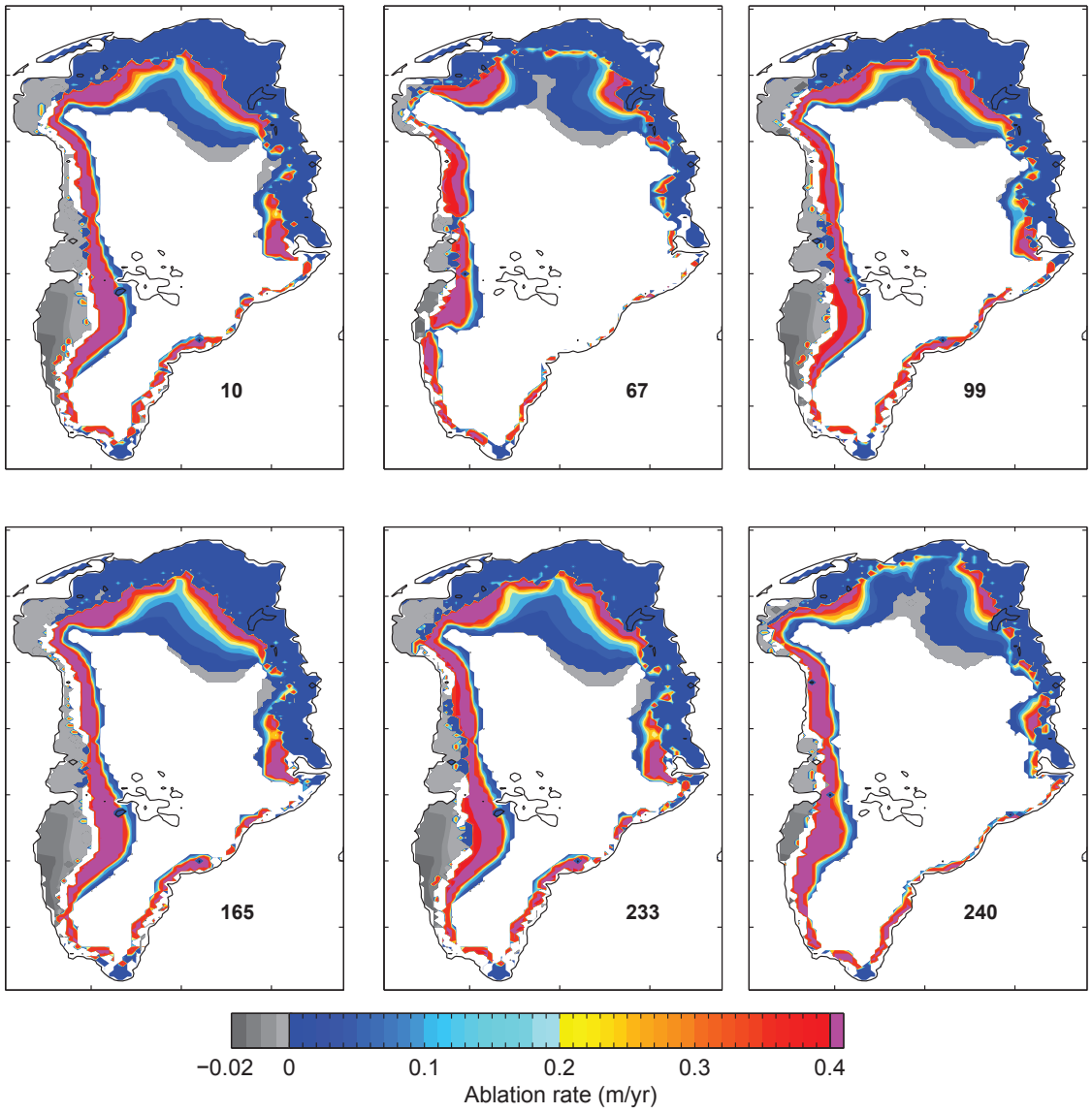

Figure 5.3 Ablation rate anomalies (410 ka minus 125 ka experiment) at model year 500 after switching from modern to interglacial climate forcing for different tuning parameter settings (see Table 5.2).

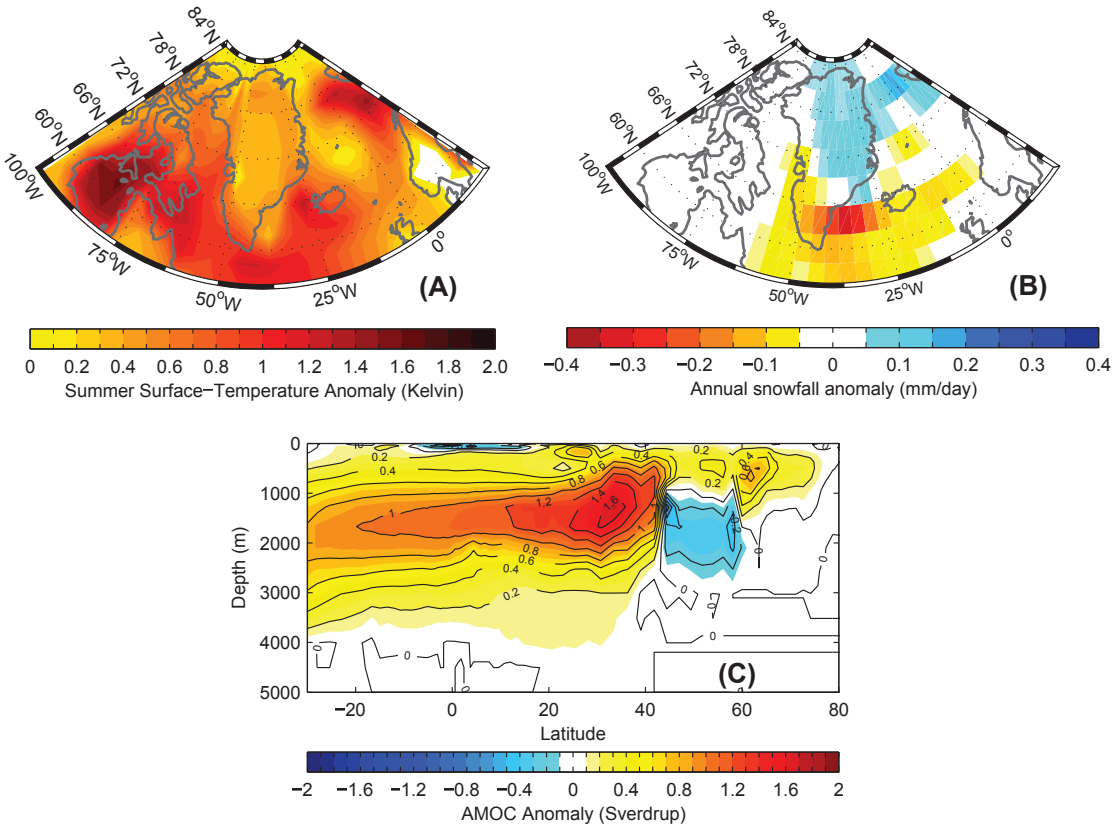

Figure 5.4 Differences between 410 ka (MIS 11 experiment) and 125 ka (MIS 5 experiment) of climatic fields simulated by CCSM3: (A) boreal summer (JJA) surface temperature in and around Greenland, (B) annual snowfall, (C) AMOC (meridional overturning streamfunction in the Atlantic Ocean).

atures during the MIS 11 peak interglacial compared to the LIG (Yin and Berger, 2012, 2015), in contrast to our results. In the absence of proxy records from Greenland which date back to MIS 11 it is not possible to assess which model result is more realistic. Paleoceanographic studies from the northern North Atlantic are inconclusive as to whether summer sea-surface temperatures where warmer or colder during the MIS 11 peak interglacial compared to the LIG, as the results depend on the paleothermometric method used (Kandiano and Bauch, 2003).

Our approach does not allow a quantitative estimate of LIG and MIS 11 GrIS volumes due to several shortcomings in the experimental setup. Firstly, the climatic forcing of the ice-sheet model is stationary (time-slice approach) rather than transient as in, (e.g., Stone et al., 2013). Moreover, the modelled ice sheet does not feedback to the other climate components (offline coupling), like the atmosphere and the ocean. In particular, GrIS meltwater flux into the ocean might further affect the AMOC, and hence North Atlantic and Greenland temperatures (Yang et al., 2016). Future studies should therefore simulate the MIS 5 and MIS 11 GrIS evolution in interactively coupled CGCM-ice sheet transient experiments. Ideally, such transient experiments would include the preceding terminations as these may precondition the evolution of the subsequent interglacials (cf. Past Interglacials Working Group of PAGES (2016)). Secondly, the semi-empirical PDD scheme used in calculating the surface mass balance may significantly underestimate surface melt associated with high insolation. van de Berg et al. (2011) have shown that surface melt is affected not only by higher ambient temperatures but also directly through stronger summertime insolation and associated non-linear feedbacks. As a result, taking insolation and albedo explicitly into account would likely lead to a greater GrIS mass loss under high insolation forcing, especially during the LIG. Thirdly, as shown by Stone et al. (2013) and in the present study, the simulation of GrIS volumes strongly depends on different tuning parameters. Even though a set of tuning parameters yields a realistic simulation of the modern GrIS, this does not ensure a realistic simulation of the LIG or MIS 11 ice-sheet using the same set of parameters. An insightful example was given by experiment 67, in which the GrIS almost completely disappeared within a few thousand years in response to LIG and MIS 11 climate forcing. A too high value for the lapse rate was identified to be the main cause for this outcome. Further caveats, mostly related to simplifications of the ice-sheet dynamics, are discussed in Stone et al. (2010) and Stone et al. (2013). In particular, the omission of basal sliding in the model likely leads to an underestimation of the dynamic ice transfer from the accumulation zone to the ablation zone, and hence an overestimation of the ice-sheet volume in warm climates. These shortcomings aside, our model results

suggest hitherto overlooked processes in the climate system that help explain the relatively strong GrIS mass loss during the interglacial of MIS 11.

5.6 Conclusions

MIS 5 and MIS 11 interglacial experiments with the Glimmer ice-sheet model driven by CCSM3 climate model output suggest a stronger sensitivity of the GrIS to MIS 11 climate forcing than to MIS 5 forcing. Beside larger GHG forcing, we attribute the greater MIS 11 ice loss relative to MIS 5 to a stronger heat transport towards high northern latitudes by the AMOC. Our model results suggest a substantial modification of orbital insolation forcing by internal climate feedbacks, which add significant complexity to the traditional Milankovitch theory.

5.7 Acknowledgments

This study was supported by the Deutsche Forschungsgemeinschaft (DFG) through the priority program INTERDYNAMIC. The CCSM3 model simulations have been carried out using the supercomputer of the Norddeutscher Verbund fuer Hoch- und Hoechstleistungsrechnen (HLRN). The Glimmer model simulations have been conducted at the School of Geographical Sciences, University of Bristol, during a research stay of R.R.

6 Summary and Outlook

6.1 Summary of the results

The following summaries conclude the research objectives proffered in Section 1.4, Chapter 1:

- The results in Chapter 3 suggest a seasonal surface temperature anomalies could largely be explained by local insolation anomalies induced by the astronomical forcing in most of regions and by GHG forcing in high latitudes and the early Brunhes interglacials MIS 13 and 15 when GHG concentrations were much lower than during the later interglacials. Climate feedbacks modify the surface temperature response in specific regions, particularly in the monsoon domains and the polar oceans. A significant role of obliquity in forcing the West African monsoon was found, whereas the Indian monsoon – as well as the other regional monsoon systems – appear to be less sensitive (or not sensitive at all) to obliquity changes during interglacials. Despite this important role of obliquity in West African monsoon variability, the response to precession is still stronger. In the 394 and 615 ka experiments, different responses to specific forcings and the anti-phase behaviour of the African and Indian monsoon systems are captured in North Africa where the rainfall anomaly has opposite sign compared to the Indian anomaly. It clearly points to the fact that the two regional monsoon systems do not always vary in concert and challenge the global monsoon concept at the astronomical timescale.

- The results in Chapter 4 support the findings of increased summer rainfall and expansion of vegetation in the early-to-mid Holocene over North Africa as in previous coupled general circulation model studies. By enabling interactive dynamic vegetation (OAV experiments), rainfall intensification is much more pronounced in this model. In the Sahara/Sahel region, the dynamic vegetation enhances the orbitally triggered summer rainfall anomaly by approximately 20 % in both the early (9 ka) and mid-Holocene (6 ka) experiments. The primary vegetation-atmosphere feedback identified here operates through surface latent heat flux anomalies by canopy evapotranspiration and their effect on the African Easterly Jet (AEJ). As such, the vegetation feedback relies on enhanced sur-

face (evaporational) cooling as opposed to the Charney feedback which operates through atmospheric instability by decreased surface albedo. Neglecting canopy evaporation, as in some previous model studies, could substantially affect the simulation of evaporative cooling such that the positive vegetation-atmosphere feedback might disappear. This type of climate-vegetation feedback over North Africa does not apply to other monsoon regions, since the feedback mechanism is closely linked to the characteristics of the regional atmospheric circulation (e.g. the presence of the AEJ). However, the North African climate-vegetation feedback should work also in other periods of time than the Holocene. Even though CCSM3-DGVM simulates a positive vegetation-precipitation feedback over North Africa, this feedback is not strong enough to produce multiple equilibrium climate-ecosystem states on a regional scale.

- The results in Chapter 5 show that sensitivity of GrIS to MIS 11 climate forcing is stronger than to MIS 5 forcing. The abcense of GrIS at 410 ka is high likely attribute to larger GHG forcing and a stronger heat transport towards high latitudes by the AMOC. The model results point out a substantial modification of orbital insolation forcing by internal climate feedbacks, which add significant complexity to the traditional Milankovitch theory. Even though a set of tuning parameters yields a realistic simulation of the modern GrIS, this does not ensure a realistic simulation of the LIG or MIS 11 ice-sheet using the same set of parameters. In this study, an example was given by one experiment 67, in which the GrIS almost completely disappeared within a few thousand years in response to LIG and MIS 11 climate forcing. A too high value for the lapse rate was identified to be the main cause for this outcome.

6.2 Outlook

This study reaffirms the different roles of obliquity, precession and GHG forcing on surface temperature and precipitation patterns between and within Quaternary interglacials based on different aspects of inter- and intra-interglacial variability and associated astronomical forcing. Nevertheless, to develop a significantly deeper understanding of interglacial climate dynamics in future studies, more simulations of earliear intergacials climates ideally coupled interactive ice-sheet models have to be done. So far, transient CGCM simulations have been performed for the present (e.g., Lorenz and Lohmann , 2004; Varma et al., 2012; Liu et al., 2014) and the last interglacial (e.g., Bakker et al., 2013; Govin et al., 2014). More-

over, the potential model-dependencies especially when DGVM is enabled remains equivocal. In order to cope with the uncertainties regarding the potential model-dependencies, further sensitivity studies are needed to assess the the robustness of the current results. Besides model resolution and PFT characteristics in the vegetation model, sensitivity studies should particularly address the effects of different parameterizations for land surface evaporation, transpiration and albedo. Furthermore, the approach done in this study does not allow a quantitative estimate of GrIS volumes due to several shortcomings in the experimental setup. Therefore, future studies should simulate the GrIS evolution in interactively coupled CGCM-ice sheet transient experiments. Ideally, such transient experiments would include the preceding terminations as these may precondition the evolution of the subsequent interglacials (cf. Past Interglacials Working Group of PAGES (2016).

References

Alley, R. B., Andrews, J. T., Brigham-Grette, J., Clarke, G. K. C., Cuffey, K. M., Fitzpatrickf, J.J., Funderg, S., Marshallh, S.J., Millerb, G.H., Mitrovicai, J.X., Muhsf, D.R., Otto-Bliesner, B.L., Polyakk, L., White, J. W. C.: History of the Greenland Ice sheet: paleoclimate insights, Quat. Sci. Rev., 29, 1728–1756, 2010.

Anderson, P., Bermike, O., Bigelow, N., Brigham-Grette, J., Duvall, M., Edwards, M., Frechette, B., Funder, S., Johnsen, S., Knies, J., Koerner, R., Lozhkin, A., Marshall, S., Matthiessen, J., Macdonald, G., Miller, G., Montoya, M., Muhs, D., Otto-Bliesner, B., Overpeck, J., Reeh, N., Sejrup, H. P., Spielhagen, R., Turner, C., Velichko, A., and Members, C.-L. I. P. a: Last Interglacial Arctic warmth conffirms polar amplification of climate change, Quat. Sci. Rev., 25, 1383–1400, 2006.

Bakker, P., Stone, E. J., Charbit, S., Groeger, M., Krebs-Kanzow, U., Ritz, S. P., and Schulz, M.: Last interglacial temperature evolutiona model inter-comparison, Clim. Past, 9, 605–619, 2013.

Bamber, J. L., Layberry, R., and Gogineni, P: A new ice thickness and bed data set for the Greenland ice sheet 1. Measurement, data reduction, and errors, J. Geophys. Res., 106, 33773–33780, 2001.

Bauch, H. A., Erlenkeuser, H., Helmke, J. P., Struck, U.: A paleoclimatic evaluation of marine oxygen isotope stage 11 in the high-northern Atlantic (Nordic seas), Global and Planetary Change, 24, 2–39, 2000.

Bauch, H. A.: Interglacial climates and the Atlantic meridional overturning circulation: Is there an Arctic controversy? Quat. Sci. Rev., 63, 1–22, 2013.

Bartlein, P. J., Harrison, S. P., Brewer, S., Connor, S., Davis, B. A. S., Gajewski, K., Guiot, J., Harrison-Prentice, T. I., Henderson, A., Peyron, O., Prentice, I. C., Scholze, M., Seppa, H., Shuman, B., Sugita, S., Thompson, R. S., Viau, A. E., Williams, J., Wu, H.: Pollen-based continental climate reconstructions at 6 and 21 ka: A global synthesis, Clim. Dynam., 37, 775–802, 2011.

Bathiany, S., Claussen, M., and Fraedrich, K.: Implications of climate variability for the detection of multiple equilibria and for rapid transitions in the atmosphere-vegetation system, Clim. Dynam., 38, 1775–1790, 2012.

Berger, A.: Long-term variations of daily insolation and Quaternary Climatic Changes, J. Atmos. Sci., 35, 2362–2367, 1978.

Berger, A. and Loutre, M. F.: Insolation values for the climate of the last 10 million years, Quat. Sci. Rev., 10, 297–317, 1991.

Beyerle, U., Rueedi, J., Leuenberger, M., Aeschbach-Hertig, W., Peeters, F., Kipfer, R., and Dodo, A.: Evidence for periods of wetter and cooler climate in the Sahel between 6 and 40 kyr BP derived from groundwater, Geophys. Res.Lett., 30, 1173, doi:10.1029/2002GL016310, 2003.

Bloemendal, J., deMenocal, P.: Evidence for a change in the periodicity of tropical climate cycles at 2.4 Myr from whole-core magnetic susceptibility measurements, Nature, 342, 897–900, 1989.

Bonan, G. B. and Levis, S.: Evaluating aspects of the Community Land and Atmosphere Models (CLM3 and CAM) using a dynamic global vegetation model, J. Climate, 19, 2290–2301, 2006.

Bonan, G. B., Levis, S., Sitch, S., Vertenstein, M., and Oleson, K. W.: A dynamic global vegetation model for use with climate models: concepts and description of simulated vegetation dynamics, Global Change Biol., 9, 1543–1566, 2003.

Born, A., and Nisancioglu, K. H.: Melting of Northern Greenland during the last interglaciation, The Cryosphere, 6, 1239–1250, 2012.

Bosmans, J. H. C., Drijfhout, S. S., Tuenter, E., Lourens, L. J., Hilgen, F. J., and Weber, S. L.: Monsoonal response to mid-holocene orbital forcing in a high resolution GCM, Clim. Past, 8, 723–740, doi:10.5194/cp-8-723-2012, 2012.

Bosmans, J. H. C., Drijfhout, S. S., Tuenter, E., Hilgen, F. J. and Lourens, L. J.: Response of the North African summer monsoon to precession and obliquity forcings in the EC-Earth GCM, Clim. Dynam., 44, 279–297, doi:10.1007/s00382-014-2260-z, 2015.

Bouimetarhan, I., Prange, M., Schefuss, E., Dupont, L., Lippold, J., Mulitza, S., and Zonneveld, K.: Sahel megadrought during Heinrich Stadial 1: evidence for a three-phase evolution of the low- and mid-level West African wind system, Quat. Sci. Rev., 58, 66–76, 2012.

Bowen, D.Q.: Sea level 400,000 years ago (MIS 11): analogue for present and future sea-level?, Clim. Past, 6, 19–29, 2010.

Braconnot, P., Loutre, M. F., Dong, B., Joussaume, S., Valdes, P.: How the simulated change in monsoon at 6 ka BP is related to the simulation of the modern climate: results from the Paleoclimate Modeling Intercomparison Project, Clim. Dynam., 19, 107–121, 2002.

Braconnot, P., Harrison, S., Joussaume, J., Hewitt, C., Kitoh, A., Kutzbach, J., Liu, Z., Otto-Bleisner, B. L., Syktus, J., Weber, S. L.: Evaluation of coupled ocean-atmosphere simulations of the mid-Holocene. In: Batterbee et al (ed) Past climate variability through Europe and Africa, Kluwer, Dordrecht, 2004.

Braconnot, P., Otto-Bliesner, B., Harrison, S., Joussaume, S., Peterchmitt, J. Y., Abe-Ouchi, A., Crucifix, M., Driesschaert, E., Fichefet, Th., Hewitt, C. D., Kageyama, M., Kitoh, A., Loutre, M.-F., Marti, O., Merkel, U., Ramstein, G., Valdes, P., Weber, L., Yu, Y., and Zhao, Y.: Results of PMIP2 coupled simulations of the Mid-Holocene and Last Glacial MaximumPart 1: experiments and large-scale features, Clim. Past, 3, 261–277, 2007.

Braconnot, P., Marzin, C., Gregoire, L., Mosquet, E., and Marti., O: Monsoon response to changes in Earths orbital parameters: comparisons between simulations of the Eemian and of the Holocene, Clim. Past, 4, 281–294, 2008.

Briegleb, B. P., Bitz, C. M., Hunke, E. C., Lipscomb, W. H., Holland, M. M., Schramm, J. L., and Moritz, R. E.: Scientific description of the sea ice component in the Community Climate System Model, Version Three, Tech. Rep. NCAR/TN-463+STR, NCAR, Boulder, CO, 2004.

Brovkin, V. and Claussen, M.: Comment on Climate-Driven Ecosystem Succession in the Sahara: The Past 6000 Years, Science, 322, 1326, doi:10.1126/science.1163381, 2008.

Brovkin, V., Claussen, M., Petoukhov, V., and Ganopolski, A.: On the stability of the atmosphere-vegetation system in the Sahel/Sahara region, J. Geophys. Res., 103, 31613–31624, 1998.

Brubaker, K. L., Entekhabi, D., and Eagleson, P. S.: Estimation of continental precipitation recycling, J. Climate, 6, 1077–1089, 1993.

Bunker A. F.:Computations of surface energy flux and annual air-sea interaction cycles of the North Atlantic Ocean, Monthly Weather Report, 104, 1122–1140, 1976.

Bunker, A. F.:Trends of variables and energy fluxes over the Atlantic Ocean from 1948 to 1972, Mon. Weather Rev., 108, 720–732, 1980.

Bunker, A. F., and Worthington, L. V.: Energy exchange charts of the North Atlantic Ocean, Bull. Am. Meteorol. Soc., 57, 670–678, 1976.

CAPE Last Interglacial Project Members, Last Interglacial Arctic warmth confirms polar amplification of climate change, Quat. Sci. Rev., 25, 1383–1400, doi: 10.1016/ j.quascirev.2006.01.033, 2006.

Charney, J. G.: Dynamics of deserts and drought in the Sahel, Q. J. Roy. Meteorol. Soc., 101, 193–202, 1975.

Charney, J. G., Stone, P. H., and Quirk, W. J.: Reply, Science, 191, 100–102, 1976.

Chen, G.S, Kutzbach, J.E, Gallimore, R., Liu, Z.: Calendar effect on phase study in paleoclimate transient simulation with orbital forcing, Clim. Dynam., 37, 1949–1960, doi:10.1007/s00382-010-0944-6, 2011.

Chen, F., Friedman, S., Gertler, C. G., Looney, J., OConnell, N., Sierks, K., and Mitrovica, J. X.: Refining estimates of polar ice volumes during the MIS11 Interglacial using sea level records from South Africa, J. Climate, 27, 8740–8746, doi: 10.1175/ JCLI-D-14-00282.1, 2014.

Church, J.A., Clark, P.U., Cazenave, A., Gregory, J. M., Jevrejeva, S., Levermann, A., Merrifield, M. A., Milne, G. A., Nerem, R. S., Nunn, P. D., Payne, A. J., Pfeffer, W. T., Stammer, D., and Unnikrishnan, A. S.: Sea Level Change. In: Climate Change 2013: The Physical Science Basis. Contribution of Working Group I to the Fifth Assessment Report of the Intergovernmental Panel on Climate Change [Stocker, T.F., D. Qin, G.-K. Plattner, M. Tignor, S.K. Allen, J. Boschung, A. Nauels, Y. Xia, V. Bex and P.M. Midgley (eds.)]. Cambridge University Press, Cambridge, United Kingdom and New York, NY, USA, 2013.

Claussen, M.: On coupling global biome models with climate models, Climate Res., 4, 203–221, 1994.

Claussen, M.: Modelling biogeophysical feedback in the African and Indian Monsoon region, Clim. Dynam., 13, 247–257, 1997.

Claussen, M.: On multiple solutions of the atmosphere-vegetation system in present-day climate, Global Change Biol., 5, 549–559, 1998.

Claussen, M.: Introduction to Climate Forcing and Climate Feedbacks, In: The Climate Past of Interglacials [Sirocko, F., Claussen, M., Goni Sanchez, M. F., and Litt, T.], Developments in Quartenary Science, 7, 2007.

Claussen, M.: Late Quaternary vegetation-climate feedbacks, Clim. Past, 5, 203–216, doi:10.5194/cp-5-203-2009, 2009.

Claussen, M. and Gayler, V.: The greening of Sahara during the mid-Holocene: Results of an interactive atmosphere-biome model, Global Ecol. Biogeogr., 6, 369–377, 1997.

Claussen, M., Brovkin, V., Ganopolski, A., Kubatzki, C., and Petoukhov, V.: Modeling global terrestrial vegetation-climate interaction, Philos. T. Roy. Soc. Lond. B, 353, 53–56, doi:10.1098/rstb.1998.0190, 1998.

Claussen, M., Kubatzki, C., Brovkin, V., Ganopolski, A., Hoelzmann, P., Pachur, H. J.: Simulation of an abrupt change in Saharan vegetation in the mid-Holocene, Geophys. Res. Lett., 26, 2037–2040, doi:10.1029/1999GL900494, 1999.

Claussen, M., Bathiany, S., Brovkin, V., and Kleinen, T.: Simulated climate-vegetation interaction in semi-arid regions affected by plant diversity, Nature Geoscience, 6(11), 954–958, 2013.

Coe, M. and Bonan, G.: Feedbacks between climate and surface water in northern Africa during the middle Holocene, J. Geophys. Res., 102, 11087–11101, doi:10.1029/97JD00343, 1997.

Collins, W. D., Rasch, P. J., Boville, B. A., Hack, J. J., McCaa, J. R., Williamson, D. L., Kiehl, J. T., Briegleb, B., Bitz, C., Jiann Lin, S., Zhang, M., and Dai, Y.: Description of the NCAR Community Atmosphere Model (CAM 3.0), Technical Report NCAR/TN-464+STR, NCAR, Boulder, CO, 2004.

Collins, W. D., Bitz, C. M., Blackmon, M. L., Bonan, G. B., Bretherton, C. S., Carton, J. A., Chang, P., Doney, S. C., Hack, J. J., Henderson, T. B., Kiehl, J. T., Large, W. G., McKenna, D. S., Santer, B. D., and Smith, R. D.:: The Community Climate System Model version 3 (CCSM3), J. Climate., 19, 2122–2143, 2006a.

Collins, W. D., Rasch, P. J., Boville, B. A., Hack, J. J., McCaa, J. R., Williamson, D. L., Briegleb, B., Bitz, C., Jiann Lin, S., and Zhang, M.: The formulation and atmospheric simulation of the Community Atmosphere Model version 3 (CAM3), J. Climate, 19, 2144–2161, 2006b.

Collins, W. D., Bitz, C. M., Blackmon, M. L., Bonan, G. B., Bretherton, C. S., Carton, J. A., Chang, P., Doney, S. C., Hack, J. J., Henderson, T. B., Kiehl, J. T., Large, W. G., McKenna, D. S., Santer, B. D., and Smith, R. D.: The Community Climate System Model version 3 (CCSM3), J. Climate, 19, 2122–2143, 2006.

Collins, J. A., Schefuss, E., Mulitza, S., Prange, M., Werner, M., Tharammal, T., Paul, A., and Wefer, G.: Estimating the hydrogen isotopic composition of past precipitation using leaf-waxes from western Africa, Quat. Sci. Rev., 65, 88–101, 2013.

Cook, K. H.: Generation of the African Easterly Jet and Its Role in Determining West African Precipitation, J. Climate, 12, 1165–1184, 1999.

Cook, K. H., and Vizy, E. K.: Coupled model simulations of the West African monsoon system: Twentieth- and twenty-first-century simulations, J. Climate, 19, 3681–3703, 2006.

Colville, E. J., Carlson, A. E., Beard, B. L., Hatfield, R. G., Stoner, J. S., Reyel, A. V., and Ullman, D. J.: Sr-Nd-Pb Isotope evidence for ice sheet presence on southern during the Last Interglacial, Science, 2011.

Cronin, T. M., Polyak, L., Reed, D., Kandiano, E. S., Marzen, R. E., and Council, E. A.: A 600-ka Arctic sea-ice record from Mendeleev Ridge based on ostracodes, Quat. Sci. Rev., 79, 157–167, doi: 10.1016/j.quascirev.2012.12.010, 2013.

Crucifix, M., Loutre, F. M.: Transient simulations over the last interglacial period (126-115 kyr BP): feedback and forcing analysis, Clim. Dynam., 19, 417–433, 2002

Dai, A., Meehl, G. A., Washington, W. M., Wigley, T. M. L., and Arblaster, J. M.: Ensemble simulation of twenty-first century climate changes: Business-as-usual versus CO_2 stabilization, Bull. Am. Meteorol. Soc., 82, 2377–2388, 2001.

Dallmeyer, A., Claussen, M., Fischer, N., Haberkorn, K., Wagner, S., Pfeiffer, M., Jin, L., Khon, V., Wang, Y., and Herzschuh, U.: The evolution of sub-monsoon systems in the Afro-Asian monsoon region during the Holocene comparison of different transient climate model simulations, Clim. Past, 11, 305–326, doi:10.5194/cp-11-305-2015, 2015.

Davis, B. A. S. and Brewer, S.: Orbital forcing and role of the latitudinal insolation/temperature gradient, Clim. Dynam., 32, 143–165, DOI:10.1007/s00382-008-0480-9, 2009.

De Abreu, C., Abrantes, F.F., Shackleton, N.J., Tzedakis, P.C., McManus, J.F., Oppo, D.W., Hall, M.A.: Ocean climate variability in the eastern North Atlantic during interglacial Marine Isotope Stage 11: A partial analogue to the Holocene? Paleoceanography, 20, PA3009, 2005.

DeConto, R. M. and Pollard, D.: Rapid Cenozoic glaciation of Antarctica induced by declining atmospheric CO_2, Nature, 421, 245–249, 2003.

DeFries, R. S., Townshend, J. R. G., and Hansen, M. C.: Continuous fields of vegetation characteristics at the global scale at 1 km resolution, J. Geophys. Res., 104, 16911–16925, 1999.

DeFries, R. S., Hansen, M. C., Townshend, J. R. G., Janetos, A. C., Loveland, T. R.: A new global 1-km dataset of percentage tree cover derived from remote sensing, Global Change Biol., 6, 247–254, 2000.

Delworth, T. L., and Greatbatch,R. J.: Multidecadal thermohaline circulation variability driven by atmospheric surface flux forcing, J. Climate, 13, 1481–1495, 2000.

deMenocal, P. B., Ruddiman, W. F., Pokras, E. K.: Influences of high-and low-latitude processes on African terrestrial climate: Pleistocene eolian records- Paleoceanography, 209–242, 1993.

deMenocal, P. B.: Plio-Pleistocene African climate, Science, 53-59, 1995.

deMenocal, P., Ortiz, J., Guilderson, T., Adkins, J., Sarnthein, M., Baker, L., and Yarusinsky, M.: Abrupt onset and termination of the African humid period: Rapid climate responses to gradual insolation forcing, Quat. Sci. Rev., 19, 347–361, 2000.

deMenocal, P. B., and Tierney, J. E.: Green Sahara: African humid periods paced by earth's orbital changes, Nature Education Knowledge, 3, 12, 2012.

de Noblet, N., Braconnot, P., Joussaume, S., and Masson, V.,: Sensitivity of simulated Asian and African boreal summer monsoons to orbitally induced variations in insolation 126, 115 and 6 kBP, Clim. Dynam., 12, 589–603, 1996.

Doherty, R. M., Kutzbach, J., Foley, J., and Pollard, D.: Fully- coupled climate/dynamical vegetation model simulations over Northern Africa during the mid-Holocene, Clim. Dynam., 16, 561–567, 2000.

Droxler, A.W., Alley, R.B., Howard, W.R., Poore, R.Z., Burckle, L.H.: Unique and exceptionally long Interglacial Marine Isotope Stage 11: Window into earth future climate. In: Droxler, A.W., Poore, R.Z., Burckle, L.H. (Eds.), Earth's climate and orbital eccentricity: The Marine Isotope Stage 11 Question, Geophysical Monograph, 137, American Geophysical Union, 2003.

Dutton, A. and Lambeck, K.: Ice volume and sea level during the Last Interglacial, Science, 337, 216–219, 2012.

Dutton, A., Carlson, A. E., Long, A. J., Milne, G. A., Clark, P. U., DeConto, R., Horton, B. P., Rahmstorf, S., and Raymo, M. E.: Sea-level rise due to polar ice-sheet mass loss during past warm periods, Science, 349, 6244, 2015.

Dutton, A., Webster, J. M., Zwartz, D., Lambeck, K., Wohlfarth, B.: Tropical tales of polar ice: Evidence of last interglacial polar ice sheet retreat recorded by fossil reefs of the granitic Seychelles islands, Quat. Sci. Rev., 107, 182–196, doi: 10.1016/ j.quascirev.2014.10.025, 2015.

ECMWF: ECMWF ERA-40 Re-Analysis data. Available from British Atmospheric Data Centre at: http://badc.nerc.ac.uk/browse/badc/ecmwf-e40/data [Accessed on 13 March 2009], 2006.

Erb, M. P., Broccoli, A. J., and Clement, A. C.: The contribution of radiative feedbacks to orbitally driven climate change, J. Climate, 26, 5897–5914, 2013.

Fischer, N. and Jungclaus, J. H.: Effects of orbital forcing on atmosphere and ocean heat transports in Holocene and Eemian climate simulations with a comprehensive Earth system model, Clim. Past, 6, 155–168, 2010.

Fleitmann, D., Burns, S. J., Mudelsee, M., Neff, U., Kramers, J., Mangini, A., and Matter, A.: Holocene forcing of the Indian monsoon recorded in a stalagmite from Southern Oman, Science, 300, 1737–1739, 2003.

Francus, P., von Suchodoletz, H., Dietze, M., Donner, R. V., Bouchard, F., Roy, A.-J., Fagot, D., Verschuren, D., and Kröpelin, S.: Varved sediments of Lake Yoa (Ounianga Kebir, Chad) reveal progressive drying of the Sahara during the last 6100 years, Sedimentology, 60, 911–934, doi:10.1111/j.1365-3091.2012.01370.x, 2013.

Gallimore, R. G., and Kutzbach, J. E.: Role of orbitally induced changes in tundra area in the onset of glaciation, Nature, 381, 503–505, 1996.

Govin, A., Varma, V., and Prange, M.: Astronomically forced variations in western African rainfall (21° N-20° S) during the Last Interglacial period, Geophys. Res. Lett., 41, 2117–2125, doi: 10.1002/2013Gl058999, 2014.

Grist, J. P. and Nicholson, S. E.: A study of the dynamic factors influencing the interannual variability of rainfall in the West African Sahel, J. Climate, 14, 1337–1359, 2001.

Gregory, J. M., P. A. Stott, D. J. Cresswell, N. A. Rayner, C. Gordon, and D. M. H. Sexton: Recent and future changes in Artic sea-ice simulated by the HadCM3 AOGCM, Geophys. Res. Lett., 29, 2175, doi:10.1029/2001GL014575, 2002.

Gregory, J. M., Dixon, K.W., Stouffer, R.J., Weaver, A.J., Driesschaert, E., Eby, M.: A model intercomparison of changes in the Atlantic thermohaline circulation in response to increasing atmospheric CO_2 concentration, Geophys. Res. Lett., 32, L12703, doi:10.1029/ 2005GL023209, 2005.

Greve, R., Saito, F., and Abe-Ouchi, A.: Initial results of the SeaRISE numerical experiments with the models SICOPOLIS and IcIES for the Greenland ice sheet, Ann. Glaciol., 52, 23–30, 2011.

Gruell, W., and Oerlemans, J.: Sensitivity studies with a mass balance nodel including temperature profile calculations inside the glacier, Zeitschrift fuer Gletscherkunde und Glazialgeologie, 22, 101–124, 1986.

Hales, K., Neelin, J. D., and Zeng, N.: Interaction of vegetation and atmospheric dynamical mechanisms in the mid-holocene African monsoon, J. Climate, 19, 4105–4120, 2006.

Hanna, E., Huybrechts, P., Janssens, I., Cappelen, J., Steffen, K., and Stephens, A. : Runoff and mass balance of the Greenland ice sheet: 1958-2003, Journal of Geophysical Research-Atmospheres, 110, doi:10.1029/2004JD005641, 2005.

Hanna, E., Huybrechts, P., Steffen, K., Cappelen, J., Huff, R., Shuman, C., Irvine-Fynn, T., Wise, S., and Griths, M.: Increased runoff from melt from the Greenland Ice Sheet: A response to global warming. J. Climate, 21,331–341, 2008.

Handiani, D., Paul, A., Prange, M., Merkel, U., Dupont, L., and Zhang, X.: Tropical vegetation response to Heinrich Event 1 as simulated with the UVic ESCM and CCSM3, Clim. Past, 9, 1683–1696, doi:10.5194/cp-9-1683-2013, 2013.

Hays, J. D., Imbrie, J., and Shackleton, N. J.: Variations in the Earth's orbit: Pacemaker of the Ice Ages, Science, 194, 1121–1132, 1976.

Hearty, P. J., Kindler, P., Cheng, H., and Edwards, R. L.: A +20m middle Pleistocene sea-level highstand (Bermuda and the Bahamas) due to partial collapse of Antarctic ice, Geology, 27, 375–378, 1999.

Helmke, J.P., Bauch, H.A., Erlenkeuser, H.: Development of glacial and interglacial conditions in the Nordic seas between 1.5 and 0.35 Ma. Quat. Sci. Rev., 22, 1717–1728, 2003.

Helsen, M. M., van de Berg, W. J., van de Wal, R. S. W., van den Broeke, M. R., and Oerlemans, J.: Coupled regional climate-ice-sheet simulation shows limited Greenland ice loss during the Eemian, Clim. Past, 9, 2013.

Herold, N., Yin, Q. Z., Karami, M. P., Berger, A.: Modelling the climatic diversity of the warm interglacials, Quat. Sci. Rev., 68, 237, 2012.

Hessler, I., Harrison, S. P., Kucera, M., Waelbroeck, C., Chen, M. T., Anderson, C., and Londeix, L.: Implication of methodological uncertainties for Mid-Holocene sea surface temperature reconstructions, Clim. Past, 10, 2237–2252, 2014.

Hoelzmann, P., Jolly, D., Harrison, S. P., Laarif, F., Bonnefille, R., and Pachur, H. J.: Mid-Holocene land surface conditions in northern Africa and the Arabian Peninsula: A data set for the analysis of biogeochemical feedbacks in the climate system, Global Biogeochem. Cy., 12, 35–52, 1998.

Howard, W.: A warm future in the past, Nature, 388, 418–419, 1997

Huybers, P.: Early Pleistocene glacial cycles and the integrated summer insolation forcing, Science, 313, 508–511, 2006.

Huybrechts, P., Gregory, J., Janssens, I., and Wild, M: Modelling Antarctic and Greenland volume changes during the 20th and 21st centuries forced by GCM time slice integrations, Global Planet. Change, 42, 83–105, 2004.

IPCC: Climate Change 2001: The Scientific Basis. Contribution of Working Group I to the Third Assessment Report of the Intergovernmental Panel on Climate Change [Houghton, J.T., Ding, Y., Griggs, D. J., Noguer, M., van der Linden, P. J., Dai, X., Maskell, K., and Johnson, C. A., (eds.)], Cambridge University Press, Cambridge, United Kingdom and New York, NY, USA, 2001.

Jansen, E., Overpeck, J., Briffa, K. R., Duplessy, J. C., Joos, F., Masson-Delmotte, V., Olago, D., Otto-Bliesner, B., Peltier, W. R., Rahmstorf, S., Ramesh, R., Raynaud, D., Rind, D., Solomina, O., Villalba, R., and Zhang, D.: Palaeo- climate. In S. Solomon, D. Qin, M. Manning, Z. Chen, M. Marquis, K. B. Averyt, M. Tignor, and H. L. Miller, editors, Climate Change 2007: The Physical Sci- ence Basis. Contribution of Working Group I to the Fourth Assessment Report of the Intergovernmental Panel on Climate Change, Cambridge University Press, Cambridge, United Kingdom and New York, NY, USA, 2007.

Jochum, M., Jahn, A., Peacock, S., Bailey, D. A., Fasullo, J. T., Kay, J., Levis, S., and Otto-Bliesner, B.: True to Milankovitch: Glacial inception in the new Community Climate System Model, J. Climate, 25, 2226–2239, 2012.

Jolly, D., Harrison, S. P., Damnati, B., and Bonnefille, R.: Simulated climate and biomes of Africa during the Late Quaternary: comparison with pollen and lake status data, Quat. Sci. Rev., 17, 629–657, 1998.

Joussaume, S., and Braconnot, P.: Sensitivity of paleoclimate simulation results to season definitions, J. Geophys. Res., 102, 1943–1956, 1997.

Jouzel, J., Masson-Delmotte, V., Cattani, O., Dreyfus, G., Falourd, S., Hoffmann, G., Minster, B., Nouet, J., Barnola, J. M., Chappellaz, J., Fischer, H., Gallet, J. C., Johnsen, S., Leuenberger, M., Loulergue, L., Luethi, D., Oerter, H., Parrenin, F., Raisbeck, G., Raynaud, D., Schilt, A., Schwander, J., Selmo, E., Souchez, R., Spahni, R., Stauffer, B., Steffensen, J. P., Stenni, B., Stocker, T. F., Tison, J. L., Werner, M., Wolff, E. W.: Orbital and millennial Antarctic climate variability over the past 800,000 years, Science, 317, 793–796, 2007.

Kandiano, E.S., and Bauch, H.A.: Surface ocean temperatures in the north-east Atlantic during the last 500,000 years: evidence from foraminiferal census data, Terra Nova 15, 265–271, 2003.

Kandiano, E. S., Van der Meer, M., Schouten, S., Fahl, K., Polyak, L., Cronin, T., Bauch, H. A., and Sinninghe Damste, J. S.: SST and salinity patterns in the northern North Atlantic and the Arctic during interglacial MIS 11c: Implications for oceanic circulation reconstruction , AGU Fall Metting, San Francisco, 9 December 2013 - 13 December 2013, 2013.

Kaspar, F., Kuhl, N., Cubasch, U., and Litt, T.: A model-data comparison of European temperatures in the Eemian interglacial, Geophys. Res. Lett., 32, doi:10.1029/2005GL022456, 2005.

Kaspar, F., and Cubasch, U.: Simulation of the Eemian interglacial and possible mechanisms for the glacial inception, Geological Society of America Special Papers, 426, 29–41, 2007.

Khodri, M., Cane, M. A., Kukla, G., Gavin, J., and Braconnot, P.: The impact of precession changes on the Arctic climate during the last interglacial-glacial transition, Earth and Planetary Science Letters, 236, 285–304, 2005.

Kleinen, T., Hildebrandt, S., Prange, M., Rachmayani, R., Müller, S., Bezrukova, S., Brovkin, V., Tarasov, P.: The climate and vegetation of Marine Isotope Stage 11 - model results and proxy-based reconstructions at global and regional scale, Quaternary International, 348, 247–265, doi:10.1016/j.quaint.2013.12.028, 2014.

Kohfeld, K. E. and Harrison, S. P.: How well can we simulate past climates? Evaluating the models using global palaeoenvironmental datasets, Quat. Sci. Rev., 19, 321–345, 2000.

Koerner, R. and Fischer, H.: Ice-core evidence for widespread Arctic glacier retreat in the last Interglacial and the early Holocene, Annals of Glaciology, 35, 19–24, 2002.

Koerner, R. M.: Ice core evidence for extensive melting of the Greenland ice-sheet in the last Interglacial, Science, 244, 964–968, 1989.

Kopp, R. E., Simons, F. J., Mitrovica, J. X., Maloof, A. C., and Oppenheimer, M.: Probabilistic assessment of sea level during the last Interglacial stage, Nature, 462, 863–868, 2009.

Kopp, R. E., Simons, F. J., Mitrovica, J. X., Maloof, A. C., and Oppenheimer, M.: A probabilistic assessment of sea level variations within the last interglacial stage, Geophys. J. Int., 193, 711–716, 2013.

Kroon, D., Alexander, I., Little, M., Lourens, L. J., Matthewson, A., Robertson, A. H., and Sakamoto, T.: Oxygen isotope and sapropel stratigraphy in the eastern Mediterranean during the last 3.2 million years, Proceedings of the Ocean Drilling Program, Scientific Results, 160, 14, 1998.

Kröpelin, S., Verschuren, D., Lézine, A.-M., Eggermont, H., Cocquyt, C., Francus, P., Cazet, J.-P., Fagot, M., Rumes, B., Russell, J. M., Darius, F., Conley, D. J., Schuster, M., von Suchodoletz, H., and Engstrom, D. R.: Climate-driven ecosystem succession in the Sahara: The past 6000 years, Science, 320, 765–768, 2008.

Krinner, G., L*é*zine, A.-M., Braconnot, P., Sepulchre, P., Ramstein, G., Grenier, C., and Gouttevin, I.: A reassessment of lake and wetland feedbacks on the North African Holocene climate, Geophys. Res. Lett., 39, L07701, doi:10.1029/2012GL050992, 2012.

Kubatzki, C., Montoya, M., Rahmstorf, S., Ganopolski, A., Claussen, M.: Comparison of a coupled global model of intermediate complexity and an AOGCM for the last interglacial, Clim. Dynam., 16, 799–814, 2000.

Kutzbach, J. E.: Monsoon climate of the early Holocene- climate experiment with the earths orbital parameters for 9000 years ago, Science, 214, 59–61, 1981.

Kutzbach, J. E. and Liu, Z.: Response of the African monsoon to orbital forcing and ocean feedbacks in the middle Holocene, Science, 278, 440–444, 1997.

Kutzbach, J. E. and Street-Perrot, E. A.: Milankovitch forcing of fluctuations in the level of tropical lakes from 18 to 0 ka, Nature, 317, 130–134, 1985.

Kutzbach, J. E., Bonan, G., Foley, J., and Harrison, S. P.: Vegetation/soil feedbacks and African monsoon response to orbital forcing in the Holocene, Nature, 384, 623–626, 1996.

Kuhn, M.: On the computation of heat transfer coefficients from energy-balance gradients on a glacier, Journal of Glacialogy, 22, 263–272, 1979.

Lang, N., and Wolff, E. W.: Interglacial and glacial variability from the last 800 ka in marine, ice and terrestrial archives, Clim. Past, 7, 361–380, 2011.

Lawrence, P. J., and Chase, T. N.: Representing a new MODIS consistent land surface in the Community Land Model (CLM3.0), J. Geophys. Res., 112, G01023, doi:10.1029/2006JG000168, 2007.

Levermann, A., Clark, P. U., Marzeion, B., Milne, G. A., Pollard, D., Radic, V., and Robinson, A.: The multimillennial sea-level commitment of global warming. Proceedings of the National Academy of Sciences, 110, 13745–13750, 2013.

Levis, S., Bonan, G. B., and Bonfils, C.: Soil feedback drives the Mid-Holocene North African monsoon northward in fully coupled CCSM2 simulations with a dynamic vegetation model, Clim. Dynam., 23, 791–802, 2004a.

Levis, S., Bonan, G. B., Vertenstein, M., and Oleson, K. W.: The Community Land Model's Dynamic Global Vegetation Model (CLM-DGVM): Technical description and user's guide, NCAR Technical Note NCAR/TN-459+IA, National Center for Atmospheric Research, Boulder, CO, 2004b.

Levitus, S., Antonov, J.I., Wang, J., Delworth, T.L., Dixon, K.W., and Broccoli, A.J.: Anthropogenic warming of Earths climate system, Science, 292, 267–270, 2001.

Lézine, A., Hély, C., Grenier, C., Braconnot, P., Krinner, G.: Sahara and Sahel vulnerability to climate changes, lessons from Holocene hydrological data, Quat. Sci. Rev., 30, 3001–3012, 2011.

Lisiecki, L. E., and Raymo, M. E.: A Pliocene-Pleistocene stack of 57 globally distributed benthic d^{18}O records, Paleoceanography, 20, PA1003, 2005.

Liu, Z., Wang, Y., Gallimore, R., Notaro, M., and Prentice, C. I.: On the mechanism of abrupt change of Northern Africa environment in the Holocene: Climate variability vs. vegetation feedback, Geophys. Res. Lett., 33, L22709, doi:10.1029/2006GL028062, 2006.

Liu, Z., Wang, Y., Gallimore, R., Gasse, F., Johnson, T., deMenocal, P., Adkins, J., Notaroa, M., Prentice, I. C., Kutzbach, J., Jacob, R., Behling, P., Wang, L., and Ong, E.: Simulating the transient evolution and abrupt change of Northern Africa atmosphere-ocean-terrestrial ecosystem in the Holocene, Quat. Sci. Rev., 26, 1818–1837, 2007.

Liu, Z., Notaro, M., and Gallimore, R.: Indirect vegetation soil moisture feedback with application to Holocene North Africa climate, Global Change Biol., 16, 1733–1743, 2010.

Liu, Z., Zhu, J., Rosenthal, Y., Zhang, X., Otto-Bliesner, B. L., Timmermann, A., Smith, R. S., Lohmann, G., Zheng, W., and Timm, O. E.: The Holocene temperature conundrum, PNAS, 111, E3501–E3505, doi:10.1073/pnas.1407229111, 2014.

Lohmann, G., Pfeiffer, M., Laepple, T., Leduc, G., and Kim, J. H.: A model-data comparison of the Holocene global sea surface temperature evolution, Clim. Past, 9, 1807–1839, 2013.

Lorenz, S. J., and Lohmann, G.: Acceleration technique for Milankovitch type forcing in a coupled atmosphere-ocean circulation model: method and application for the Holocene, Clim. Dynam., 23, 727–743, 2004.

Loulergue, L., Schilt, A., Spahni, R., Masson-Delmotte, V., Blunier, T., Lemieux, B., Barnola, J.-M., Raynaud, D., Stocker, T. F., and Chappellaz, J.: Orbital and millennial-scale features of atmospheric CH_4 over the past 800,000 years, Nature, 453, 383–386, 2008.

Loutre, M. F. and Berger, A.: Future climatic changes: Are we entering an exceptionally long interglacial?, Climatic Change, 46, 61–90, 2000.

Loutre, M. F., and Berger, A.: Marine Isotope Stage 11 as an analogue for the present interglacial, Global and Planetary Change, 36, 209–217, 2003.

Loutre, M. F., Paillard, D., Vimeux, F., and Cortijo, E.: Does mean annual insolation have the potential to change the climate?, Earth Planet. Sci. Lett., 221, 1–14, 2004.

Lundberg, J., McFarlane, D.: Isotope stage 11 sea level in the Netherlands Antilles, Geol. Soc. Am. Abstr. Programs, 34, 31, 2002.

Lunt, D. J., Foster, G. L., Haywood, A. M., and Stone, E. J.: Late Pliocene Greenland glaciation controlled by a decline in atmospheric CO_2 levels. Nature, 454, 1102–1105, 2008.

Lunt, D. J., Haywood, A. M., Foster, G. L., and Stone, E. J.: The Arctic cryosphere in the Mid-Pliocene and the future. Philosophical Transactions of the Royal Society a-Mathematical Physical and Engineering Sciences, 367, 49–67, 2009.

Lunt, D. J., Abe-Ouchi, A., Bakker, P., Berger, A., Braconnot, P., Charbit, S., Fischer, N., Herold, N., Jungclaus, J. H., Khon, V. C., Krebs-Kanzow, U., Langebroek, P. M., Lohmann, G., Nisancioglu, K. H., Otto-Bliesner, B. L., Park, W., Pfeiffer, M., Phipps, S. J., Prange, M., Rachmayani, R., Renssen, H., Rosenbloom, N., Schneider, B., Stone, E. J., Takahashi, K., Wei, W., Yin, Q., and Zhang, Z. S.: A multimodel assessment of last interglacial temperatures, Clim. Past, 9, 699–717, doi:10.5194/cp-9-699-2013, 2013.

Lüthi, D., Le Floch, M., Bereiter, B., Blunier, T., Barnola, J.-M., Siegenthaler, U., Raynaud, D., Jouzel, J., Fischer, H., Kawamura, K., and Stocker, T. F.: High-resolution carbon dioxide concentration record 650,000 - 800,000 years before present, Nature, 453, 379–382, 2008.

Mantsis, D. F., Clement, A. C., Broccoli, A. J., and Erb, M. P.: Climate feedbacks in response to changes in obliquity, J. Climate, 24, 2830–2845, 2011.

Mantsis, D. F., Lintner, B. R., Broccoli, A. J., Erb, M. P., Clement, A. C., and Park, H. S.: The response of large-scale circulation to obliquity-induced changes in meridional heating gradients, J. Climate, 27, 5504–5516, 2014.

Marcott, S. A., Clark, P. U., Padman, L., Klinkhammer, G. P., Springer, S. R., Liu, Z., Otto-Bliesner, B. L.: Ice-shelf collapse from subsurface warming as a trigger for Heinrich events, Proc. Natl. Acad. Sci. U.S.A., 108, 13415–13419, doi: 10.1073/pnas.1104772108; pmid: 21808034, 2011.

Marzin, C., Braconnot, P., Kageyama, M.: Relative impacts of insolation changes, meltwater fluxes and ice sheets on African and Asian monsoons during the Holocene, Clim. Dynam., 41, 2267–2286, 2013.

Masson-Delmotte, V., B. Stenni, K. Pol, P. Braconnot, O. Cattani, S. Falourd, M. Kageyama: EPICA Dome C record of glacial and interglacial intensities, Quat. Sci. Rev., 29, 113–128, 2010.

Masson-Delmotte, V., Braconnot, P., Hoffmann, G., Jouzel., J., Kageyama, M., Landais, A., Lejeune, Q., Risi, C., Sime, L., Sjotte, J., Swingdouw, D., and VInther, B.: Sensitivity of interglacial Greenland temperature and d^{18}O: ice core data, orbital and increased CO_2 climate simulations, Clim. Past, 7, 1041–1059, 2011.

Masson-Delmotte, V., Schulz, M., Abe-Ouchi, A., Beer, J., Ganopolski, A., Rouco, J. F. G., Jansen, E., Lambeck, K., Luterbacher, J., Naish, T., Osborn, T., Otto-Bliesner, B., Quinn, T., Ramesh, R., Rojas, M., Shao, X., and Timmermann, A.: Information from Paleoclimate Archives. In: Climate Change 2013: The Physical Science Basis. Contribution of Working Group I to the Fifth Assessment Report of the Intergovernmental Panel on Climate Change [Stocker, T.F., D. Qin, G.-K. Plattner, M. Tignor, S.K. Allen, J. Boschung, A. Nauels, Y. Xia, V. Bex and P.M. Midgley (eds.)]. Cambridge University Press, Cambridge, United Kingdom and New York, NY, USA, 2013.

McClure, H. A.: Radiocarbon chronology of late Quaternary lakes in the Arabian Desert, Nature, 263, 755–756, 1976.

McCulloch, M. T., and Esat, T.: The coral record of last interglacial sea levels and sea surface temperatures, Chem. Geol, 169, 107–129, 2000.

McFarlane, D.A., Lundberg, J.: Amiddle Pleistocene age and biogeography for the extinct rodent Megalomys curazensis from Curaao, Netherlands Antilles, Caribb. J. Sci. 38, 278–281, 2002.

McManus, J. F., Oppo, D. W., and Cullen, J. L.: A 0.5-millionyear record of millennial-scale climate variability in the North Atlantic, Science, 283, 971–975, 1999.

McMurtry, G. M., Tappin, D. R., Sedwick, P. N., Wilkinson, I., Fietzked, J., Sellwood, B.: Elevated marine deposits in Bermuda record a late Quaternary megatsunami, Sedimentary Geology, 200, 3–4, 155–165, 2007.

Melles, M., Brigham-Grette, J., Minyuk, P. S., Nowaczyk, N. R., Wennrich, V., DeConto, R. M., Anderson, P. M., Andreev, A. A.,Coletti, A., Cook, T. L., Haltia-Hovi, E., Kukkonen, M., Lozhkin A. V., Rosen, P., Tarasov, P., Vogel, H., and Wagner, B.: 2.8 million years of Arctic climate change from Lake Elgygytgyn, NE Russia, Science, 337, 315–320, 2012.

Meissner, K. J., Weaver, A. J., Matthews, H. D., Cox, P. M.: The role of land-surface dynamics in glacial inception: a study with the UVic Earth System Climate Model, Clim. Dynam., 21, 519–537, 2003.

Milker, Y., Rachmayani, R., Weinkauf, M. F. G., Prange, M., Raitzsch, M., Schulz, M., and Kucera, M.: Global and regional sea surface temperature trends during Marine Isotope Stage 11, Clim. Past, 9, 2231–2252, doi:10.5194/cp-9-2231-2013, 2013.

Montoya, M., von Storch, H., and Crowley, T. J.: Climate simulation for 125 kyr BP with a coupled ocean-atmosphere general circulation model, J. Climate, 13, 1057–1072, 2000.

Muhs, D.R., Simmons, K.R., Schumann, R.R., Halley, R.B.: Sea-level history of the past two interglacial periods: new evidence from U-series dating of reef corals from south Florida, Quat. Sci. Rev., 30, 570–590, 2011.

Muhs, D.R., Pandolfi, J.M., Simmons, K.R., Schumann, R.R.: Sea-level history of past interglacial periods from uranium-series dating of corals, Curaao, Leeward Antilles islands, Quat. Res., 78, 157–169, 2012.

Muhs, D.R, Meco, J., Simmons, K. R.: Uranium-series ages of corals, sea level history, and palaeozoogeography, Canary Islands, Spain: An exploratory study for two Quaternary interglacial periods, Palaeogeography, Palaeoclimatology, Palaeoecology, 394, 99–118, 2014.

Mulitza, S., Prange, M., Stuut, J. B., Zabel, M., von Dobeneck, T., Itambi, C. A., Nizou, J., Schulz, M., and Wefer, G.: Sahel megadroughts triggered by glacial slowdowns of Atlantic meridional overturning, Paleoceanography, 23, PA4206, doi:10.1029/2008PA001637, 2008.

Muri, H., Berger, A., Yin, Q., Karami, M., Barriat, P. V.: The Climate of the MIS-13 Interglacial according to HadCM3, J. Climate, 26, 9696–9712, 2013.

NEEM community members: Eemian interglacial reconstructed from a Greenland folded ice core, Nature, 493, 489–494, 2013.

Notaro, M., Wang, Y., Liu, Z., Gallimore, R., and Levis, S.: Combined statistical and dynamical assessment of simulated vegetation-rainfall interactions in North Africa during the mid-Holocene, Global Change Biol., 14, 347–368, 2008.

NorthGRIP: High-resolution record of Northern Hemisphere climate extending into the last interglacial period, Nature, 431, 147–151, 2004.

Nicholson, S. E.: The intensity, location and structure of the tropical rainbelt over West Africa as a factor in interannual variability, Int. J. Climatol., 28, 1775–1785, 2008.

Nicholson, S. E. and Grist, J. P.: A conceptual model for understanding rainfall variability in the West African Sahel on interannual and interdecadal timescales, Int. J. Climatol., 21, 1733–1757, 2001.

Niedermeyer, E. M., Prange, M., Mulitza, S., Mollenhauer, G., Schefuss, E., and Schulz, M.: Extratropical forcing of Sahel aridity during Heinrich stadials, Geophys. Res. Lett., 36, L20707, doi:10.1029/2009GL039687, 2009.

Nikolova, I., Yin, Q., Berger, A., Singh, U. K., and Karami, M. P.: The last interglacial (Eemian) climate simulated by LOVECLIM and CCSM3, Clim. Past, 9, 1789–1806, 2013.

O'Leary, M. J., Hearty, P. J., Thompson, W. G., Raymo, M. E, Mitrovica, J. X., and Webster, J. M.: Ice sheet collapse following a prolonged period of stable sea level during the last interglacial. Nat. Geosci., 6, 796–800, doi: 10.1038/ngeo1890, 2013.

Oleson, K. W., Dai, Y., Bonan, G., Dickinson, R. E., Dirmeyer, P. A., Hoffman, F., Houser, P., Levis, S., Niu, G.-Y., Thornton, P., Vertenstein, M., Yang, Z.-L., and Zeng, X.: Technical description of the Community Land Model (CLM), Tech. Rep. NCAR/TN-461, National Center for Atmospheric Research, Boulder, CO, 174, 2004.

Oleson, K. W., Niu, G. Y., Yang, Z. L., Lawrence, D. M., Thornton, P. E., Lawrence, P. J., Stockli, R., Dickinson, R. E. G., Bonan, B., Levis, S., Dai, A., and Qian, T.: Improvements to the Community Land Model and their impact on the hydrological cycle, J. Geophys. Res., 113, G01021, doi:10.1029/2007JG000563, 2008.

Olson, S. L. and Hearty, P. J.: A sustained +21 m sea-level highstand during MIS 11 (400 ka): direct fossil and sedimentary evidence from Bermuda, Quat. Sci. Rev., 28, 271–285, 2009.

Otterman, J.: Baring high-albedo soils by overgrazing: a hypothesised desertification mechanism, Science, 186, 531–533, 1974.

Otto-Bliesner, B. L., Tomas, R., Brady, E. C., Ammann, C., Kothavala, Z., and Clauzet, G.: Climate sensitivity of moderate and low resolution versions of CCSM3 to preindustrial forcings, J. Climate, 19, 2567–2583, 2006.

Otto-Bliesner, B. L., Stone, E. J:, McKay, N. P., Lunt, D. J., Brady, E. C., Overpeck, J. T.: How warm was the last interglacial? New model-data comparisons. Philos. Trans. R. Soc. London Ser. A 371, 20130097, doi: 10.1098/rsta.2013.0097; pmid: 24043870, 2013.

Past Interglacials Working Group of PAGES: Interglacials of the last 800,000years, Rev. Geophys., 54, doi:10.1002/2015RG000482, 2016.

Paterson, W. S. B: Ice-sheets and ice shelves, In Colbeck, S.C. (ed.), Dynamics of Snow and Ice Masses, Academic Press, New York, 1–78, 1994.

Patricola, C. M. and Cook, K. H.: Dynamics of the West African Monsoon under Mid-Holocene Precessional Forcing: Regional Climate Model Simulations, J. Climate, 20, 694–716, 2007.

Patricola, C. M. and Cook, K. H.: Atmosphere/vegetation feedbacks: A mechanism for abrupt climate change over northern Africa, J. Geophys. Res., 113, D18102, doi:10.1029/2007JD009608, 2008.

Payne, A. J.: A thermomechanical model of ice flow in West Antarctica, Clim. Dynam., 15, 115–125, 1999.

Poore, R. Z., and Dowsett, H. J.: Pleistocene reduction of polar ice caps: Evidence from Cariaco Basin marine sediments, Geology, 29, 71–74, 2001.

Prell, W., L., and Kutzbach, J.,E.: Monsoon variability over the past 150,000 years, J. Geophys. Res., 92, 8411–8425, 1987.

Prentice, I. C. and Jolly, D.: BIOME 6000 participants: Mid-Holocene and glacial-maximum vegetation geography of the northern continents and Africa, J. Biogeogr., 27, 507–519, 2000.

Prokopenko, A. A., Bezrukova, E. V., Khursevich, G. K., Solotchina, E. P., Kuzmin, M. I., and Tarasov, P. E.: Climate in continental interior Asia during the longest interglacial of the past 500 000 years: the new MIS 11 records from Lake Baikal, SE Siberia, Clim. Past, 6, 31–48, 2010.

Quiquet, A., Ritz, C., Punge, H. J., and Salas y Milia, D.: Greenland ice sheet contribution to sea level rise during the last interglacial period: a modelling study driven and constrained by ice core data, Clim. Past, 9, 353–366, 2013.

Rachmayani, R., Prange, M., and Schulz, M.: North African vegetation-precipitation feedback in early and mid-Holocene climate simulations with CCSM3-DGVM, Clim. Past, 11, 175–185, doi:10.5194/cp-11-175-2015, 2015.

Rachmayani, R., Prange, M., and Schulz, M.: Intra-interglacial climate variability: model simulations of Marine Isotope Stages 1, 5, 11, 13, and 15, Clim. Past, 12, 1–19, doi:10.5194/cp-12-1-2016, 2016.

Raynaud, D., Loutre, M. F., Ritz, C., Chappellaz, J., Barnola, J-M., Jouzel, J., Lipenkov, V. Y., Petit, J-R., and Vimeux, F.: Marine Isotope Stage (MIS) 11 in the Vostok ice core: CO_2 forcing and stability of East Antarctica, Geophysical Monograph Series, 137, 27–40, 2003.

Raynaud, D., Barnola, J.-M., Souchez, R., Reginald, L., Petit, J.-R., Duval, P., and Lipenkov, V. Y.: Paleoclimatology: The record for marine isotopic stage 11, Nature, 436, 39–40, 2005.

Raymo, M. E., Nisancioglu, K. H.: The 41 kyr world: Milankovitch's other unsolved mystery, Paleoceanography, 18, 1011, doi: 10.1029/2002PA000791, 2003.

Raymo, M. E., Mitrovica, J. X.: Collapse of polar ice sheets during the stage 11 interglacial, Nature, 2012/03/22/print, 483, 7390, 453–456, 2012.

Reeh, N.: Paramterization of melt rate and surface temperature on the Greenland ice-sheet, Polarforschung, 59, 113–128, 1991.

Renssen, H., Brovkin, V., Fichefet, T., and Goosse, H.: Holocene climate instability during the termination of the African Humid Period, Geophys. Res. Lett., 30, 1184, doi:10.1029/2002GL016636, 2003.

Renssen, H., Brovkin, V., Fichefet, T., and Goosse, H.: Simulation of the Holocene climate evolution in Northern Africa: The termination of the African Humid Period. Quaternary International, 150, 95–102, 2006a.

Renssen, H., Driesschaert, E., Loutre, M.F., and Fichefet, T.: On the importance of initial conditions for simulations of the mid-Holocene climate, Clim. Past, 2, 91–97, 2006b.

Renssen, H., Seppä, H., Heiri, O., Roche, D. M., Goosse, H., and Fichefet, T.: The spatial and temporal complexity of the Holocene thermal maximum, Nature Geoscience, 2, 411–414, 2009.

Reyes, A. V., Carlson, A. E., Beard, B. L., Hatfield, R. G., Stoner, J. S., Winsor, K., Welke, B., Ullman, D. J.:South Greenland ice-sheet collapse during Marine Isotope Stage 11, Nature, 510, 525–528, 2014.

Ripley, E. A.: Drought in the Sahara: insufficient bio-geophysical feedback?, Science, 191, 100-102, doi:10.1126/science.191.4222.100, 1976.

Ritz, C., Fabre, A., and Letreguilly, A.: Sensitivity of a Greenland ice sheet model to ice flow and ablation parameters: Consequences for the evolution through the last climatic cycle, Clim. Dynam., 13, 11, 1997.

Roberts, D. L., Karkanas, P., Jacobs, Z., Marean, C. W., and Roberts, R. G: Melting ice sheets 400,000 yr ago raised sea level by 13 m: Past analogue for future trends, Earth Planet. Sci. Lett., 357, 226–237, 2012.

Robinson, A., Calov, R., and Ganopolski, A.: Greenland ice sheet model parameters constrained using simulations of the Eemian Interglacial, Clim. Past, 7, 381–396, 2011.

Robinson, A., Calov, R., and Ganopolski, A.: Multistability and critical thresholds of the Greenland ice sheet, Nature Climate Change, 2, 429–432, doi:10.1038/nclimate1449, 2012.

Rowell, D. P., Folland, C. K., Maskell, K., Owen, J. A., and Ward, M. N.: Modelling the influence of global sea surface temperatures on the variability and predictability of seasonal Sahel rainfall, Geophys. Res. Lett., 19, 905–908, 1992.

Rowell, D. P.: The impact of Mediterranean SSTs on the Sahelian rainfall Season, J. Climate, 16, 849–862, 2003.

Rutt, I. C., Hagdorn, M., Hulton, N. R. J., and Payne, A. J.: The Glimmer community ice sheet model, J. Geophys. Res.-Earth Surface, 114, 2009.

Scherer, R. P., Aldahan, A., Tulaczyk, S., Possnert, G., Engelhardt, H., and Kamb, B.: Pleistocene collapse of the West Antarctic Ice Sheet, Science, 281, 82–85, 1998.

Schilt, A., Baumgartner, M., Blunier, T., Schwander, J., Spahni, R., Fischer, H., Stocker, T. F.: Glacial-interglacial and millennial-scale variations in the atmospheric nitrous oxide concentration during the last 800.000 years, Quat. Sci. Rev., 29, 182–192, 2010.

Sitch, S., Smith, B., Prentice, I. C., Arneth, A., Bondeau, A., Cramer, W., Kaplan, J. O., Levis, S., Lucht, W., Sykes, M. T., Thonicke, K., and Venevsky, S.: Evaluation of ecosystem dynamics, plant geography and terrestrial carbon cycling in the LPJ dynamic vegetation model, Global Change Biol., 9, 161–185, 2003.

Smith, R. D., and Gent, P. R.: Reference manual for the Parallel Ocean Program (POP), ocean component of the Community Climate System Model (CCSM2.0 and 3.0), Technical Report, LA-UR-02-2484, Los Alamos National Laboratory, 2002.

Stirling, C. H., Esat, T. M., Lambeck, K., and McCulloch, M. T.: Timing and duration of the Last Interglacial: evidence for a restricted interval of widespread coral reef growth, Earth and Planetary Science Letters, 160, 745–762, 1998.

Stone, E. J., Lunt, D. J., Rutt, I. C., and Hanna, E.: Investigating the sensitivity of numerical model simulations of the modern state of the Greenland ice-sheet and its future response to climate change, The Cryosphere, 4, 397–417, doi:10.5194/tc-4-397-2010, 2010.

Stone, E. J., Lunt, D. J., Annan, J. D., and Hargreaves, J. C.: Quantification of the Greenland ice sheet contribution to Last Interglacial sea-level-rise, Clim. Past, 9, 621–639, doi:10.5194/cp-9-621-2013, 2013.

Street-Perrott, F. A. and Perrott, R. A.: Holocene vegetation, lake levels and climate of Africa, in: Global climates since the Last Glacial Maximum, University of Minnesota Press, Minneapolis, 318–356, 1993.

Sugden, D.E: Case against deep erosion of shileds by ice-sheets, Geology, 4, 580–582, 1976.

Tiedemann, R., Sarnthein, M., and Shackleton, N. J.: Astronomic timescale for the Pliocene Atlantic 18O and dust flux records of Ocean Drilling Program Site 659, Paleoceanography, 9, 619–638, 1994.

Timm, O., Timmermann, A., Abe-Ouchi, A., Saito, F., and Segawa, T.: On the definition of seasons in paleoclimate simulations with orbital forcing, Paleoceanography, 23, PA2221, doi:10.1029/2007PA001461, 2008

Tuenter, E., Weber, S., Hilgen, F., Lourens, L.: The response of the African boreal summer monsoon to remote and local forcing due to precession and obliquity, Global Planet. Change, 36, 219–235, 2003.

Trenberth, K. E., Stepaniak, D. P., and Caron, J. M.: The global monsoon as seen through the divergent atmospheric circulation, J. Climate, 13, 3969–3993, 2000.

Tzedakis, P. C., Hooghiemstra, H., and Palike, H.: The last 1.35 million years at Tenaghi Philippon: revised chronostratigraphy and long-term vegetation trends, Quat. Sci. Rev., 25, 3416–3430, 2006.

Tzedakis, P. C., Raynaud, D., McManus, J. F., Berger, A., Brovkin, V. and Kiefer, T.: Interglacial diversity, Nature Geoscience, 2, 751–755, 2009.

van de Berg, W. J., van den Broeke, M., Ettema, J., van Meijgaard, E., and Kaspar, F.: Significant contribution of insolation to Eemian melting of the Greenland ice sheet, Nat. Geosci., 4, 679–683, doi:10.1038/ngeo1245, 2011.

van Hengstrum, P. J., Scott, D. B., Javaux, E. J.: Foraminifera in elevated Bermudian caves provide further evidence for 21 m eustatic sea level during Marine Isotope Stage 11, Quat. Sci. Rev., 28, 1850–1860, 2009.

van Nes, E. H., Scheffer, M., Brovkin, V., Lenton, T. M., Ye, H., Deyle, E., Sugihara, G.: Casual feedbacks in climate change, Nature Climate Change, doi:10.1038/nclimate2568, 2015.

Varma, V., Prange, M., Merkel, U., Kleinen, T., Lohmann, G., Pfeiffer, M., Renssen, H., Wagner, A., Wagner, S., and Schulz, M.: Holocene evolution of the Southern Hemisphere westerly winds in transient simulations with global climate models, Clim. Past, 8, 391–402, doi:10.5194/cp-8-391-2012, 2012.

Vogel, H., Meyer-Jacob, C., Melles, M., Brigham-Grette, J., Andreev, A. A., Wennrich, V., Tarasov, P. E., and Rosn, P.: Detailed insight into Arctic climatic variability during MIS 11c at Lake El'gygytgyn, NE Russia, Clim. Past, 9, 1467–1479, doi:10.5194/cp-9-1467-2013, 2013.

Wang, G. and Eltahir, E. A. B.: Biosphere-Atmosphere Interactions over West Africa, 2. Multiple Equilibria, Q. J. Roy. Meteorol. Soc., 126, 1261–1280, 2000.

Wang, Y., Notaro, M., Liu, Z., Gallimore, R., Levis, S., and Kutzbach, J. E.: Detecting vegetation-precipitation feedbacks in mid-Holocene North Africa from two climate models, Clim. Past, 4, 59–67, doi:10.5194/cp-4-59-2008, 2008.

Wang, P. X., Wang, B., Cheng, H., Fasullo, J., Guo, Z. T., Kiefer, T., and Liu, Z. Y.: The global monsoon across timescales: coherent variability of regional monsoons, Clim. Past, 10, 2007–2052, doi:10.5194/cp-10-2007-2014, 2014.

Willerslev, E., Cappellini, E., Boomsma, W., Nielsen, R., Hebsgaard, M. B., Brand, T. B., Hofreiter, M., Bunce, M., Poinar, H. N., Dahl-Jensen, D., Johnsen, S., Stevensen, J. P., Bennike, O., Schwenninger, J. L., Nathan, R., Armitage, S., de Hoog, C. J., Alfimov, V., Christl, M., Beer, J., Muscheler, R., Barker, J., Sharp, M., Penkman, K. E. H., Haile, J., Taberlet, P., Gilbert, M. T. P., Casoli, A., Campani, E., and Collins, M. J.: Ancient biomolecules from deep ice cores reveal a forested Southern Greenland, Science, 317, 111–114, 2007.

Williams, J. W., Blois, J. L., and Shuman, B. N.: Extrinsic and intrinsic forcing of abrupt ecological change: case studies from the late Quaternary, J. Ecol., 99, 664–677, 2011.

Xue, Y. and Shukla, J.: The influence of land-surface properties on Sahel climate, Part 1: Desertification, J. Climate, 6, 2232–2245, 1993.

Xue, Y. and Shukla, J.: The influence of land surface properties on Sahel climate, Part II: Afforestation, J. Climate, 9, 3260–3275, 1996.

Yang, Q., Dixon, T. H., Myers, P. G., Bonin, J., Chambers, D., van den Broeke, M. R.: Recent increases in Arctic freshwater flux affects Labrador Sea convection and Atlantic overturning circulation, Nature Communications, 7, 10525, doi:10.1038/ncomms10525, 2016.

Yeager, S. G., Shields, C. A., Large, W. G., and Hack, J. J.: The low-resolution CCSM3, J. Climate, 19, 2545–2566, 2006.

Yin, Q., Berger, A., Driesschaert, E., Goosse, H., Loutre, M. F., and Crucifix, M.: The Eurasian ice sheet reinforces the East Asian boreal summer monsoon during the interglacial 500 000 years ago, Clim. Past, 4, 79–90, 2008.

Yin, Q. Z., Berger A, and Crucifix, M.: Individual and combined effects of ice sheets and precession on MIS13 climate, Clim. Past, 5, 229–243, 2009.

Q. Z. Yin, and A. Berger: Insolation and CO_2 contribution to the interglacial climate before and after the Mid-Brunhes Event. Nat. Geosci., 3, 243–246, doi: 10.1038/ngeo771, 2010.

Yin Q. Z., and Berger, A.: Individual contribution of insolation and CO_2 to the interglacial climates of the past 800,000 years, Clim. Dynam., 38, 709–724, 2012.

Yin Q. Z., and Berger, A.: Interglacial analogues of the Holocene and its natural near future, Quat. Sci. Rev., 20, doi:10.1016/j.quascirev.2015.04.008, 2015.

Zhao, Y., Braconnot, P., Marti, O., Harrison, S. P., Hewitt, C., Kitoh, A., Liu, Z., Mikolajewicz, U., Otto-Bliesner, B., and Weber, S. L.: A Multi-Model Analysis of the Role of the Ocean on the African and Indian Monsoon During the Mid-Holocene, Clim. Dynam., 25, 777–800, 2005.

Zhao, Y. and Harrison, S. P.: Mid-Holocene monsoons: A multi-model analysis of the inter-hemispheric differences in the responses to orbital forcing and ocean feedbacks, Clim. Dynam., 39, 1457–1487, 2012.

Zeng, N. and Neelin, J. D.: The Role of Vegetation-Climate Interaction and Interannual Variability in Shaping the African Savanna, J. Climate, 13, 2665–2670, 2000.

Zheng, W. and Braconnot, P.: Characterization of Model Spread in PMIP2 Mid-Holocene Simulations of the African Monsoon, J. Climate, 26, 1192–1210, 2013.